Reaction Crystallization Field to Control Crystal Characteristics

結晶特性を制御するための反応晶析場

February 2014

Mikiyasu INOUE

井上　幹康

Reaction Crystallization Field to Control Crystal Characteristics

結晶特性を制御するための反応晶析場

February 2014

Waseda University
Graduate School of Advanced Science and Engineering
Major in Applied Chemistry,
Research on Chemical Engineering

Mikiyasu INOUE

井上　幹康

JUDGING COMMITTEE

Referee in chief

Waseda University: Prof. Izumi Hirasawa

Referees

Waseda University: Prof. Suguru Noda

Martin-Luther-Univetsity Halle-Wittenberg: Dr. Ing. Joachim Ulrich

CONTENTS

Chapter 1

Characteristics of reaction crystallization and effects of polyelectrolyte reaction field

Chapter 1

Reaction crystallization is one of liquid phase method obtaining crystal product by mixing liquid raw materials. Reaction crystallization has advantages and disadvantages. The greatest advantage of reaction crystallization is rapid reaction rate resulting from supersaturation generated by reaction. In addition, reaction crystallization can save energy because reaction occurs at ordinary temperatures and ordinary pressures. On the other hand, the most serious disadvantage of reaction crystallization is difficulties to control crystal nucleation and crystal growth caused by large supersaturation and consequent crystal aggregation. In addition, not target materials but amorphous precursor of them can be formed in reaction crystallization. For example, ceramics requiring high temperature or high pressure to crystallize are likely to form amorphous precursor synthesized by reaction crystallization. YBO_3 applied as Vacuum ultraviolet (VUV) red phosphor is one example to form amorphous precursor synthesized by reaction crystallization. Moreover, $CaCO_3$ can form amorphous other than three polymorphs, vaterite, aragonite and calcite, and some hydroxide can form gel-like solid showing low crystallinity and bad solid-liquid separation properties.

To control crystal nucleation and crystal growth, and to prevent aggregation, reaction crystallization using polyelectrolyte as reaction field is proposed. Reaction crystallization using polyelectrolyte intends to divide whole process of crystallization into nucleation process and growth process by preventing continuous nucleation and secondary nucleation. Polyelectrolyte reaction field will prevent overgrowth and aggregation of crystals by electrostatic attractive force between polyelectrolyte and solute molecules or crystal nuclei, and by steric hindrance of polymer chain. As a result, mono-dispersed microcrystals free from aggregation will be formed. In fact, this method has provided remarkable results on synthesis of mono-dispersed microcrystals of poorly-soluble sulfates: $SrSO_4$, $BaSO_4$, and $PbSO_4$ [1, 2, 3]. The problem forming amorphous precursor is hard to solve because it is almost defined by fundamental characteristics of materials whether crystal precursor or amorphous precursor is formed in reaction crystallization. However, confirmation of synthesis

method of crystal precursor will enable us to control crystal shape and crystal size more easily not only in reaction crystallization but also in lower processes considering amorphous has structural proximity to liquid phase.

Chapter 2

Characteristics of target materials:

$(Y,Gd)BO_3:Eu^{3+}$ and $CaSO_4 \cdot 2H_2O$

2.1 Characteristics of $(Y,Gd)BO_3:Eu^{3+}$

2.1.1 Crystal characteristics and luminescent characteristics of $(Y,Gd)BO_3:Eu^{3+}$

$(Y,Gd)BO_3:Eu^{3+}$ is one of VUV red phosphors doped Eu^{3+} as luminescent center into YBO_3 host lattice. Y^{3+} in the host lattice is partly substituted with Gd^{3+} to enhance energy transfer efficiency. $(Y,Gd)BO_3:Eu^{3+}$ is widely used for plasma display panels (PDP) and is examined to apply to Hg-free fluorescent lump in the future. PDP is one of light-emitting flat display panel with VUV phosphors. PDP is comprised of two glass screens; front screen with display electrodes and rear screen with address electrodes coated with phosphors. Xe containing Ne is enclosed between two screens. Ne showing high discharge generation efficiency helps to decrease discharge voltage of Xe. Discharged Xe generates VUV excitation light whose wavelength is 147 nm and 173 nm by impressing a voltage between these two electrodes, and as a result, phosphors excited by VUV emit fluorescence. $(Y,Gd)BO_3:Eu^{3+}$ phosphor particles about 3 μm are uniformly applied on electrode and form phosphor layer about 20 μm [4, 5, 6, 7, 8] (Fig. 2.1).

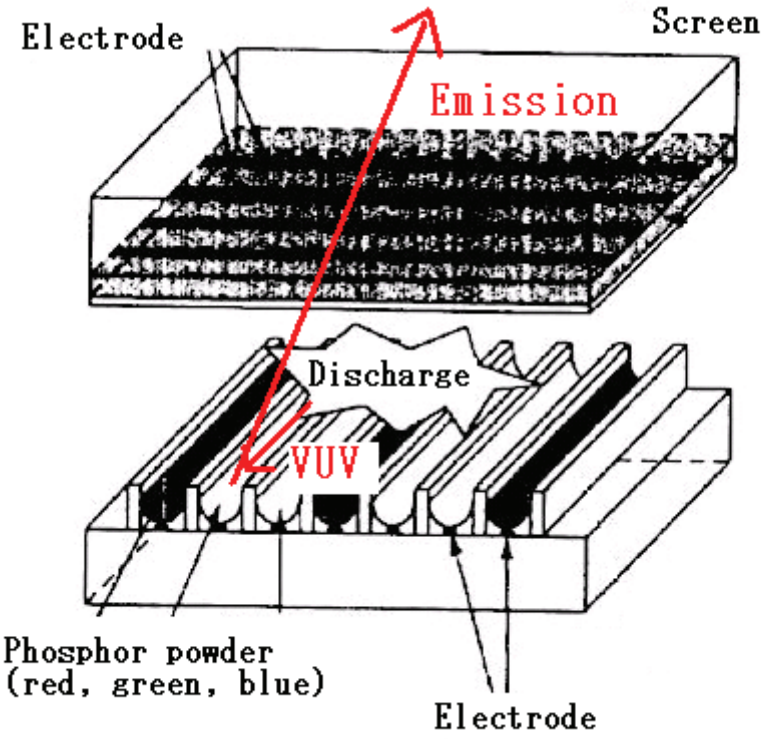

Figure 2.1 Structure of PDP

Ideal phosphor requires abilities in excitation energy absorption, energy transfer efficiency, wide color region and stability against heat and chemicals. $(Y,Gd)BO_3:Eu^{3+}$ has the advantages of strong VUV absorption and high luminescent intensity. This is because energy transfer from VUV excitation light to Eu^{3+} luminescent center efficiently proceeds due to the existence of B-O bonds; B-O bonds can efficiently absorb VUV excitation light which Eu^{3+} cannot directly absorb due to its energy level (Fig. 2.2) [9]. However, $(Y,Gd)BO_3:Eu^{3+}$ has disadvantages, too. Disadvantages of $(Y,Gd)BO_3:Eu^{3+}$ can be classified into two major types: originating from this material and originating from synthesis method. Disadvantage of $(Y,Gd)BO_3:Eu^{3+}$ originating from this material is poor chromaticity, that is, $(Y,Gd)BO_3:Eu^{3+}$ contains orange fluorescence. This is because $(Y,Gd)BO_3$ host lattice has parity symmetry and therefore orange fluorescence produced by magnetic dipole transition is dominant. Deviance from color standard requires complicated control to produce

desired color. On the other hand, disadvantages of $(Y,Gd)BO_3:Eu^{3+}$ originating from synthesis method, solid-state reaction, are large size and non-uniform shape. These size and shape result from repetition of firing process at a high temperature above 1000℃ for some hours, and following grinding process. Eu^{3+} locating inside of phosphor particle where VUV excitation light does not reach cannot emit fluorescence and be wasted, however, phosphor particles smaller than micrometer order cannot be synthesized by solid-state reaction. In addition, large and non-uniform phosphors are difficult to apply in high packing density and to form flat surface with small amount of phosphors [10], which increases market price.

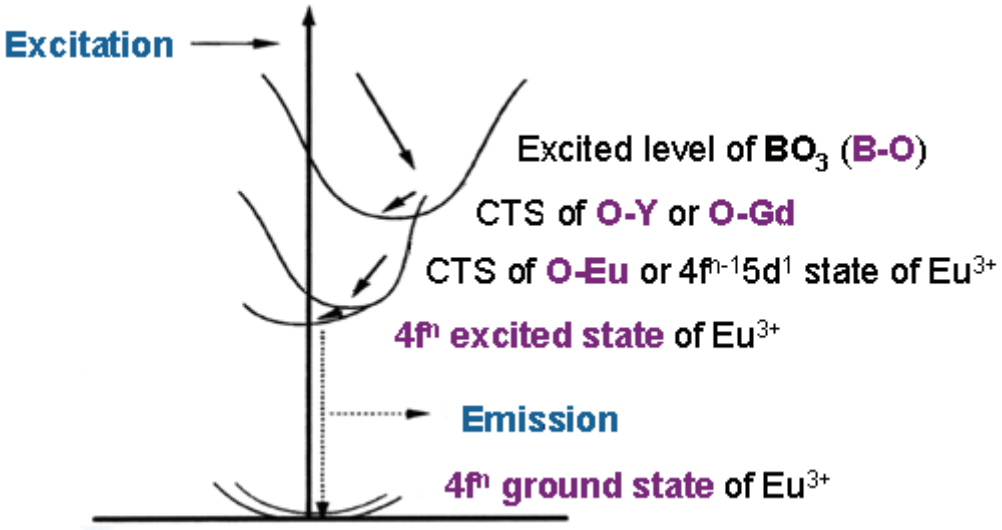

Figure 2.2 Emission process of $(Y,Gd)BO_3:Eu^{3+}$

To solve these problems, several synthesis methods have been proposed: sol-gel method [11], hydrothermal synthesis [12, 13], reaction crystallization [12, 14, 15], spray pyrolysis [16] and microwave heating [13]. In this research, reaction crystallization was applied. By reaction crystallization, $(Y,Gd)BO_3:Eu^{3+}$ microcrystals with uniform shape will be formed. Final objective of

this research is to synthesize (Y,Gd)BO_3:Eu^{3+} microcrystals satisfying following requirements by reaction crystallization; 1. crystal size smaller than 300 nm, that of phosphors synthesized by solid-state reaction, 2. mono-dispersity whose C.V. is lower than 0.1, and 3. higher luminance and better chromaticity than those of crystals synthesized by solid-state reaction. However, firing process is required to change amorphous precursor into (Y,Gd)BO_3:Eu^{3+} crystals when applying reaction crystallization though repetition of firing is not needed like solid-state reaction. Firing temperature and time in this research are fixed 1000℃ and 6 hours, respectively. (Y,Gd)BO_3:Eu^{3+} will not melt in this firing condition because melting point of YBO_3 is about 1650℃ [17, 18]. However, melting point may decrease when (Y,Gd)BO_3:Eu^{3+} microcrystals or nano-crystals are formed or when using additives functioning as flux.

Uniform microcrystals will shorten firing time, which will save the energy during firing. In addition, uniform microcrystals will allow making flat emission surface with less phosphor particles in high packing density, which will reduce market price. Moreover, uniform microcrystals will also improve their chromaticity. The ratio of surface area to particle volume will increase by minifying, which will increase surface effects such as roughness. Rough surface with low parity symmetry will show better chromaticity [11, 12, 13]. Chromaticity can also be improved by breaking parity symmetry around Eu^{3+} by incorporating impurity ions into host lattice [12, 13, 19].

2.1.2 Precursor before firing and product after firing possible to form in reaction crystallization of (Y,Gd)BO_3:Eu^{3+}

In reaction crystallization of (Y,Gd)BO_3:Eu^{3+}, amorphous precursor is formed by mixing two raw materials, aqueous solutions of rare earth nitrate ($RE(NO_3)_3$) and H_3BO_3, and following pH adjustment by basic pH adjuster such as NH_3. Solubility of YBO_3 precursor is high in acidic conditions, however, it rapidly decreases as pH rises. Solution pH should be adjusted carefully to

form uniform microcrystals because rapid pH change causes mass nucleation, particle overgrowth and particle aggregation.

Amorphous precursor is changed into YBO_3 by firing, however, by-products such as Y_3BO_6 and Y_2O_3 may be formed according to reaction condition. Y_3BO_6 is likely to incorporate in such cases adding NH_3 massively. Y_3BO_6 incorporation often decreases luminance and chromaticity terribly though luminescent characteristics of Y_3BO_6 itself has not been revealed. On the other hand, Y_2O_3 is likely to form in such cases using strong base like NaOH massively. Y_2O_3 shows opposite luminescent characteristics to YBO_3: low luminance and good chromaticity. Low luminance of Y_2O_3 results from low energy transfer efficiency from VUV excitation light to Eu^{3+} luminescent center due to lack of B-O bonds absorbing VUV excitation light efficiently. Maximum luminance of Y_2O_3 is 2/3 of commercial YBO_3 at the best. Meanwhile, good chromaticity of Y_2O_3 results from lack of parity symmetry of Y_2O_3 host lattice and therefore red fluorescence produced by electric dipole transition is dominant. XRD charts of YBO_3, Y_3BO_6 and Y_2O_3 are shown in Fig. 2.3. XRD peak intensities of YBO_3, Y_3BO_6 and Y_2O_3 are referred to PDF#00-016-0277, PDF#00-034-0291 and PDF#01-086-1107, respectively.

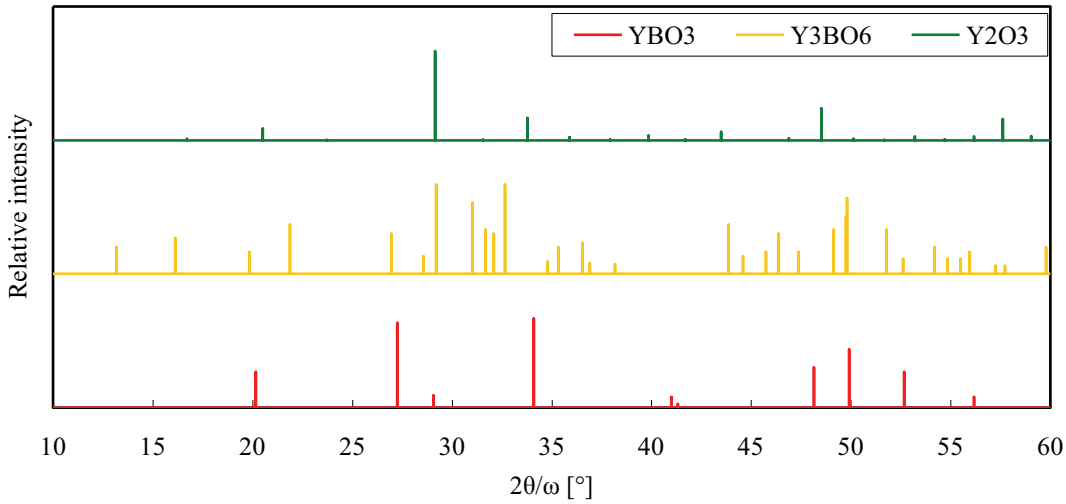

Figure 2.3 XRD charts of YBO_3, Y_3BO_6 and Y_2O_3

2.1.3 Evaluation of (Y,Gd)BO_3:Eu^{3+} characteristics

Phosphors for PDP require following major seven properties: luminance, chromaticity, afterglow, process-degradation resistance, lifetime, powder characteristics and electrical characteristics. In this research, we focused on two luminescent properties, luminance and chromaticity, among those seven properties. In addition, we focused on crystal shape, crystal size and crystal composition (crystallinity). The followings are evaluation methods of each property of (Y,Gd)BO_3:Eu^{3+} phosphor.

(a) Crystal shape and crystal size

Commercial (Y,Gd)BO_3:Eu^{3+} crystals synthesized by solid-state reaction have large size and non-uniform shape. Meanwhile, (Y,Gd)BO_3:Eu^{3+} crystals synthesized by reaction crystallization are relatively small and relatively uniform but tend to aggregate. Mono-dispersed uniform microcrystals are desirable for making flat emission surface with less phosphor particles in high packing density.

Crystal shape and crystal size both before firing and after firing were observed by scanning electron microscope (SEM). By observing particles both before firing and after firing, whether

crystal shape and crystal size were maintained or not during firing was determined.

(b) Crystal composition (Crystallinity)

Precursor synthesized by reaction crystallization between $RE(NO_3)_3$ and H_3BO_3 is generally amorphous with non-uniform shape and non-uniform size. However, crystal precursor may be formed according to reaction condition, and crystal precursor will enable us to control crystal shape and crystal size more easily. On the other hand, main product after firing is generally YBO_3, the target material, however, by-product Y_3BO_6 or Y_2O_3 showing low luminance and/or poor chromaticity may be incorporated according to reaction condition. Host lattice of pure YBO_3 showing high crystallinity is required to achieve high luminance by efficient energy transfer.

Crystal composition (Crystallinity) was examined both before firing and after firing. Composition of product and crystallinity of each component were examined by X-ray diffraction (XRD). Crystallinity was determined from the strongest diffraction peak of each component.

(c) Luminance

Luminance is the amount of light per unit area emitted from particular direction. Ideal white fluorescence is achieved by equalizing luminance of three primary colors. In addition, luminance of three primary colors is required to be strong enough to brighten display.

Luminance was measured by luminance and color meter, and relative luminance to commercial $(Y,Gd)BO_3:Eu^{3+}$ synthesized by solid-state reaction (NP-360-03, NICHIA CORPORATION) was calculated.

(d) Chromaticity

Chromaticity is mixing ratio of three primary colors and is determined from x-y chromaticity diagram (Fig. 2.4). Three primary colors are required to be as pure as possible to display desired colors by mixing them.

Chromaticity was measured in parallel with luminance by luminance and color meter.

Calculation process of chromaticity from x-y chromaticity diagram is as follows: 1. Distances of r_1 and r_2 are measured. Here, r_1 is a distance between chromaticity coordinate of reference (commercial $(Y,Gd)BO_3:Eu^{3+}$ synthesized by solid-state reaction) and chromaticity coordinate of ideal red, and r_2 is a distance between chromaticity coordinate of sample synthesized by reaction crystallization and chromaticity coordinate of ideal red. 2. $1/r_1$ and $1/r_2$ are calculated. 3. Relative chromaticity to commercial $(Y,Gd)BO_3:Eu^{3+}$ is calculated by following equation: Relative chromaticity = $(1/r_2)$ / $(1/r_1)$ · 100

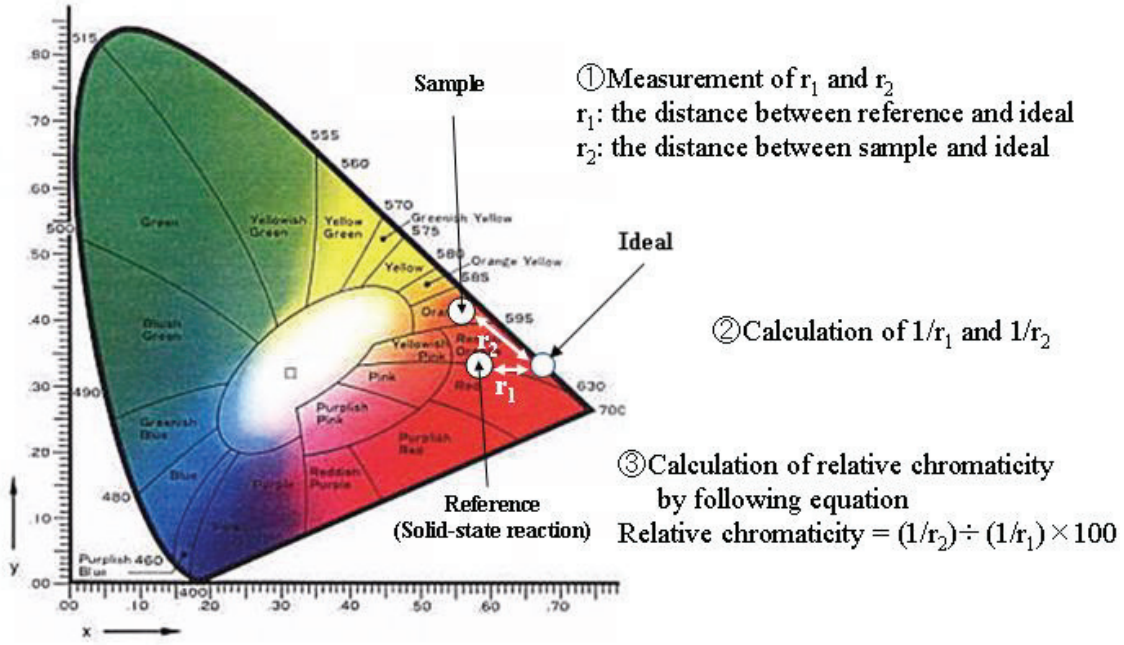

Figure 2.4 x-y chromaticity diagram and calculation procedure of relative chromaticity

2.2 Crystal characteristics of $CaSO_4 \cdot 2H_2O$

$CaSO_4 \cdot 2H_2O$ has the smallest formula weight and the highest solubility in water among alkaline-earth metal sulfates though it is categorized in poorly-soluble salts among all materials. $CaSO_4 \cdot 2H_2O$ is worthwhile to develop the method to synthesize mono-dispersed microcrystals successfully as well as poorly-soluble sulfates examined in previous studies [1, 2, 3] because of its

difficulty to control crystal nucleation and crystal growth, and to prevent aggregation.

Calcium sulfate anhydride has following three polymorphs. Polymorph Ⅲ has hexagonal structure and is soluble in water. Polymorph Ⅱ formed by heating polymorph Ⅲ at 300-600℃ has orthorhombic structure and is poorly-soluble in water. Polymorph Ⅰ formed by heating polymorph Ⅱ at 1150-1200℃ has cubic structure and is stable in high temperature [20]. On the other hand, calcium sulfate also has pseudo-polymorphs with different hydration numbers. Calcium sulfate is usually crystallized as dihydrate ($CaSO_4 \cdot 2H_2O$) by reaction crystallization from water solution under ordinary temperature and ordinary pressure, however, sometimes another hydrate such as hemihydrate ($CaSO_4 \cdot 0.5H_2O$) may be crystallized. Both anhydride polymorphs and hydrate polymorphs can have various crystal habits.

Polymorphs are essentially different from crystal habits. Polymorphs are substances with same chemical composition, which have various crystal structures. Morphologies are fundamentally different among polymorphs due to a difference of crystal phase, resulting in a difference of XRD charts. In addition, each polymorph has peculiar thermodynamically stable zone because physical and chemical properties are different among polymorphs. On the other hand, crystal habit is a difference of crystal shape resulting from the difference of growth rate of each crystal face. Growth rates of equivalent crystal faces can be different according to reaction conditions though targets are identical substances with the same number of constituent faces and identical ideal forms, resulting in a difference of crystal habit. Although crystal shape and crystal size are different among crystals showing different crystal habits, XRD peak positions are identical because chemical compositions, physical properties and chemical properties are identical among them. However, intensities of each diffraction peak are different among them because total area of each crystal face is different according to crystal habit.

Major diffraction peaks of $CaSO_4 \cdot 2H_2O$ crystals in the range of 10-60° are (020), (021),

(130), (041), and (-221) peaks. Positions (2θ) of these peaks are 11.6°, 20.7°, 23.4°, 29.1°, and 31.1°, respectively (Fig. 2.5). Miller indices of these peaks were referred to PDF#00-033-0311. Concerning $CaSO_4 \cdot 2H_2O$ crystals synthesized from raw material solutions with appropriate concentrations without additives, their typical morphologies are needle-like or plate-like (Fig. 2.6), and (020) diffraction peak is much stronger than any other peaks (Fig. 2.5). XRD absolute intensities of other diffraction faces are usually negligibly low. On the other hand, PDF#00-033-0311 has two strongest peaks, (020) diffraction peak and (021) diffraction peak, and differences of peak intensities among diffraction peaks are smaller than those synthesized by reaction crystallization (Fig. 2.7). These differences result from the difference of crystal habit caused by the difference of synthesis method or synthesis condition of $CaSO_4 \cdot 2H_2O$.

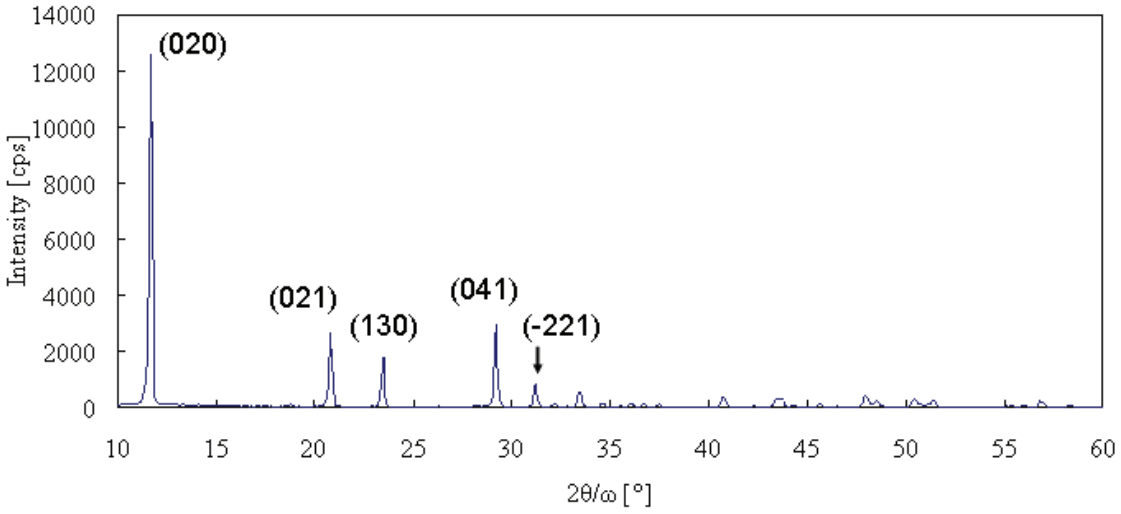

Figure 2.5 Typical XRD chart and major diffraction peaks of $CaSO_4 \cdot 2H_2O$ synthesized by reaction crystallization

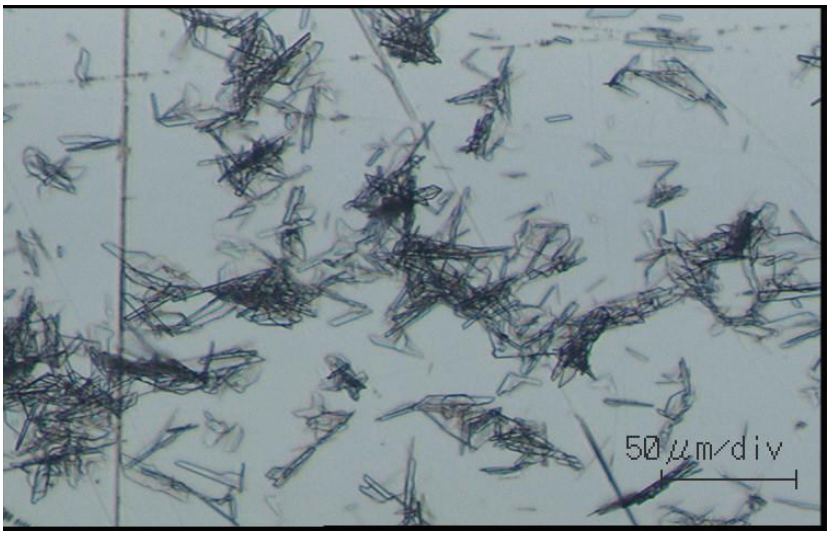

Figure 2.6 Typical $CaSO_4 \cdot 2H_2O$ crystals synthesized by reaction crystallization

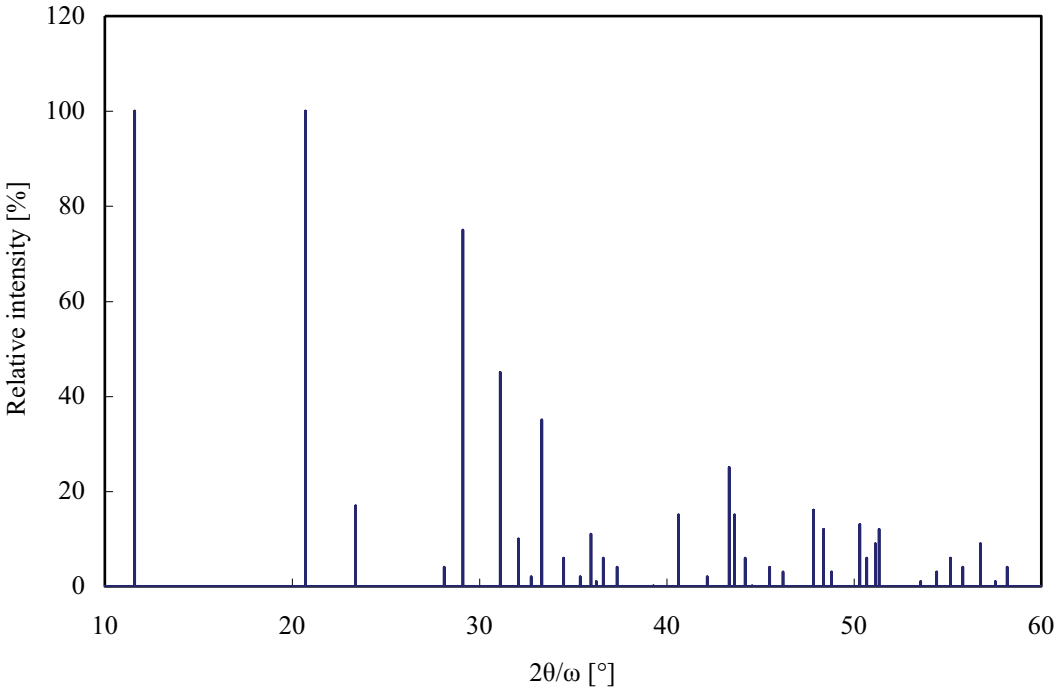

Figure 2.7 XRD chart of PDF#00-033-0311

Crystal structure of $CaSO_4 \cdot 2H_2O$ and Miller index of each crystal face have been defined by several authors [21, 22, 23] (Fig. 2.8), however, some Miller indices defined by them do not correspond with JCPDS or major peaks on XRD charts. Therefore, crystal structure of $CaSO_4 \cdot 2H_2O$ and Miller index of each crystal face are worthwhile to investigate.

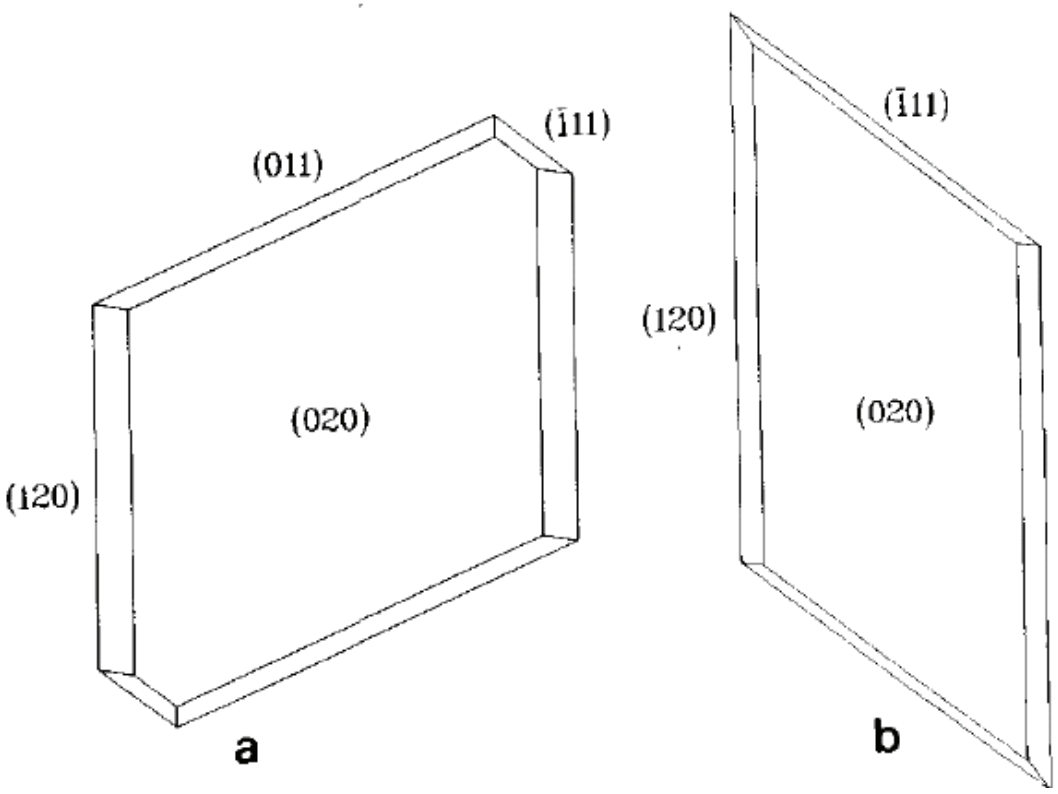

Figure 2.8 Crystal structure and Miller indices of $CaSO_4 \cdot 2H_2O$

(a) theoretical habit derived by Heijnen and Hartman

(b) observed habit from an aqueous solution

Chapter 3

Synthesis of $(Y,Gd)BO_3:Eu^{3+}$ mono-dispersed microcrystals by reaction crystallization

3.1 Synthesis of (Y,Gd)BO_3:Eu^{3+} mono-dispersed microcrystals by reaction crystallization using polyelectrolyte reaction field

3.1.1 Introduction

In reaction crystallization of (Y,Gd)BO_3:Eu^{3+} precursor by mixing raw materials, solutions of *RE*$(NO_3)_3$ and H_3BO_3, and following pH adjustment to basic state, amorphous precursor whose shape and size are not uniform is formed. These shape and size remain non-uniform after YBO_3 precursor changed into YBO_3 crystal by firing. These shape and size of YBO_3 precursor and YBO_3 crystal were tried to be improved by applying polyelectrolyte reaction field.

In this research, polyelectrolytes having possibility to interact electrostatically with rare earth ion (RE^{3+}), polyethyleneimine (PEI) and polyacrylic acid (PAA), were selected as candidates of polyelectrolyte reaction field. Average molecular weights of PEI and PAA are 70000 and 250000, respectively. Concerning PEI, not only non-acidified PEI but also acidified PEI was examined because acidified PEI is more likely to prevent overgrowth and aggregation of crystals than non-acidified PEI [1, 2, 3]. Effect of polyelectrolyte on precursor type, crystal shape and crystal size both before firing and after firing, and relative luminance and relative chromaticity after firing, were evaluated in reaction crystallization using polyelectrolyte reaction field, and suitable polyelectrolyte type and its reaction condition were discussed.

3.1.2 Experimental procedure

(Y,Gd)BO_3:Eu^{3+} was synthesized by reaction crystallization in polyelectrolyte reaction field. Applied materials are shown in Table 3.1.1. PEI and PAA were used as polyelectrolyte reaction field. Polyelectrolytes were sufficiently dissolved into deionized water by stirring for more than 24 hours. 0.3 mol/L *RE*$(NO_3)_3$ solution and 0.3 mol/L H_3BO_3 solution were used as raw materials. *RE*$(NO_3)_3$ solution was composed of $Y(NO_3)_3 \cdot 6H_2O$, $Gd(NO_3)_3 \cdot 6H_2O$ and $Eu(NO_3)_3 \cdot 6H_2O$ mixed in a ratio

of 0.9 : 0.1 : 0.03, based on the previous research by Kee-Sun Sohn et. al. [24]. This mixing ratio can achieve the best fluorescent properties at the lowest material cost. Reaction crystallization was carried out in a batch reactor at room temperature.

Table 3.1.1 Materials

Reagent	Grade	Purity [%]	Production company
H_3BO_3	special	99.5	Kanto Chemical Co. Inc
$Y(NO_3)_3 \cdot 6H_2O$	high purity	99.99	Kanto Chemical Co. Inc
$Gd(NO_3)_3 \cdot 6H_2O$	high purity	99.95	Kanto Chemical Co. Inc
$Eu(NO_3)_3 \cdot 6H_2O$	—	99.9	Shin-Etsu Chemical Co., Ltd.
HNO_3	special	60.0-61.0	Wako Pure Chemical Industries, Ltd.
NH_3	special	28.0-30.0	Kanto Chemical Co. Inc
PEI70000	P-1000	29.0-31.0	Nippon Shokubai Co., Ltd.
PAA250000	first	—	Wako Pure Chemical Industries, Ltd.
N_2	—	—	Kotobuki Sangyo Co., Ltd.
$(Y,Gd)BO_3:Eu^{3+}$	NP-360-03	—	Nichia Corporation

PEI70000 (P-1000, EPOMIN) is provided by Nippon Shokubai.

N_2 is applied as pressurization gas for pressure filtration.

$(Y,Gd)BO_3:Eu^{3+}$ (NP-360-03) is commercial red phosphor synthesized by solid-state reaction, and is used as reference to calculate relative luminance and relative chromaticity.

500 mL of polyelectrolyte solution were put into 1 L beaker reactor. In the condition using acidified PEI, solution pH was adjusted below 3 by 60% HNO_3. 100 mL of 0.3 mol/L $RE(NO_3)_3$ solution and 100 mL of 0.3 mol/L H_3BO_3 solution were added in order, and stirred for 1 day after adding respectively. Through this operation YBO_3 precursor was formed. In the condition using acidified PEI, pH adjuster was additionally added until pH was reached to 7 in order to precipitate YBO_3 precursor and stirred for 20 min. Precursor slurry was separated into precipitate and supernatant by centrifugation (4000 rpm, 60 min). Precipitate was washed by adding deionized water to centrifuge bottle and shaking. Washed precursor was separated from suspension by pressured

filtration, and dried in oven at 150℃ for 24 hours. Dried precursor was ground in mortar and fired at 1000℃ for 6 hours. Precursor transforms into YBO_3 by firing.

Crystal shape and crystal size were observed by SEM (VE-8800, KEYENCE), and composition and crystallinity were examined by XRD (Rint-UltimaⅢ, Rigaku) on synthesized samples before firing and after firing. In addition, luminance and chromaticity on samples after firing were determined by luminance and color meter (CS-200, Konica Minolta).

Whole synthesis procedure is shown in Fig. 3.1.1. This figure shows synthesis procedure becomes complicated and prolonged by introducing polyelectrolyte reaction field.

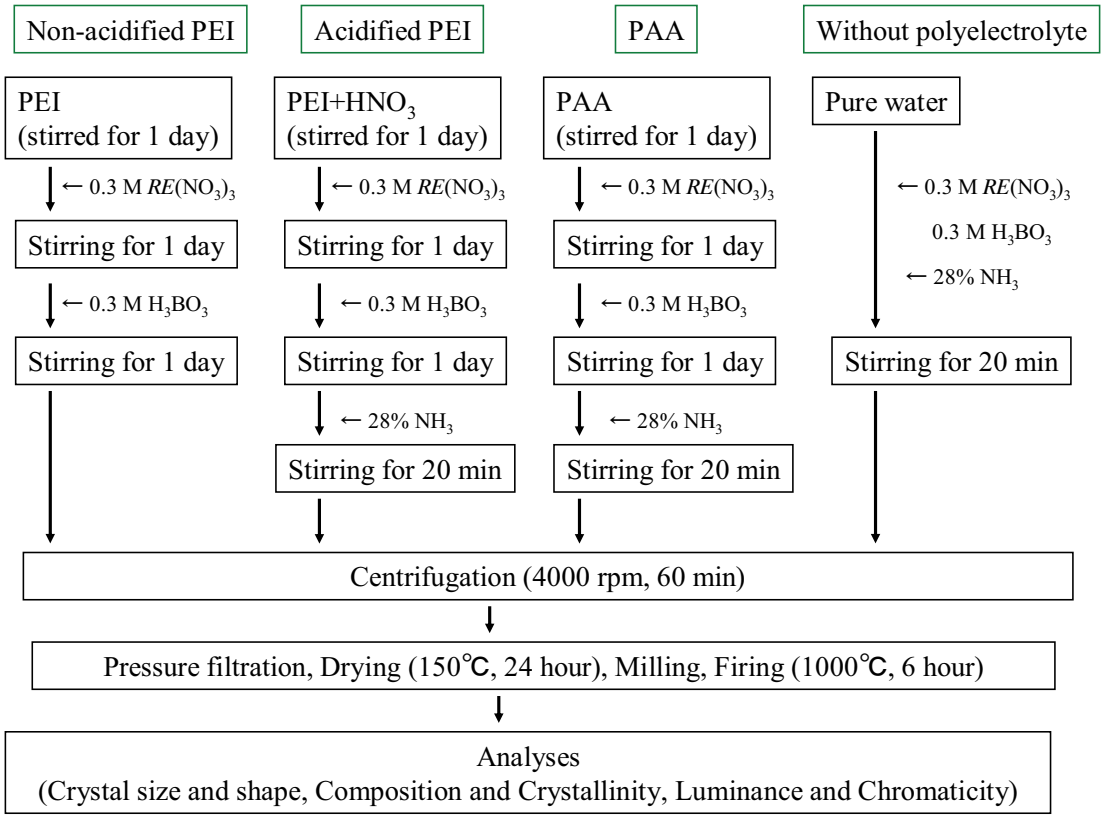

Figure 3.1.1 Synthesis procedure

3.1.3 Results and discussions

Experimental results before firing and after firing are shown in Table 3.1.2 and Table 3.1.3, respectively. At first, candidates of polyelectrolyte concentrations were widely selected from 1, 10, 50, 100 g/L. However, PEI whose concentration was over 50 g/L precipitated by reacting with HNO_3 acidifier or $RE(NO_3)_3$. In addition, PAA whose concentration was over 10 g/L precipitated by reacting with $RE(NO_3)_3$. Therefore, polyelectrolyte candidates were narrowed to following five types: 1 g/L non-acidified PEI, 10 g/L non-acidified PEI, 1 g/L acidified PEI, 10 g/L acidified PEI, and 1 g/L PAA.

Table 3.1.2 Experimental results (before firing)

Polyelectrolyte	pH		Crystal shape and Crystal size		Precursor	
	Initial [-]	Adjusted [-]	Shape	Size [μm]	Type	Crystallinity [cps]
1g/L non-acidified PEI	8.30	5.47	spherical microcrystals	0.1-1	$YB(OH)_4CO_3$	1284
10g/L non-acidified PEI	10.41	6.49	coarse crystals and aggregated microcrystals	0.1-120	$YB(OH)_4CO_3$	475
1g/L acidified PEI	2.83	7.04	coarse crystals and aggregated microcrystals	0.1-50	amorphous	360
10g/L acidified PEI	2.86	7.01	coarse crystals and aggregated microcrystals	0.1-30	amorphous	372
1g/L PAA	3.38	8.56	coarse crystals and aggregated microcrystals	0.1-40	amorphous	348
without polyelectrolyte	7	8.5	coarse crystals and aggregated microcrystals	0.1-70	amorphous	448

Table 3.1.3 Experimental results (after firing)

Polyelectrolyte	Crystal shape and Crystal size		Crystallinity			Relative	Relative
	Shape	Size [μm]	YBO_3 [cps]	Y_3BO_6 [cps]	Y_2O_3 [cps]	luminance [%]	chromaticity [%]
1g/L non-acidified PEI	spherical microcrystals	0.2-1	2672	287	0	34.4	95.0
10g/L non-acidified PEI	coarse crystals and aggregated microcrystals	0.2-40	1322	499	1058	32.6	85.7
1g/L acidified PEI	aggregated microcrystals	0.2-40	3548	0	0	93.8	97.1
10g/L acidified PEI	aggregated microcrystals	0.2-50	3938	0	0	89.9	97.2
1g/L PAA	coarse crystals and aggregated microcrystals	0.2-70	2306	247	0	55.8	92.2
without polyelectrolyte	coarse crystals and aggregated microcrystals	0.1-50	2268	298	0	63.0	91.7

Examined polyelectrolytes can be classified into four types according to observed effects of polyelectrolytes and characteristics of synthesized phosphors: (a) 1 g/L non-acidified PEI, (b) 10 g/L non-acidified PEI, (c) 1 g/L acidified PEI and 10 g/L acidified PEI, and (d) 1 g/L PAA.

(a) 1 g/L non-acidified PEI

In the case using 1 g/L non-acidified PEI, the smallest and the most uniform crystals were formed. In addition, not amorphous precursor but uniform $YB(OH)_4CO_3$ microcrystals whose mean size was about 300 nm were formed before firing. This is supposed to be the result of pH history changing from weakly-basic condition to weakly-acidic condition assumed to be appropriate for synthesizing $YB(OH)_4CO_3$ crystal precursor. Moreover, size and uniformity of these crystals were kept after $YB(OH)_4CO_3$ changed to YBO_3 by firing (Fig. 3.1.2).

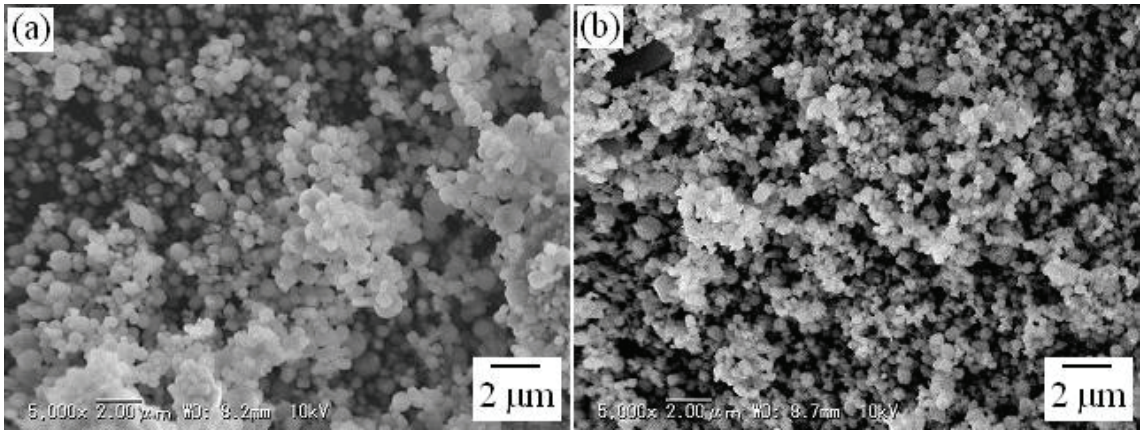

Figure 3.1.2 SEM images of crystals synthesized with 1 g/L non-acidified PEI

(a) before firing (b) after firing

Assumed mechanisms to form mono-dispersed YBO_3 microcrystals in the 1 g/L non-acidified PEI reaction field are as follows: 1. Coordination bond was formed between unshared electron pairs on N atoms in PEI and RE^{3+}, resulting in preventing nuclei aggregation. 2. Steric hindrance of PEI chains interrupts overgrowth of crystals, resulting in forming uniform microcrystals. 3. Remained PEI protects crystal surface, resulting in preventing adhesion and aggregation of crystals during firing. Through these mechanisms, 1 g/L non-acidified PEI will show significant suppressing effect on crystal growth and crystal aggregation, and will enable to form mono-dispersed YBO_3 microcrystals.

Formation of coordination bond between N atoms in PEI and RE^{3+} was investigated by FT-IR (Nicolet 6700, Thermo SCIENTIFIC). IR absorbance around 1140 cm^{-1} corresponding to C-N bond of amine in PEI disappeared when $RE(NO_3)_3$ was added to PEI (Fig. 3.1.3). However, this IR absorbance remained when H_3BO_3 was added to PEI (Fig. 3.1.4). This result indicates the state of C-N bond in PEI changed by forming coordination bond between N atoms in PEI and RE^{3+}.

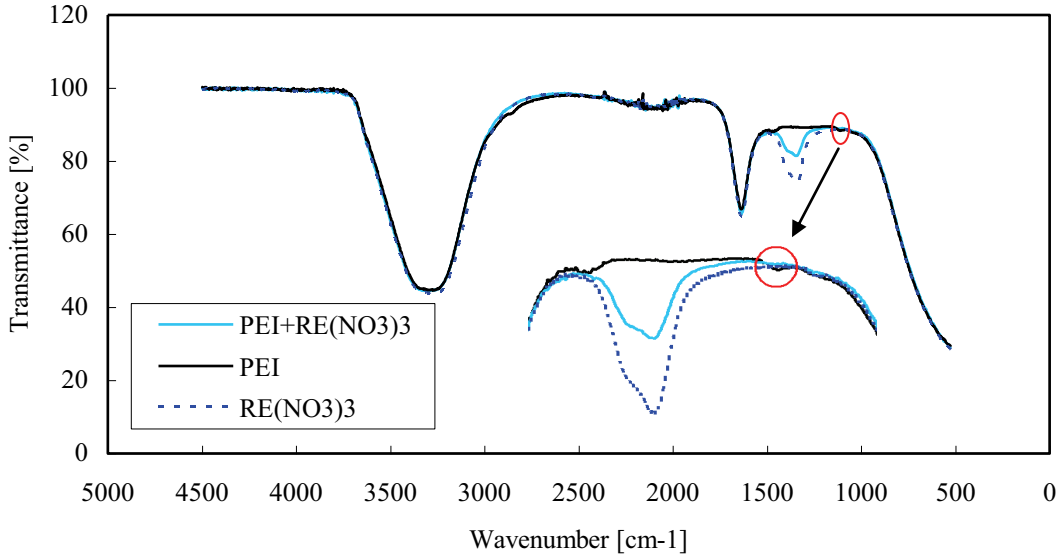

Figure 3.1.3 IR chart of non-acidified PEI and $RE(NO_3)_3$

and enlargement in the range of 1500 - 1000 cm^{-1}

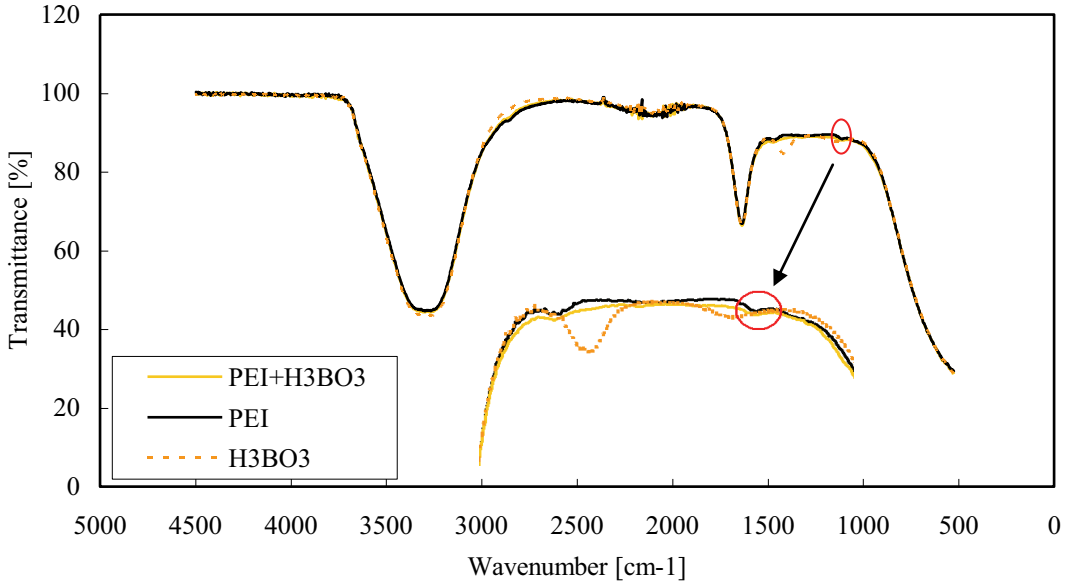

Figure 3.1.4 IR chart of non-acidified PEI and H_3BO_3

and enlargement in the range of 1500 - 1000 cm^{-1}

Thus, 1 g/L non-acidified PEI is the most suitable for reaction field to synthesize mono-dispersed YBO_3 microcrystals among investigated conditions. However, low luminance and low yield had better be improved. Low luminance is ascribed not only to addition order of raw materials but also to remaining PEI inside of crystals; PEI attached on crystal surface are removed during firing, however, PEI taken in crystals can remain after firing and can decrease luminance by preventing energy transfer. Low yield results from mildly-acidic final pH in which solubility of YBO_3 is relatively high. Yield of YBO_3 can be improved by raising final pH to around 8.5, the most suitable pH to synthesize YBO_3 in relatively high yield without by-products.

(b) 10 g/L non-acidified PEI

When using 10 g/L non-acidified PEI, $YB(OH)_4CO_3$ crystals were formed before firing similarly to the case using 1 g/L non-acidified PEI. However, formed crystals were not uniform but mixture of coarse crystals and aggregated microcrystals both before firing and after firing (Fig. 3.1.5). This is because thick PEI interacts with itself by its intermolecular attractive force and suppressing effect on crystal growth and crystal aggregation does not work well. In addition, product after firing was a mixture of YBO_3, Y_3BO_6 and Y_2O_3, showing low luminance and bad chromaticity. This is because reaction system is kept strong basic condition for a long time, and in such a condition RE^{3+} is likely to react not with BO_3^{3-} but with OH^-. Moreover, filtration time was extremely prolonged. This is because thick PEI increased water content of precursor as well as thick PEI blocked filter pore. From these reasons, 10 g/L non-acidified PEI is unsuitable for reaction field. These results show non-acidified PEI is favorable for reaction field to synthesize mono-dispersed YBO_3 microcrystals, however, appropriate concentration of non-acidified PEI exists.

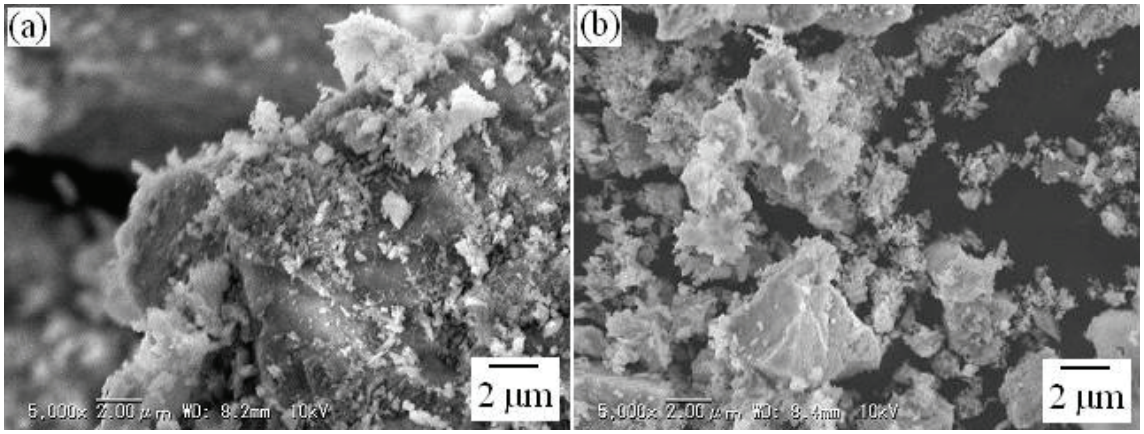

Figure 3.1.5 SEM images of crystals synthesized with 10 g/L non-acidified PEI

(a) before firing (b) after firing

(c) 1 g/L and 10 g/L acidified PEI

Acidified PEI is promising reaction field in reaction crystallization of $(Y,Gd)BO_3:Eu^{3+}$ because it has provided remarkable results on synthesis of mono-dispersed poorly-soluble sulfates microcrystals [1, 2, 3]. In the case using 1 g/L acidified PEI and 10 g/L acidified PEI, pure YBO_3 showing high luminance and good chromaticity was formed. This is because formation of by-products Y_2O_3 resulting from direct reaction between RE^{3+} and OH^- is prevented in acidic condition. Therefore, high luminance and good chromaticity were led by not the presence of PEI but appropriate pH history. Although luminance and chromaticity were improved when using acidified PEI, precursor was coarse and aggregated amorphous similarly to the case without polyelectrolyte. YBO_3 crystals formed after firing were relatively uniform but aggregated (Fig. 3.1.6, 3.1.7). These results mean that acidified PEI is ineffective to prevent aggregation in YBO_3 system. In addition, when using 10 g/L acidified PEI, filtration time was extremely prolonged similarly to the case using 10 g/L non-acidified PEI.

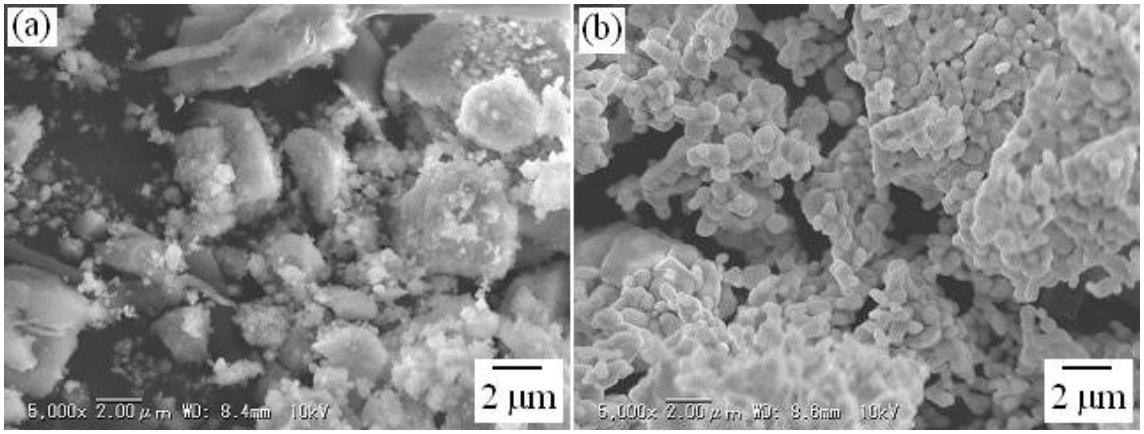

Figure 3.1.6 SEM images of crystals synthesized with 1 g/L acidified PEI

(a) before firing (b) after firing

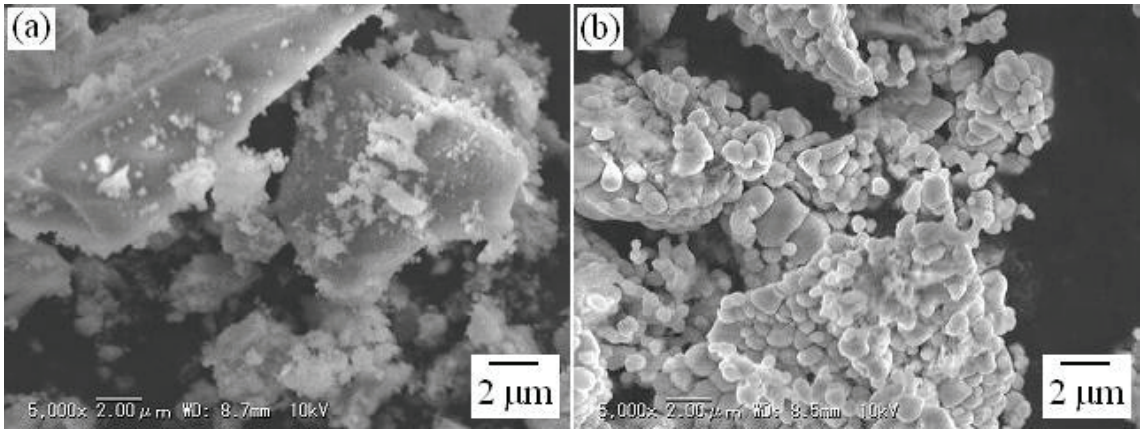

Figure 3.1.7 SEM images of crystals synthesized with 10 g/L acidified PEI

(a) before firing (b) after firing

Interaction between N atoms in PEI and RE^{3+} when using acidified PEI was investigated in the same way to the conditions using non-acidified PEI. However, IR absorbance around 1140 cm^{-1} corresponding to C-N bond of amine in PEI disappeared when PEI was acidified by HNO_3 (Fig. 3.1.8). Moreover, IR absorbance originating from PEI unchanged when $RE(NO_3)_3$ was added to PEI. This result indicates acidified PEI does not interact with RE^{3+}.

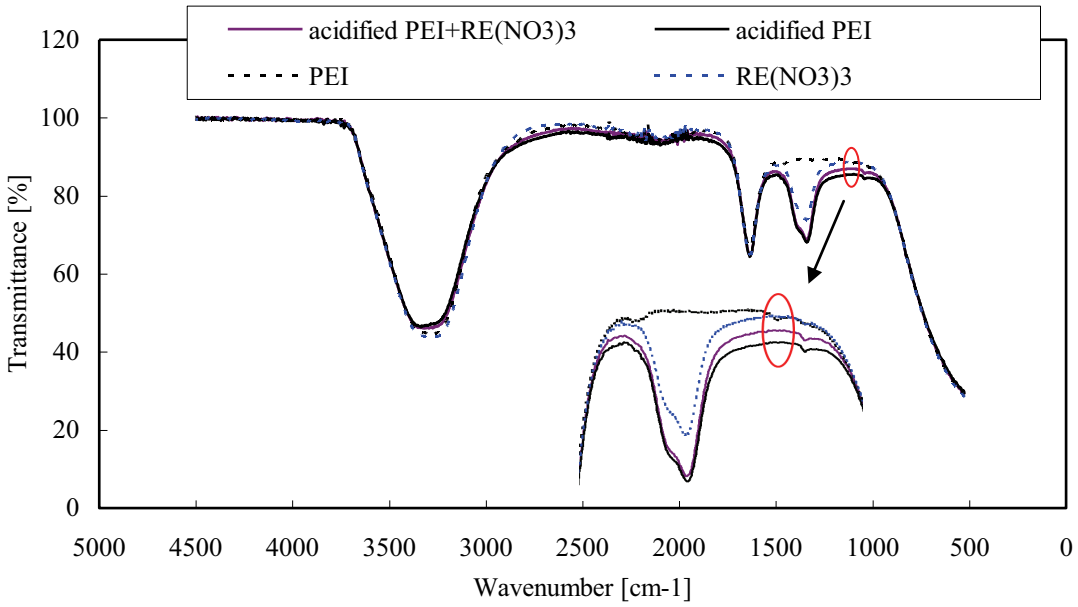

Figure 3.1.8 IR chart on acidified PEI and *RE*$(NO_3)_3$

and enlargement in the range of 1600 - 900 cm^{-1}

The reasons acidified PEI is ineffective for YBO_3 while it is effective for poorly-soluble sulfates containing Sr, Ba or Pb in previous studies are supposed to be as follows. Direct reaction between metal ions and non-acidified PEI immediately forms hydroxide precipitation. Although target materials will form by continuous stirring, it will take a long time to exchange OH^- for target anion and forming crystals will be mixture of target compound and hydroxide with non-uniform shape and non-uniform size. However, acidified PEI prevents direct reaction between metal ions and unshared electron pairs on N atoms in PEI by blocking unshared electron pairs through formation of coordination bond between N atoms in PEI and H^+, and as a result, incorporation of hydroxide will be prevented. Above mechanisms are common regardless of metal ions, however, suppressing effect of acidified PEI on crystal growth and crystal aggregation works only for target materials containing relatively heavy metal ions such as Sr, Ba and Pb. In such cases, displacement reaction between H^+ and metal ions occurs due to attractive force between metal ions and N atoms

in PEI to form coordination bond. Although unshared electron pairs on N atoms are masked by H^+, large difference of electronegativity between N atoms and relatively heavy metals drives this reaction. Through this displacement reaction, crystal nucleation of poorly-soluble sulfates will proceed mildly on N atoms in PEI, and crystal overgrowth and crystal aggregation will be prevented by steric hindrance of PEI chains. As a result, mono-dispersed microcrystals of target materials free from aggregation will be properly synthesized. On the other hand, relatively light metal ions like rare earth ions cannot displace H^+ on N atom in acidified PEI due to weakness of coordination bond between PEI and metal ions and high stability of metal ions resulting from high solubility of target materials in acidic conditions. As a result, crystallization will occur everywhere similarly to the case without PEI reaction field and aggregated crystals will be formed though uniformity of crystal shape and crystal size may be slightly improved by steric hindrance of PEI chains. From above mechanisms, acidified PEI is ineffective for YBO_3.

(d) 1 g/L PAA

When using 1 g/L PAA, white particle assumed to be PAA salt or micro amount of YBO_3 precipitated in acidic condition. This result suggests precipitation cannot be controlled by pH adjustment when using PAA. Moreover, PAA gelated and precipitated in basic condition. This result means PAA is deactivated in basic condition. Furthermore, crystal shape, crystal size and aggregation were not improved (Fig. 3.1.9) compared with the case polyelectrolyte reaction field was not used (Fig. 3.1.10). From these reasons, 1 g/L PAA is clearly unsuitable for reaction field.

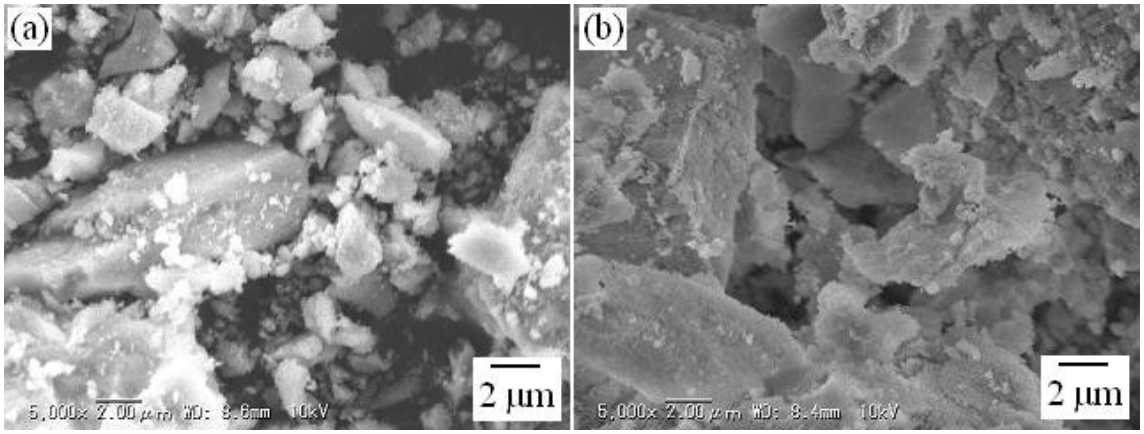

Figure 3.1.9 SEM images of crystals synthesized with 1 g/L PAA

(a) before firing (b) after firing

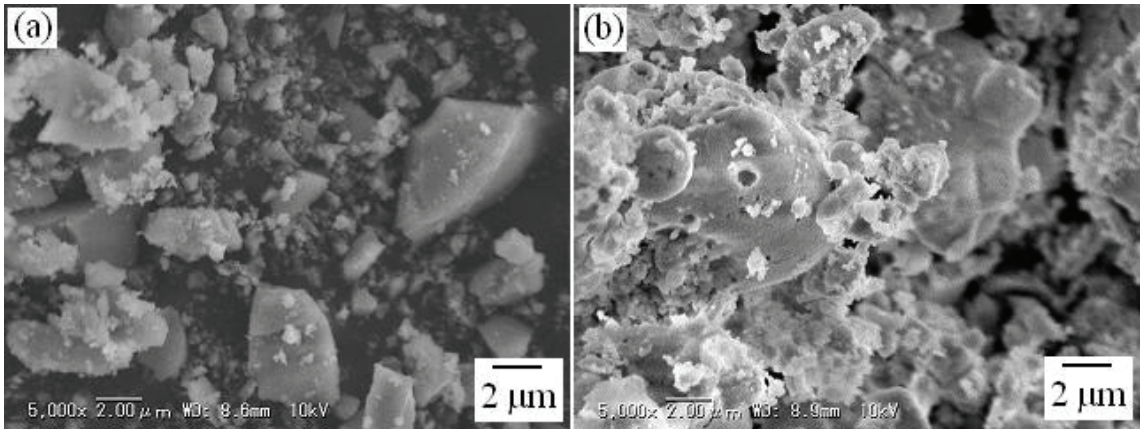

Figure 3.1.10 SEM images of crystals synthesized without polyelectrolyte

(a) before firing (b) after firing

3.1.4 Conclusions

1 g/L non-acidified PEI reaction field enables to form uniform $YB(OH)_4CO_3$ crystal precursor through its pH history changing from weakly-basic condition to weakly-acidic condition. Moreover, 1 g/L non-acidified PEI shows obvious suppressing effect on crystal growth and crystal aggregation not only during reaction crystallization but also during firing; 1 g/L non-acidified PEI prevents nuclei aggregation by forming coordination bond between unshared electron pairs on N atoms in PEI

and RE^{3+}, prevents overgrowth of crystals by its steric hindrance, and prevents adhesion and aggregation of crystals during firing by protecting crystal surface. On the other hand, suppressing effect of 10 g/L non-acidified PEI on crystal growth and crystal aggregation is insufficient because of self-interaction of thick PEI. In addition, acidified PEI shows no suppressing effect on crystal growth and crystal aggregation contrary to the cases synthesizing mono-dispersed microcrystals of poorly-soluble sulfates. Therefore, suitable concentration range and suitable pH range on PEI reaction field exist according to target materials.

3.2 Identification of formation condition of $YB(OH)_4CO_3$ crystal precursor

3.2.1 Introduction

When using non-acidified PEI as reaction field, $YB(OH)_4CO_3$ crystal precursor formed nevertheless CO_3^{2-} source was not added. Four possible reasons $YB(OH)_4CO_3$ crystal precursor formed in non-acidified PEI reaction field are as follows: 1. CO_2, necessary as raw materials to form $YB(OH)_4CO_3$, was dissolved massively from air because reaction was started from basic state. 2. PEI showing basicity reacted with RE^{3+} before reacting with H_3BO_3 due to adding order of raw materials, which promotes to form crystal precursor. 3. Final pH was slightly acidic state (pH 5-6), which offers appropriate supersaturation to form $YB(OH)_4CO_3$ crystal precursor. 4. Precursor suspension was stirred for sufficiently long time (1 day) after reaching to final pH. Among these reasons, long stirring time is assumed to be necessary to form crystal precursor showing high crystallinity by dissolving CO_2 massively from air and reacting dissolved CO_2 with raw materials sufficiently. In this research, the condition to form $YB(OH)_4CO_3$ crystal precursor was tried to be clarified. YBO_3 precursor was synthesized in various conditions changing addition order of raw materials, final pH and volume of water solvent.

3.2.2 Experimental procedure

Applied materials and experimental conditions are shown in Table 3.2.1 and Table 3.2.2, respectively. 100 mL of 0.3 mol/L $RE(NO_3)_3$ solution and 100 mL of 0.3 mol/L H_3BO_3 solution were used as raw materials, and 28% NH_3 was used as pH adjuster. Reaction crystallization was carried out in a batch reactor at room temperature.

Table 3.2.1 Materials

Reagent	Grade	Purity [%]	Production company
H_3BO_3	special	99.5	Kanto Chemical Co. Inc
$Y(NO_3)_3 \cdot 6H_2O$	high purity	99.99	Kanto Chemical Co. Inc
$Gd(NO_3)_3 \cdot 6H_2O$	high purity	99.95	Kanto Chemical Co. Inc
$Eu(NO_3)_3 \cdot 6H_2O$	—	99.9	Shin-Etsu Chemical Co., Ltd.
NH_3	special	28.0-30.0	Kanto Chemical Co. Inc
N_2	—	—	Kotobuki Sangyo Co., Ltd.
$(Y,Gd)BO_3:Eu^{3+}$	NP-360-03	—	Nichia Corporation

N_2 is applied as pressurization gas for pressure filtration.

$(Y,Gd)BO_3:Eu^{3+}$ (NP-360-03) is commercial red phosphor synthesized by solid-state reaction, and is used as reference to calculate relative luminance and relative chromaticity.

Table 3.2.2 Experimental conditions

No.		Deionized water [mL]	NH_3 (28%) [mL]	Raw materials added in first	pH Initial [-]	pH Final [-]
1		100	20	*RE* $(NO_3)_3$+H_3BO_3	3.65	9.55
2	basic	100	20	NH_3	10.93	8.38
3	conditions	100	20	NH_3+H_3BO_3	10.2	9.34
4		100	20	NH_3+*RE* $(NO_3)_3$	9.34	9.01
5		100	2.5	*RE* $(NO_3)_3$+H_3BO_3	3.87	6.13
6	mildly-acidic	100	2.5	NH_3	12.46	6.8
7	conditions	100	2.5	NH_3+H_3BO_3	10.29	6.83
8		100	2.5	NH_3+*RE* $(NO_3)_3$	7.03	6.07
9	mildly-acidic	500	2.5	*RE* $(NO_3)_3$+H_3BO_3	4.32	6.84
10	conditions	500	2.5	NH_3	11.05	6.55
11	(diluted)	500	2.5	NH_3+H_3BO_3	9.07	6.5
12		500	2.5	NH_3+*RE* $(NO_3)_3$	6.8	6.43

Synthesis procedure is shown in Fig. 3.2.1. Raw materials were added to pure water according to predetermined order and stirred for predetermined time. Precursor was separated from suspension by pressured filtration, and dried in oven at 150℃ for 24 hours. Dried precursor was ground in mortar and fired at 1000℃ for 6 hours.

Crystal shape and crystal size were observed by SEM (VE-8800, KEYENCE), and composition and crystallinity were examined by XRD (Rint-UltimaⅢ, Rigaku) on synthesized samples before firing and after firing. In addition, luminance and chromaticity on samples after firing were determined by luminance and color meter (CS-200, Konica Minolta).

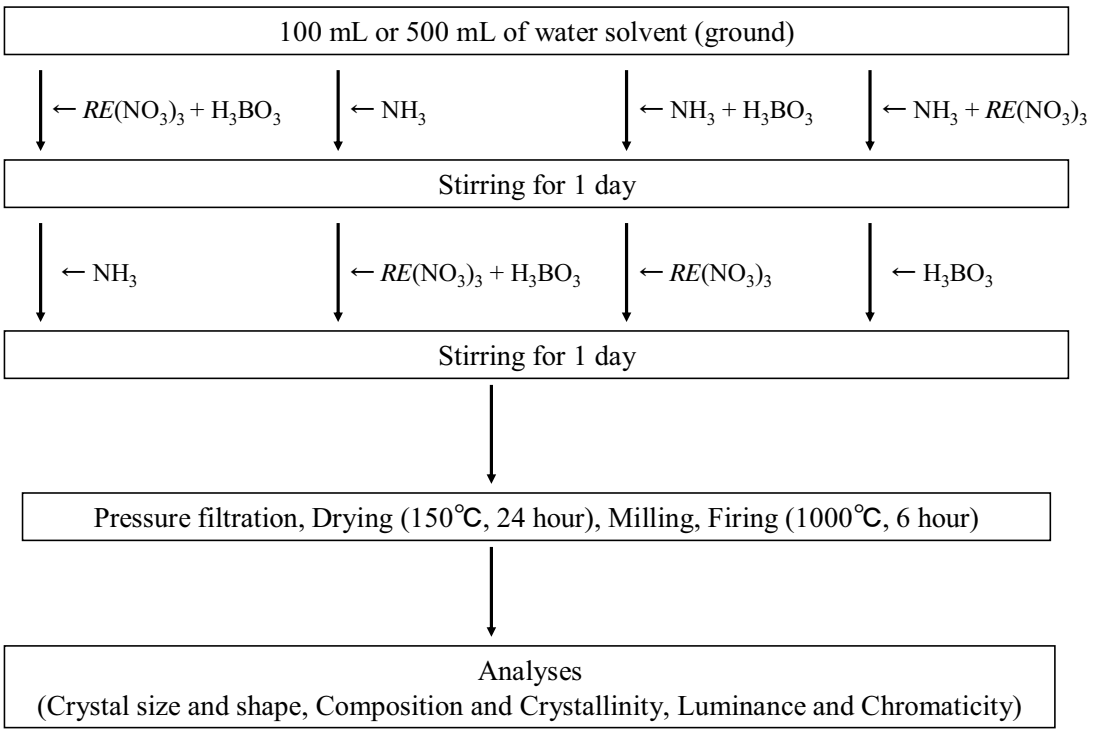

Figure 3.2.1 Synthesis procedure

3.2.3 Results and discussions

Experimental results before firing and after firing are shown in Table 3.2.3 and Table 3.2.4, respectively.

Table 3.2.3 Experimental results (before firing)

	Raw materials added in first	Crystal shape and crystal size Shape	Size [μm]	Precursor Type	Crystallinity [cps]
basic conditions	*RE* $(NO_3)_3$ H_3BO_3	coarse crystals and microcrystals	0.05-20	amorphous	348
	NH_3	coarse crystals and microcrystals	0.05-40	amorphous	367
	NH_3 H_3BO_3	coarse crystals and microcrystals	0.05-40	amorphous	380
	NH_3 *RE* $(NO_3)_3$	coarse crystals and microcrystals	0.05-70	amorphous	383
mildly-acidic conditions	*RE* $(NO_3)_3$ H_3BO_3	coarse crystals and aggregated microcrystals	0.1-10	amorphous	348
	NH_3	coarse crystals and microcrystals	0.1-50	amorphous	328
	NH_3 H_3BO_3	coarse crystals and microcrystals	0.05-50	amorphous	356
	NH_3 *RE* $(NO_3)_3$	coarse crystals and microcrystals	0.05-30	$Y_2(OH)_{5.14}(NO_3)_{0.86}\cdot H_2O$	1023
mildly-acidic conditions (diluted)	*RE* $(NO_3)_3$ H_3BO_3	coarse crystals and microcrystals	0.1-80	$YB(OH)_4CO_3$	711
	NH_3	coarse crystals and aggregated microcrystals	0.1-60	$YB(OH)_4CO_3$	1615
	NH_3 H_3BO_3	coarse crystals and aggregated microcrystals	0.1-30	$YB(OH)_4CO_3$	1228
	NH_3 *RE* $(NO_3)_3$	coarse crystals and aggregated microcrystals	0.05-80	$Y_2(OH)_{5.14}(NO_3)_{0.86}\cdot H_2O$ $YB(OH)_4CO_3$	1057

Table 3.2.4 Experimental results (after firing)

	Raw materials added in first	Crystal shape and crystal size Shape	Size [μm]	Crystallinity YBO_3 [cps]	Y_3BO_6 [cps]	Y_2O_3 [cps]	Relative luminance [%]	Relative chromaticity [%]
basic conditions	*RE* $(NO_3)_3$ H_3BO_3	aggregated microcrystals and porous crystals	0.1-50	2347	275	0	81.3	91.5
	NH_3	aggregated microcrystals and porous crystals	0.1-70	2583	277	0	85.7	94.2
	NH_3 H_3BO_3	aggregated microcrystals and porous crystals	0.1-50	1985	319	0	68.4	91.6
	NH_3 *RE* $(NO_3)_3$	aggregated microcrystals and porous crystals	0.1-50	1702	435	0	62.2	94
mildly-acidic conditions	*RE* $(NO_3)_3$ H_3BO_3	microcrystals	0.3-10	2651	0	0	80.2	98.7
	NH_3	aggregated microcrystals	0.1-3	3188	274	0	66.7	98.1
	NH_3 H_3BO_3	aggregated microcrystals	0.1-10	2603	0	0	81.3	97.7
	NH_3 *RE* $(NO_3)_3$	coarse crystals and aggregated microcrystals	0.1-50	308	507	2417	27.4	110.1
mildly-acidic conditions (diluted)	*RE* $(NO_3)_3$ H_3BO_3	aggregated microcrystals	0.1-10	4236	0	0	80.2	97.8
	NH_3	aggregated microcrystals	0.2-5	3653	358	0	82.6	103.3
	NH_3 H_3BO_3	aggregated microcrystals	0.1-10	3489	0	0	89.4	103
	NH_3 *RE* $(NO_3)_3$	coarse crystals and aggregated microcrystals	0.05-60	553	869	2775	15.4	85.9

The results were examined by classifying into following two cases according to final pH: (a) maintaining basic conditions through reaction crystallization and (b) final pH was adjusted to mildly-acidic conditions. In the latter case, diluted condition was also discussed.

(a) In the cases maintaining basic conditions

In the cases maintaining basic conditions through reaction crystallization, amorphous precursor was formed in all conditions regardless of addition order of raw materials. However, porous crystals were incorporated after firing (Fig. 3.2.2). This result suggests that precursor contains dissolved CO_2 molecules and releases them during firing though $YB(OH)_4CO_3$ is not

formed before firing. The mechanisms why $YB(OH)_4CO_3$ is not formed in these cases are assumed to be as follows. In basic conditions, plenty of CO_2 molecules are dissolved into precursor slurry and they are taken in precursor precipitation. However, because of low solubility of YBO_3 precursor in basic condition, nucleation and growth of YBO_3 precursor proceed too rapidly to form $YB(OH)_4CO_3$ crystal structure. As a result, amorphous precursor will be formed in all cases maintaining basic conditions.

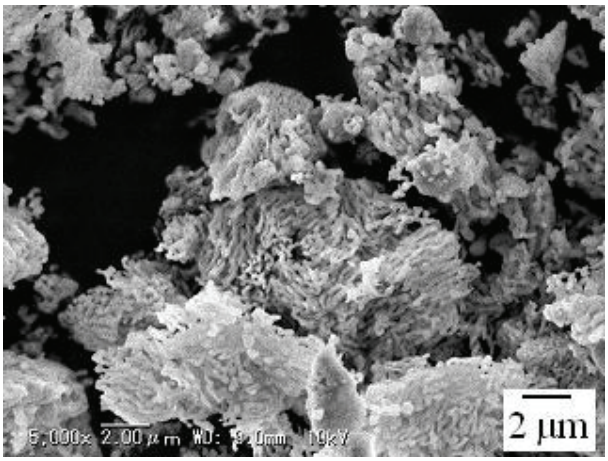

Figure 3.2.2 Examples of porous crystals formed after firing

(b) In the cases final pH was adjusted to mildly-acidic conditions

In the cases final pH was adjusted to mildly-acidic conditions, amorphous precursor was formed regardless of addition order of raw materials when using 100 mL of water solvent. However, $YB(OH)_4CO_3$ crystal precursor was formed when using 500 mL of water solvent. These results indicate that two requirements other than long stirring time are needed to form $YB(OH)_4CO_3$ crystal precursor: final pH is sufficiently low (about 6) and volume of water solvent is sufficiently large (dilute condition).

The procedure to satisfy requirements to form $YB(OH)_4CO_3$ crystal precursor is assumed to be

as follows. In mildly-acidic conditions, reaction of forming YBO_3 precursor proceeds mildly because solubility of YBO_3 precursor is relatively high. However, solubility of CO_2 and abundance of CO_3^{2-} in precursor slurry are too low to form $YB(OH)_4CO_3$ crystal precursor. When starting from basic conditions, CO_2 is sufficiently dissolved in precursor slurry while the system is maintained in basic conditions. However, in the cases the volume of solvent water is small, amorphous precursor forms due to rapid reaction rate caused by high supersaturation. Therefore, the volume of solvent water must be increased to form $YB(OH)_4CO_3$ crystal precursor. By increasing the volume of water solvent, solubility of CO_2 and abundance of CO_3^{2-} in precursor increase even in the cases starting from acidic conditions. In addition, suspension density or concentrations of raw materials, in other words, supersaturation of YBO_3 precursor decreases by increasing the volume of water solvent. This is important especially in the cases starting from basic conditions in which solubility of YBO_3 precursor is low. As a result, reaction of forming YBO_3 precursor will proceed mildly with enough CO_3^{2-} to form $YB(OH)_4CO_3$ crystal precursor.

When volume of water solvent was 500 mL, not only $YB(OH)_4CO_3$ crystal precursor was formed before firing but also pure YBO_3 showing high crystallinity and good chromaticity was formed after firing. Although crystallinity of $YB(OH)_4CO_3$ was relatively low in synthesis from acidic condition, it will be able to be improved by increasing of abundance of CO_3^{2-} by injecting CO_2 gas. However, in the cases $RE(NO_3)_3$ and NH_3 can react in first, crystal precursor assumed to be basic nitrate ($Y_2(OH)_{5.14}(NO_3)_{0.86}\cdot H_2O$) was incorporated before firing, and Y_2O_3 showing low luminance was formed as main product after firing. This result means the conditions $RE(NO_3)_3$ and NH_3 can react directly should be avoided to form $YB(OH)_4CO_3$ crystal precursor and pure YBO_3. In terms of purity and chromaticity of YBO_3 after firing, the condition NH_3 and H_3BO_3 are added in first to 500 mL of water solvent is the most appropriate procedure to synthesize $YB(OH)_4CO_3$ crystal precursor.

$YB(OH)_4CO_3$ crystal precursor was formed when following three requirements were satisfied: long stirring time, low final pH and large volume of water solvent. However, formed $YB(OH)_4CO_3$ crystal precursor showed non-uniform shape and non-uniform size, and partly aggregated. These non-uniformity of shape and size, and aggregation were not improved after $YB(OH)_4CO_3$ was changed into YBO_3 by firing (Fig. 3.2.3). These results indicate some strategies such as PEI reaction field are necessary to improve crystal shape and crystal size, and to prevent aggregation. In addition, low yield of YBO_3 resulting from low final pH had better be improved.

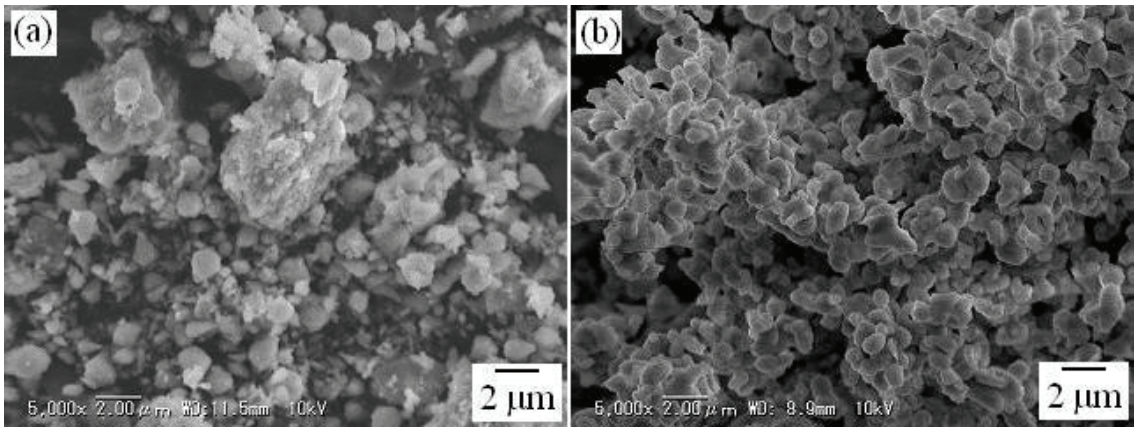

Figure 3.2.3 Examples of aggregated crystals with non-uniform shape and size

(a) before firing ($YB(OH)_4CO_3$ crystal precursor) (b) after firing

Although crystal shape, crystal size, aggregation and yield must be improved, this result is remarkable with respects that $YB(OH)_4CO_3$ crystal precursor and pure YBO_3 can be formed without adding another reagent. This result is meaningful as an example that target materials likely to form as amorphous can be obtained as crystals with relatively-high purity. This synthesis method will be applicable to other systems intended to synthesize target materials without additives or to crystallize target materials usually formed as amorphous.

3.2.4 Conclusions

$YB(OH)_4CO_3$ crystal precursor forms without adding CO_3^{2-} source when following three requirements are satisfied: long stirring time (1 day), low final pH (about 6) and large volume of water solvent (dilute condition). In addition, when $YB(OH)_4CO_3$ crystal precursor is synthesized in mildly-acidic condition, pure YBO_3 showing high crystallinity and good chromaticity is formed after firing unless $RE(NO_3)_3$ and pH adjuster react directly. However, $YB(OH)_4CO_3$ precursor and YBO_3 after firing shows non-uniform shape and non-uniform size, and partly aggregates. This suggests importance of PEI reaction field to improve crystal shape and crystal size, and to prevent aggregation.

3.3 Synthesis of $YB(OH)_4CO_3$ crystal precursor using Na_2CO_3 pH adjuster

3.3.1 Introduction

The major cause of formation of mono-dispersed YBO_3 microcrystals when using 1 g/L non-acidified PEI may be formation of $YB(OH)_4CO_3$ spherical microcrystals before firing rather than effects of PEI such as prevention of crystal aggregation and crystal overgrowth during reaction crystallization and during firing. Formation of mono-dispersed $YB(OH)_4CO_3$ microcrystals as precursor without PEI reaction field will shorten reaction time and will simplify synthesis procedure. Confirming reaction condition to form crystal precursor certainly will enable us to control crystal size and crystal shape more easily not only in reaction crystallization but also in following processes. Such improvements of synthesis procedure will contribute to various materials likely to form as amorphous, not just for YBO_3 precursor.

It has been proved that $YB(OH)_4CO_3$ crystal precursor forms without PEI reaction field and without adding CO_3^{2-} source when following three requirements are satisfied: long stirring time (1 day), low final pH (about 6) and large volume of water solvent (dilute condition). However, both

$YB(OH)_4CO_3$ precursor and YBO_3 after firing showed non-uniform shape and non-uniform size, and aggregated. In addition, yield of YBO_3 was low because of reaction at low pH.

Without such complicated requirements, $YB(OH)_4CO_3$ crystal precursor may be formed more easily and more certainly by adding CO_3^{2-} source. In addition, yield of YBO_3 may be improved by raising final pH in the presence of CO_3^{2-} source.

In this research, Na_2CO_3 was newly applied as pH adjuster to form $YB(OH)_4CO_3$ crystal precursor successfully by CO_3^{2-} contained in Na_2CO_3. Additive amount of Na_2CO_3 was standardized on molar ratio of B atom to C atom: B : C = 1 : 1. Concentration and amount of raw material H_3BO_3 were 0.3 mol/L and 100 mL, respectively. Therefore, concentration and amount of pH adjuster Na_2CO_3 were standardized on 3 mol/L and 10 mL, respectively. Additive amount of Na_2CO_3 was changed as 5, 10, 15, 20 mL. Reaction time was 20 min or 1 day. In some conditions, 28% NH_3 was also used as pH adjuster with Na_2CO_3 to improve yield by raising final pH to about 8.5.

3.3.2 Experimental procedure

Applied materials and experimental conditions are shown in Table 3.3.1 and Table 3.3.2, respectively. 0.3 mol/L $RE(NO_3)_3$ and 0.3 mol/L H_3BO_3 solution were used as raw materials. 3 mol/L Na_2CO_3 and 28% NH_3 were used as pH adjuster. Reaction crystallization was carried out in a batch reactor at room temperature.

Table 3.3.1 Materials

Reagent	Grade	Purity [%]	Production company
H_3BO_3	special	99.5	Kanto Chemical Co. Inc
$Y(NO_3)_3 \cdot 6H_2O$	high purity	99.99	Kanto Chemical Co. Inc
$Gd(NO_3)_3 \cdot 6H_2O$	high purity	99.95	Kanto Chemical Co. Inc
$Eu(NO_3)_3 \cdot 6H_2O$	—	99.9	Shin-Etsu Chemical Co., Ltd.
Na_2CO_3	special	99.8	Wako Pure Chemical Industries, Ltd.
NH_3	special	28.0-30.0	Kanto Chemical Co. Inc
N_2	—	—	Kotobuki Sangyo Co., Ltd.
$(Y,Gd)BO_3:Eu^{3+}$	NP-360-03	—	Nichia Corporation

N_2 is applied as pressurization gas for pressure filtration.

$(Y,Gd)BO_3:Eu^{3+}$ (NP-360-03) is commercial red phosphor synthesized by solid-state reaction, and is used as reference to calculate relative luminance and relative chromaticity.

Table 3.3.2 Experimental conditions

pH adjuster Type	Volume [mL]	Final pH [-]	Stirring time	pH adjuster Type	Volume [mL]	Final pH [-]	Stirring time	pH adjuster Type	Volume [mL]	Final pH [-]	Stirring time
Na_2CO_3	5	5.22	20 min	Na_2CO_3 NH_3	5 5.5	9.05	20 min				
Na_2CO_3	10	5.25	20 min	Na_2CO_3 NH_3	10 3.5	9.03	20 min				
Na_2CO_3	15	6.08	20 min	Na_2CO_3 NH_3	15 2	9.07	20 min				
Na_2CO_3	20	8.38	20 min	Na_2CO_3 NH_3	20 1	9.33	20 min				
Na_2CO_3	5	4.84	1 day	Na_2CO_3 NH_3	5 5.5	8.46	1 day	Na_2CO_3 NH_3	5 5.5	8.55	1 day 20 min
Na_2CO_3	10	5.21	1 day	Na_2CO_3 NH_3	10 3.5	8.61	1 day	Na_2CO_3 NH_3	10 3.5	8.81	1 day 20 min
Na_2CO_3	15	7.84	1 day	Na_2CO_3 NH_3	15 2	8.67	1 day	Na_2CO_3 NH_3	15 0.6	9.1	1 day 20 min
Na_2CO_3	20	8.41	1 day	Na_2CO_3 NH_3	20 1	8.64	1 day	Na_2CO_3 NH_3	20 0.2	8.5	1 day 20 min

Synthesis procedure is shown in Fig. 3.3.1. Raw materials, 100 mL of $RE(NO_3)_3$ and 100 mL of H_3BO_3, and predetermined volume of Na_2CO_3 were added to 100 mL of pure water and stirred for predetermined time. In the conditions NH_3 was combined with Na_2CO_3, NH_3 was added simultaneously with Na_2CO_3 or added after Na_2CO_3. Precipitate was separated from precursor slurry

by pressured filtration, and dried in oven at 150℃ for 24 hours. Dried precursor was ground in mortar and fired at 1000℃ for 6 hours.

Crystal shape and crystal size were observed by SEM (VE-8800, KEYENCE), and composition and crystallinity were examined by XRD (Rint-UltimaⅢ, Rigaku) on synthesized samples before firing and after firing. In addition, luminance and chromaticity on samples after firing were determined by luminance and color meter (CS-200, Konica Minolta).

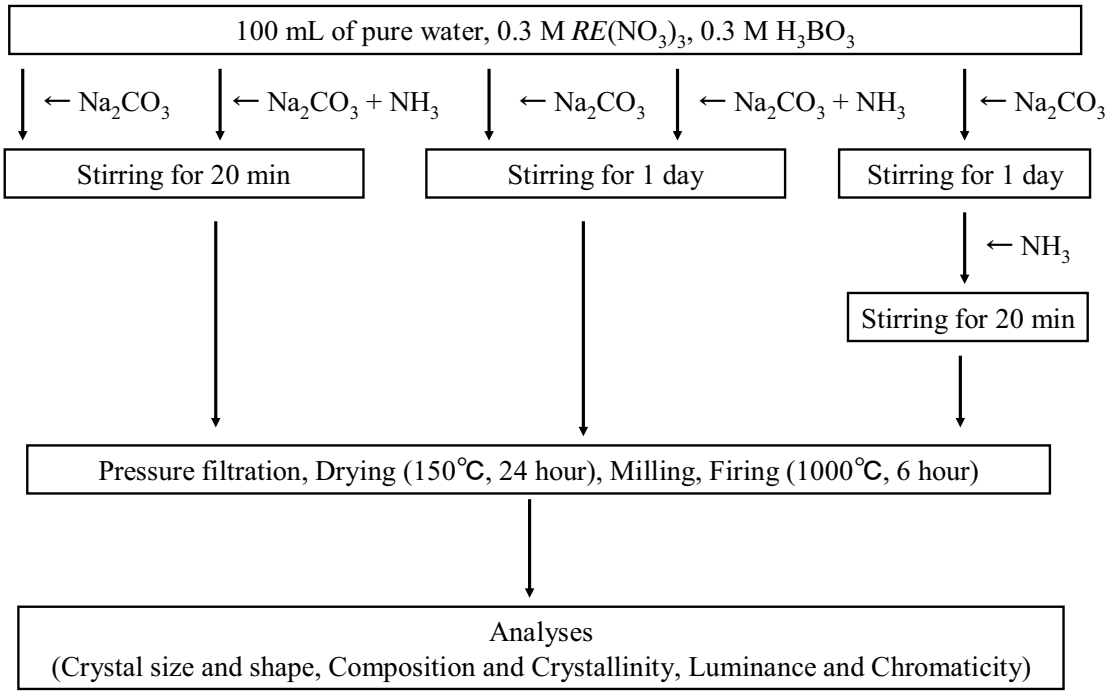

Figure 3.3.1 Synthesis procedure

3.3.3 Results and discussions

3.3.3.1 General results

(a) pH history and yield

When Na_2CO_3 only was used as pH adjuster, precursor started to precipitate around pH 5, and did not dissolve again once pH reached to buffering area: pH 5.1-5.6. Although precursor started to precipitate at mildly-acidic condition around pH 5 when using NH_3 only, precursor slurry was clearly dilute and dissolved again by continuous stirring at the same pH. This result indicates that Na_2CO_3 makes precursor start and finish precipitating at lower pH than the cases using NH_3. Although thick slurry was formed when using Na_2CO_3, yield of precursor remained low because of high solubility of YBO_3 precursor at low pH.

On the other hand, when combining NH_3 with Na_2CO_3, yield of precursor was improved in all conditions. In addition, pH change when adding NH_3 was different by additive timing of NH_3 in the cases additive amount of Na_2CO_3 was over 15 mL; pH increased rapidly by a few drop of NH_3 in the cases NH_3 was added after Na_2CO_3 stirred for 1 day, however, pH did not increase easily in the cases NH_3 was added simultaneously with Na_2CO_3. In the cases NH_3 was added simultaneously with Na_2CO_3, additive amount of NH_3 required to raise solution pH to 8.5 was two times as much as that in the cases NH_3 was added after Na_2CO_3 stirred for 1 day.

(b) Separation property

Filtration speed was greatly improved when using Na_2CO_3 only. It took more than 24 hours for pressure filtration of 300 mL precursor slurry when using NH_3 only, and in addition, it took further time when precursor was synthesized at lower pH around 7. On the other hand, it took about 1 hour for pressure filtration of 300 mL precursor slurry when using Na_2CO_3 only, and in addition, it took less time when stirring for 1 day: some minutes.

However, when NH_3 was combined with Na_2CO_3, filtration speed was fast only in the cases additive amount of Na_2CO_3 was over 15 mL. Filtration speeds of other cases were almost the same when using NH_3 only as pH adjuster. In other words, filtration speed was decreased when additive amount of Na_2CO_3 was decreased and additive amount of NH_3 was increased. At the same time, precursor changed from opaque white to translucent and hardened like the cases NH_3 only was used. These results are attributed to difference of water content in precursor, that is, Na_2CO_3 decreases water content in precursor and increases filtration speed, while NH_3 increases water content in precursor and decreases filtration speed.

(c) Precursor type

When using Na_2CO_3 as pH adjuster, $YB(OH)_4CO_3$ crystal precursor was formed in almost all conditions. This is because CO_3^{2-} exists from beginning of reaction incomparably greater than the conditions relying on CO_2 natural dissolution. Na_2CO_3 pH adjuster is very useful to improve flexibility of synthesis condition considering $YB(OH)_4CO_3$ crystal precursor is only formed in specific conditions when using NH_3 pH adjuster or using PEI reaction field.

(d) Density of precursor and product after firing

Precursor was further bulky only when using 20 mL of Na_2CO_3, however, this precursor shrank during firing and bonded to crucible. This phenomenon is ascribed to composition difference of product before and after firing changed by additive amount of Na_2CO_3.

In the cases NH_3 was combined with Na_2CO_3, density of precursor was also different by additive timing of NH_3; precursor became more bulky when Na_2CO_3 and NH_3 were simultaneously added. This phenomenon was remarkable in the cases additive amount of Na_2CO_3 was less than 10 mL.

(e) Another by-product: $Na_2Y_2B_2O_7$

Y_3BO_6 and Y_2O_3 are known as by-products in reaction crystallization of YBO_3. When using Na_2CO_3 as pH adjuster, another by-product assumed to be $Na_2Y_2B_2O_7$ was sometimes incorporated. An example of XRD chart of sample containing $Na_2Y_2B_2O_7$ and JCPDS of $Na_2Y_2B_2O_7$ (PDF#00-054-1118) are shown in Fig. 3.3.2. Influence of $Na_2Y_2B_2O_7$ on luminance and chromaticity has been uncertain, however, synthesis condition preventing incorporation of $Na_2Y_2B_2O_7$ will be desirable unless it improves luminance and/or chromaticity.

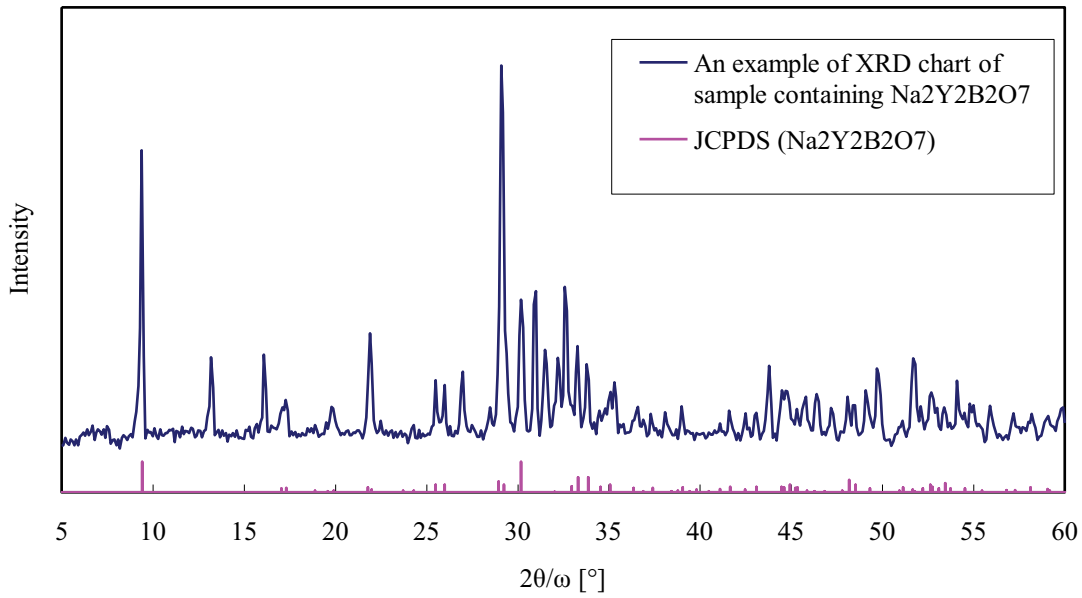

Figure 3.3.2 An example of XRD chart of sample containing $Na_2Y_2B_2O_7$ and JCPDS of $Na_2Y_2B_2O_7$ (PDF#00-054-1118)

3.3.3.2 Analysis of results classified by pH adjuster and stirring time

The results are examined by classifying into following four categories according to pH adjuster and stirring time: (a) Na_2CO_3 only, stirring for 20 min, (b) Na_2CO_3 and NH_3, stirring for 20 min, (c) Na_2CO_3 only, stirring for 1 day, and (d) Na_2CO_3 and NH_3, stirring for 1 day. In last category, following two cases were examined: the case Na_2CO_3 and NH_3 were added simultaneously and

stirred for 1 day, and the case NH_3 was added after Na_2CO_3 stirred for 1 day and stirred another 20 min.

(a) Na_2CO_3 only, stirring for 20 min

Experimental results in the cases Na_2CO_3 only was used and stirred for 20 min are shown in Table 3.3.3 and Table 3.3.4. SEM images of crystals before firing and after firing are shown in Fig. 3.3.3.

Table 3.3.3 Experimental results (crystal shape and crystal size)

pH adjuster Type	Volume [mL]	Final pH [-]	Stirring time	Before firing Shape	Size [μm]	After firing Shape	Size [μm]
Na_2CO_3	5	5.22	20 min	coarse crystals and aggregated microcrystals	0.05-60	aggregated microcrystals (partly coarse)	0.1-50
Na_2CO_3	10	5.25	20 min	coarse crystals and aggregated microcrystals	0.1-80	porous crystals and aggregated microcrystals	0.3-60
Na_2CO_3	15	6.08	20 min	coarse crystals and aggregated microcrystals	0.05-40	aggregated microcrystals	0.1-10
Na_2CO_3	20	8.38	20 min	plate-like coarse crystals and microcrystals	0.05-20	coarse crystals and aggregated microcrystals	0.1-40

Table 3.3.4 Experimental results (crystallinity, relative luminance and relative chromaticity)

pH adjuster Type	Volume [mL]	Final pH [-]	Stirring time	Crystallinity (before firing) [cps]	Crystallinity (after firing) YBO_3 [cps]	Y_3BO_6 [cps]	Y_2O_3 [cps]	$Na_2Y_2B_2O_7$ [cps]	Relative luminance [%]	Relative chromaticity [%]
Na_2CO_3	5	5.22	20 min	738	474	731	5478	0	65.1	156
Na_2CO_3	10	5.25	20 min	525	0	342	5298	423	72.5	186.6
Na_2CO_3	15	6.08	20 min	488	0	0	4769	456	82.1	158.3
Na_2CO_3	20	8.38	20 min	415	0	0	2382	0	3.6	25.1

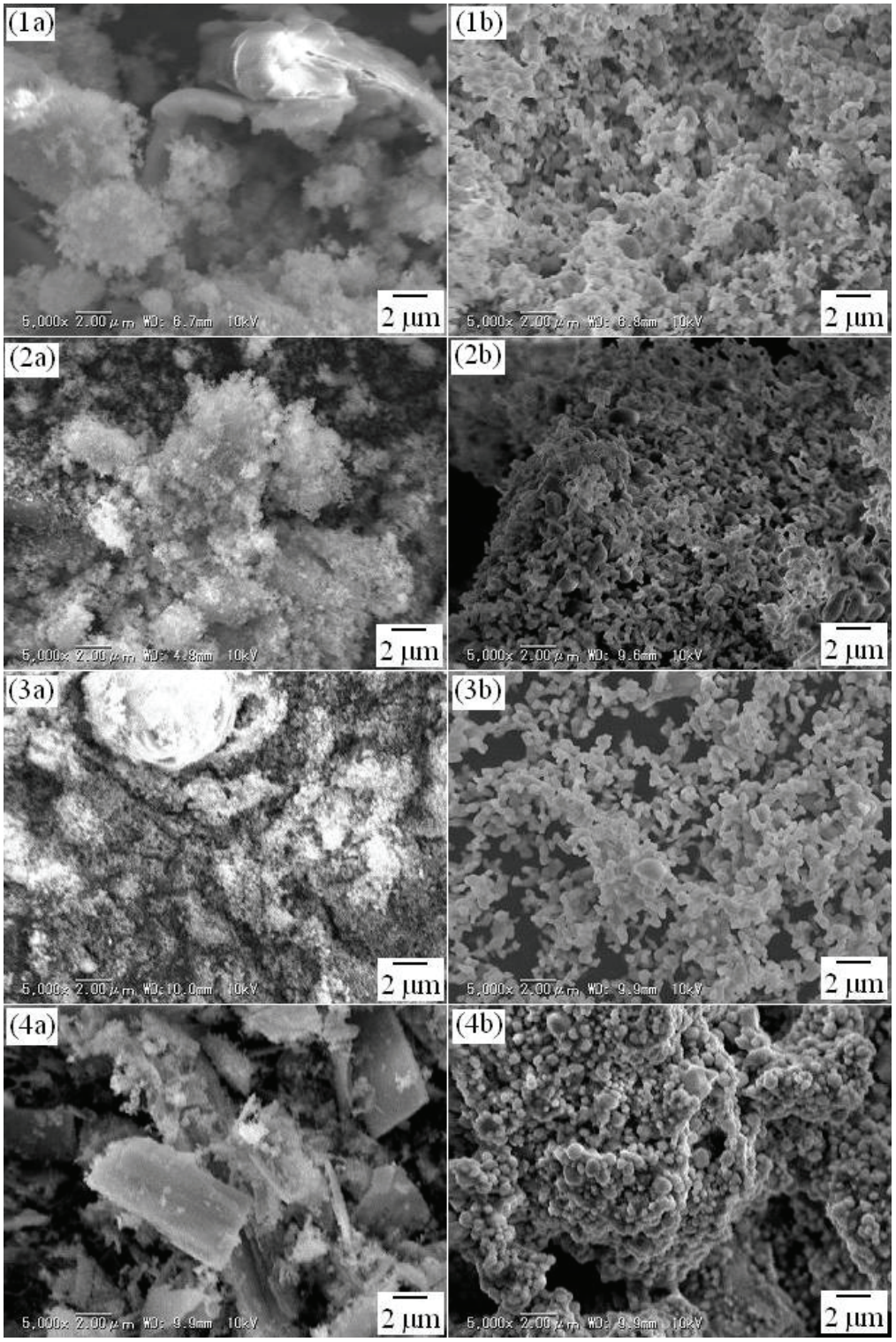

Figure 3.3.3 SEM images of crystals

Additive amount of Na_2CO_3 is (1) 5 mL, (2) 10 mL, (3) 15 mL, and (4) 20 mL.

(a) before firing (b) after firing

In the cases Na_2CO_3 was only used as pH adjuster and stirred for 20 min, $YB(OH)_4CO_3$ precursor composed of coarse crystals and aggregated microcrystals was formed regardless of additive amount of Na_2CO_3. Crystallinity of $YB(OH)_4CO_3$ decreased as additive amount of Na_2CO_3 increased. Main product after firing was Y_2O_3 comprised mainly of aggregated microcrystals. Amount of formed YBO_3 and Y_3BO_6 was very few, and decreased as additive amount of Na_2CO_3 increased. This result indicates CO_3^{2-} or OH^- is more likely to be taken in precursor than BO_3^{3-} at the beginning of reaction when using Na_2CO_3 as pH adjuster.

Maximum luminance of Y_2O_3, main product in these cases, is 2/3 of commercial YBO_3 at the best because Y_2O_3 does not have B atom helping energy transfer. On the other hand, chromaticity of Y_2O_3 is superior to YBO_3 because red luminescence is dominant contrary to YBO_3 which orange luminescence is dominant. In fact, chromaticity of these phosphors whose main product is Y_2O_3 was improved. Moreover, luminance of these phosphors was over 70% of commercial YBO_3 nevertheless main product was Y_2O_3. Luminance increased as additive amount of Na_2CO_3 increased, and reached to 82.1% when 15 mL of Na_2CO_3 was added, while good chromaticity of Y_2O_3 was maintained. This is assumed to be the result that energy transfer efficiency was improved by incorporating B atom slightly not to decrease chromaticity by forming of Y_3BO_6. This result suggests Y_2O_3 showing better luminance is able to be synthesized in the cases Na_2CO_3 is only used and stirred for 20 min. However, luminance and chromaticity was drastically decreased when additive amount of Na_2CO_3 reached to 20 mL. In addition, sticky paste-like crystals were formed in the case using 20 mL of Na_2CO_3, which indicates decrease of chemical resistance.

(b) Na_2CO_3 and NH_3, simultaneous addition, stirring for 20 min

Experimental results in the cases Na_2CO_3 and NH_3 were added simultaneously and stirred for 20 min are shown in Table 3.3.5 and Table 3.3.6. SEM images of crystals before firing and after

firing are shown in Fig. 3.3.4.

Table 3.3.5 Experimental results (crystal shape and crystal size)

pH adjuster Type	Volume [mL]	Final pH [-]	Stirring time	Before firing Shape	Size [μm]	After firing Shape	Size [μm]
Na_2CO_3	5	9.05	20 min	coarse crystals and aggregated microcrystals	0.05-70	aggregated microcrystals	0.2-15
NH_3	5.5						
Na_2CO_3	10	9.03	20 min	coarse crystals and aggregated microcrystals	0.05-30	aggregated microcrystals	0.1-10
NH_3	3.5						
Na_2CO_3	15	9.07	20 min	coarse crystals and aggregated microcrystals	0.05-30	aggregated microcrystals	0.1-30
NH_3	2						
Na_2CO_3	20	9.33	20 min	coarse crystals and aggregated microcrystals	0.1-50	coarse crystals and aggregated microcrystals	0.2-60
NH_3	1						

Table 3.3.6 Experimental results (crystallinity, relative luminance and relative chromaticity)

pH adjuster Type	Volume [mL]	Final pH [-]	Stirring time	Crystallinity (before firing) [cps]	Crystallinity (after firing) YBO_3 [cps]	Y_3BO_6 [cps]	Y_2O_3 [cps]	$Na_2Y_2B_2O_7$ [cps]	Relative luminance [%]	Relative chromaticity [%]
Na_2CO_3	5	9.05	20 min	759	3053	400	0	338	66.6	89.6
NH_3	5.5									
Na_2CO_3	10	9.03	20 min	49982	1613	1481	0	579	32.8	78.6
NH_3	3.5									
Na_2CO_3	15	9.07	20 min	1395	388	429	4984	1253	48.2	123.8
NH_3	2									
Na_2CO_3	20	9.33	20 min	940	0	0	3393	0	2.7	21.8
NH_3	1									

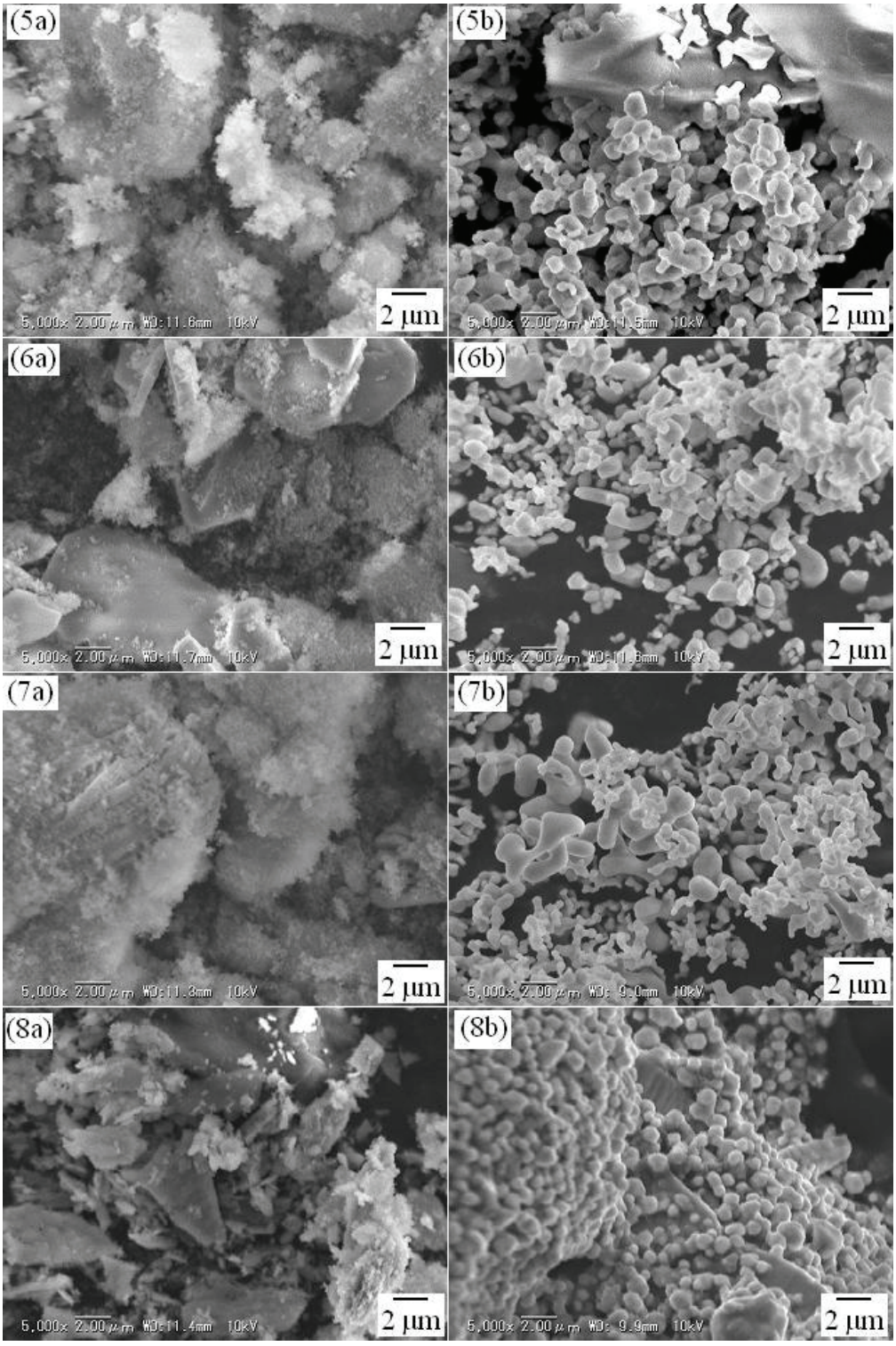

Figure 3.3.4 SEM images of crystals

Additive amount of Na_2CO_3 is (1) 5 mL, (2) 10 mL, (3) 15 mL, and (4) 20 mL.

(a) before firing (b) after firing

In the cases Na_2CO_3 and NH_3 were added simultaneously and stirred for 20 min, crystallinity of $YB(OH)_4CO_3$ wholly increased compared to the cases Na_2CO_3 was only used while crystal shape was similar to those cases. However, correlation between crystallinity of $YB(OH)_4CO_3$ and additive amount of Na_2CO_3 was unclear.

Main product after firing was varied according to additive amount of Na_2CO_3, which was different result from the cases Na_2CO_3 only was used. Main product after firing changed from YBO_3 (and Y_3BO_6) to Y_2O_3 as additive amount of Na_2CO_3 increased from 5 mL to 15 mL. When 20 mL of Na_2CO_3 was added, almost pure Y_2O_3 formed. As additive amount of Na_2CO_3 decreased, in other words, additive amount of NH_3 increased, products containing B atom tended to form after firing.

At beginning of reaction (or in short-stirring conditions), CO_3^{2-} and OH^- tended to be taken in precursor in the cases Na_2CO_3 was used as pH adjuster. However, when NH_3 was combined with Na_2CO_3, crystallinity of $YB(OH)_4CO_3$ increased before firing and products containing B atom like YBO_3 or Y_3BO_6 were likely to form after firing. There results indicate NH_3 promotes BO_3^{3-} intake and corrects abundance ratio between BO_3^{3-} and CO_3^{2-} or OH^- in precursor. As a result, not only crystallinity of $YB(OH)_4CO_3$ precursor will increase but also main product after firing will change from Y_2O_3 to YBO_3.

When NH_3 was combined with Na_2CO_3, luminance and chromaticity were decreased compared to the cases Na_2CO_3 only was used. Main product changed from Y_2O_3 to Y_3BO_6 and YBO_3 as additive amount of Na_2CO_3 was decreased, however, tendencies of low luminance and poor chromaticity were unchanged. Even in the case using 5 mL of Na_2CO_3 with NH_3, product after firing showed low luminance and poor chromaticity considering main product was YBO_3.

(c) Na_2CO_3 only, stirring for 1 day

Experimental results in the cases Na_2CO_3 only was used and stirred for 1 day are shown in

Table 3.3.7 and Table 3.3.8. SEM images of crystals before firing and after firing are shown in Fig. 3.3.5.

Table 3.3.7 Experimental results (crystal shape and crystal size)

pH adjuster Type	Volume [mL]	Final pH [-]	Stirring time	Before firing Shape	Size [μm]	After firing Shape	Size [μm]
Na_2CO_3	5	4.84	1 day	spherical microcrystals	0.1-1	aggregated microcrystals	0.2-2
Na_2CO_3	10	5.21	1 day	spherical microcrystals and coarse crystals	0.1-40	aggregated microcrystals	0.1-3
Na_2CO_3	15	7.84	1 day	discoid microcrystals and spherical microcrystals	0.1-1	aggregated microcrystals	0.1-4
Na_2CO_3	20	8.41	1 day	coarse crystals and aggregated microcrystals	0.2-50	aggregated spherical microcrystals	0.3-30

Table 3.3.8 Experimental results (crystallinity, relative luminance and relative chromaticity)

pH adjuster Type	Volume [mL]	Final pH [-]	Stirring time	Crystallinity (before firing) [cps]	Crystallinity (after firing) YBO_3 [cps]	Y_3BO_6 [cps]	Y_2O_3 [cps]	$Na_2Y_2B_2O_7$ [cps]	Relative luminance [%]	Relative chromaticity [%]
Na_2CO_3	5	4.84	1 day	1288	2724	290	0	0	78.6	101.7
Na_2CO_3	10	5.21	1 day	1463	2983	328	0	0	82.5	98.7
Na_2CO_3	15	7.84	1 day	1125	2195	1089	0	258	50.6	89.9
Na_2CO_3	20	8.41	1 day	384	0	0	3739	218	34.6	128.7

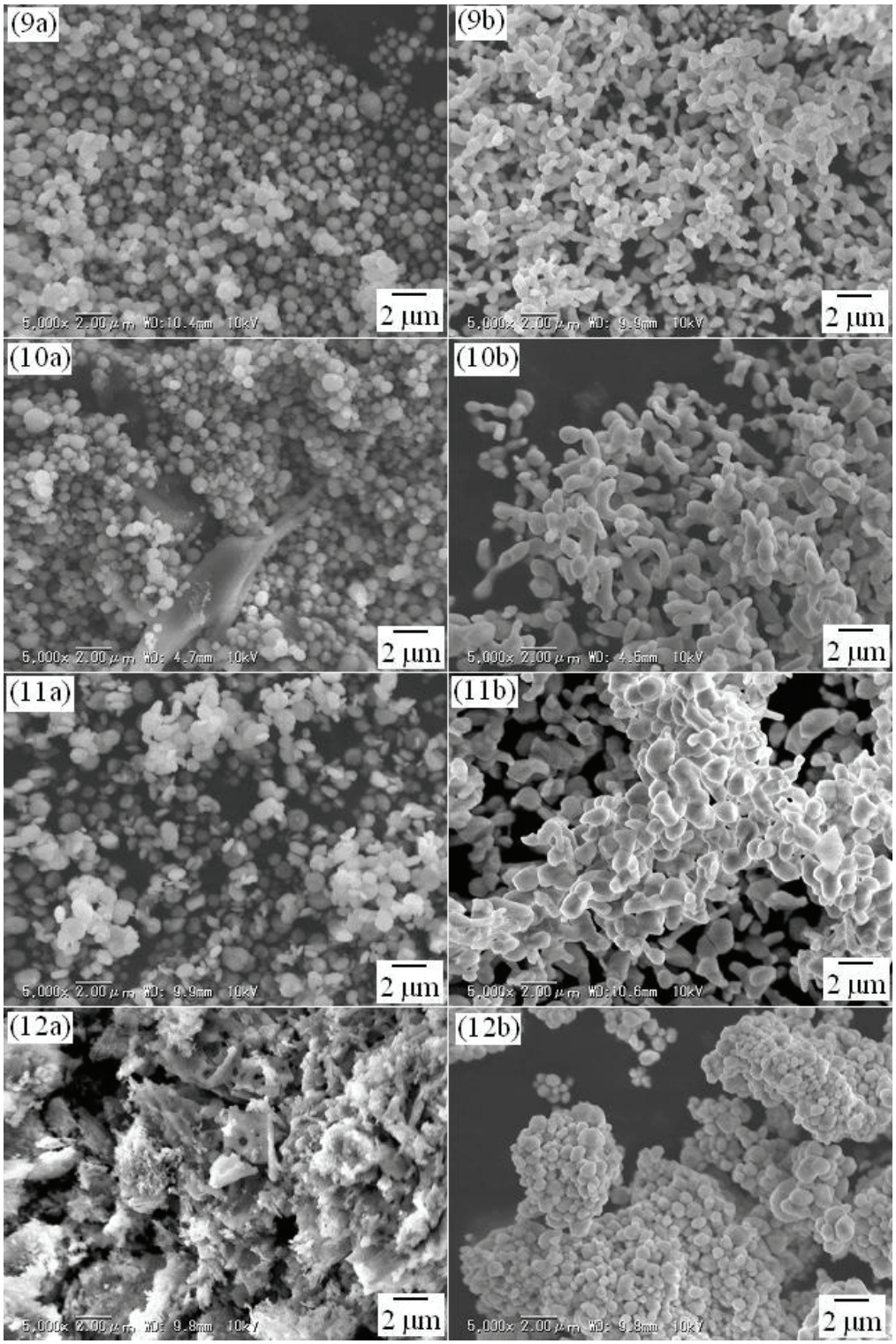

Figure 3.3.5 SEM images of crystals

Additive amount of Na_2CO_3 is (1) 5 mL, (2) 10 mL, (3) 15 mL, and (4) 20 mL.

(a) before firing (b) after firing

In the cases Na_2CO_3 only was used and stirred for 1 day, $YB(OH)_4CO_3$ spherical microcrystals without aggregation were formed when additive amount of Na_2CO_3 was less than 15 mL. The reason spherical microcrystals are unlikely to aggregate is ascribed to one of characteristics of sphere with the least surface area. Irregularly-shaped crystals were likely to incorporate as additive amount of Na_2CO_3 increased. When 20 mL of Na_2CO_3 was used, coarse crystals and aggregated microcrystals composed of $YB(OH)_4CO_3$ and Y_2O_3 precursor with uncertain formula were formed. XRD chart of precursor containing $YB(OH)_4CO_3$ and Y_2O_3 precursor with uncertain formula and JCPDS of $YB(OH)_4CO_3$ (PDF#00-040-0508) are shown in Fig. 3.3.6. Crystallinity of $YB(OH)_4CO_3$ was increased compared with the cases stirring for 20 min except for the case additive amount of Na_2CO_3 was 20 mL. These results were ascribed to increase of BO_3^{3-} amount in precursor caused by increase of stirring time and consequent correction of ion balance of BO_3^{3-} to CO_3^{2-} and OH^-. Main product after firing was YBO_3 in the conditions $YB(OH)_4CO_3$ spherical microcrystals were formed before firing; additive amount of Na_2CO_3 was less than 15 mL. However, Y_3BO_6 were incorporated in all conditions. This result suggests incorporation of Y_3BO_6 is inevitable when using Na_2CO_3. Amount of Y_3BO_6 was increased as additive amount of Na_2CO_3 was increased, and only Y_2O_3 was formed when using 20 mL of Na_2CO_3. Crystal size was mostly maintained during firing in the conditions $YB(OH)_4CO_3$ spherical microcrystals were formed before firing. This result means formation of $YB(OH)_4CO_3$ spherical microcrystals before firing is essential to form YBO_3 microcrystals after firing. However, crystals changed their shape from spherical into angular and aggregated by firing. This result indicates PEI reaction field or PEI addition during firing is necessary to maintain crystal shape and to prevent aggregation though formation of mono-dispersed $YB(OH)_4CO_3$ spherical microcrystals before firing is the most important to form mono-dispersed YBO_3 microcrystals after firing. Crystallinity of YBO_3 after firing was correlated with crystallinity of $YB(OH)_4CO_3$ before firing, that is, crystallinity after firing increased as crystallinity before firing increased.

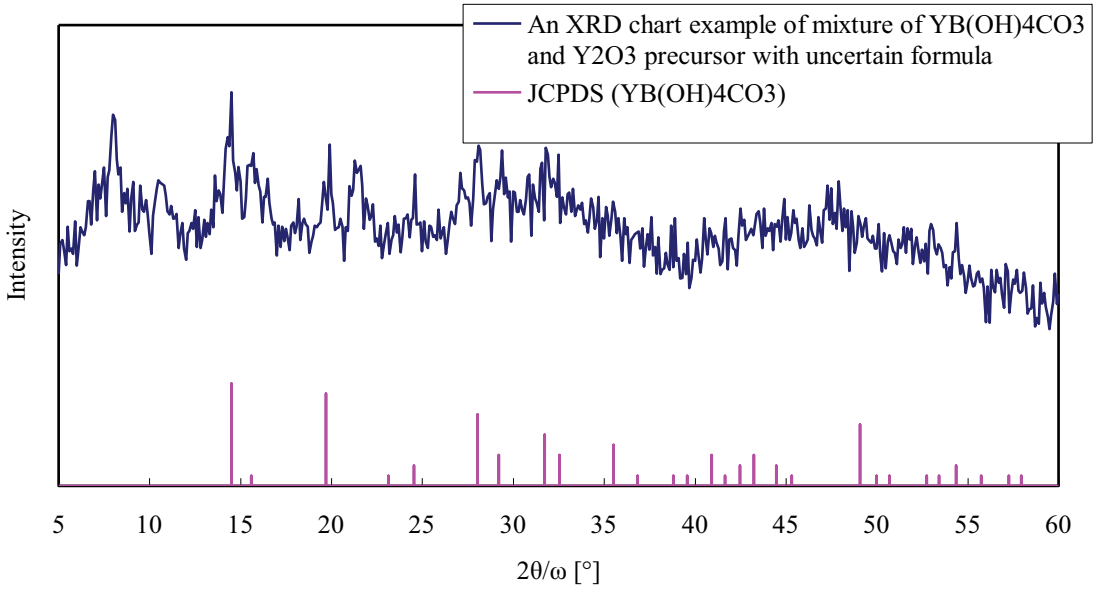

Figure 3.3.6 An example of XRD chart containing $YB(OH)_4CO_3$ and Y_2O_3 precursor with uncertain formula and JCPDS of $YB(OH)_4CO_3$ (PDF#00-040-0508)

Luminance was maximized when using 10 mL of Na_2CO_3. Crystallinity before firing was also maximized when using 10 mL of Na_2CO_3, the same condition as luminance was maximized. This result suggests high crystallinity improves energy transfer efficiency, that is, high crystallinity improves luminance. On the other hand, chromaticity was maximized when using 5 mL of Na_2CO_3. This result is ascribed to decrease of parity symmetry of YBO_3 after firing by lattice defect formed by disproportion of B/C. Similar mechanism is assumed to work when using 15 mL of Na_2CO_3, however, decrease of luminance and chromaticity caused by Y_3BO_6 is greater than chromaticity improvement by decrease of parity symmetry in this case. Maximum chromaticity was superior to the value of solid-state reaction and that of the cases NH_3 only was used. This result suggests YBO_3 forming in the cases using Na_2CO_3 inherits better chromaticity, the characteristics of Y_2O_3 forming mainly in the cases stirring time is relatively short.

(d) Na_2CO_3 and NH_3, stirring for 1 day

Experimental results in the cases Na_2CO_3 and NH_3 were adding simultaneously and stirred for 1 day are shown in Table 3.3.9 and Table 3.3.10. SEM images of crystals before firing and after firing are shown in Fig. 3.3.7. At the same time, experimental results in the cases NH_3 was added after Na_2CO_3 stirred for 1 day and stirred for another 20 min are shown in Table 3.3.11 and Table 3.3.12. SEM images of crystals before firing and after firing are shown in Fig. 3.3.8.

Table 3.3.9 Experimental results (crystal shape and crystal size)

pH adjuster Type	Volume [mL]	Final pH [-]	Stirring time	Before firing Shape	Size [μm]	After firing Shape	Size [μm]
Na_2CO_3 NH_3	5 5.5	8.46	1 day	coarse crystals and aggregated microcrystals	0.05-70	aggregated microcrystals (partly needle-like)	0.2-10
Na_2CO_3 NH_3	10 3.5	8.61	1 day	spherical microcrystals	0.05-4	aggregated microcrystals	0.2-10
Na_2CO_3 NH_3	15 2	8.67	1 day	spherical microcrystals and discoid microcrystals	0.1-10	aggregated microcrystals (partly needle-like)	0.5-10
Na_2CO_3 NH_3	20 1	8.64	1 day	plate-like microcrystals	0.1-15	microcrystals (partly aggregated)	0.1-5

Table 3.3.10 Experimental results (crystallinity, relative luminance and relative chromaticity)

pH adjuster Type	Volume [mL]	Final pH [-]	Stirring time	Crystallinity (before firing) [cps]	Crystallinity (after firing) YBO_3 [cps]	Y_3BO_6 [cps]	Y_2O_3 [cps]	$Na_2Y_2B_2O_7$ [cps]	Relative luminance [%]	Relative chromaticity [%]
Na_2CO_3 NH_3	5 5.5	8.46	1 day	604	2144	390	0	0	60.5	91.5
Na_2CO_3 NH_3	10 3.5	8.61	1 day	1572	3133	370	0	0	74.3	95.3
Na_2CO_3 NH_3	15 2	8.67	1 day	898	2083	488	0	0	57.5	93
Na_2CO_3 NH_3	20 1	8.64	1 day	783	0	418	2555	1512	32.6	89.1

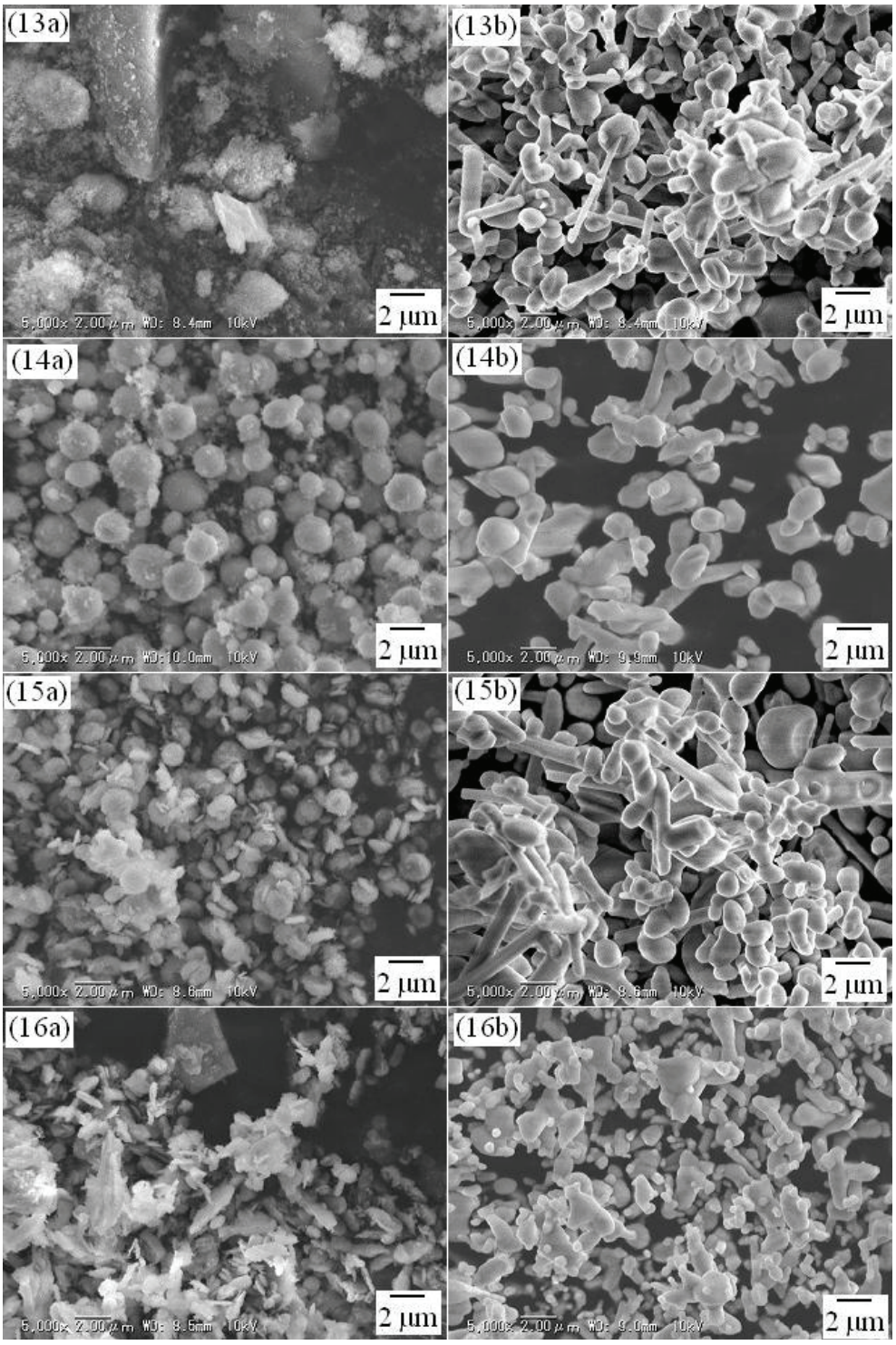

Figure 3.3.7 SEM images of crystals

Additive amount of Na_2CO_3 is (1) 5 mL, (2) 10 mL, (3) 15 mL, and (4) 20 mL.

(a) before firing (b) after firing

Table 3.3.11 Experimental results (crystal shape and crystal size)

pH adjuster Type	Volume [mL]	Final pH [-]	Stirring time	Before firing Shape	Size [μm]	After firing Shape	Size [μm]
Na_2CO_3	5	8.55	1 day 20 min	spherical microcrystals and aggregated microcrystals	0.05-20	aggregated microcrystals	0.4-10
NH_3	5.5						
Na_2CO_3	10	8.81	1 day 20 min	spherical microcrystals and coarse crystals	0.05-5	aggregated microcrystals	0.1-2
NH_3	3.5						
Na_2CO_3	15	9.1	1 day 20 min	spherical microcrystals	0.1-4	microcrystals	0.1-5
NH_3	0.6						
Na_2CO_3	20	8.5	1 day 20 min	plate-like and needle-like crystals	0.1-15	aggregated microcrystals (partly needle-like)	0.2-15
NH_3	0.2						

Table 3.3.12 Experimental results (crystallinity, relative luminance and relative chromaticity)

pH adjuster Type	Volume [mL]	Final pH [-]	Stirring time	Crystallinity (before firing) [cps]	Crystallinity (after firing) YBO_3 [cps]	Y_3BO_6 [cps]	Y_2O_3 [cps]	$Na_2Y_2B_2O_7$ [cps]	Relative luminance [%]	Relative chromaticity [%]
Na_2CO_3	5	8.55	1 day 20 min	484	3083	289	0	0	80.5	95.4
NH_3	5.5									
Na_2CO_3	10	8.81	1 day 20 min	756	3878	247	0	246	82.4	95.8
NH_3	3.5									
Na_2CO_3	15	9.1	1 day 20 min	1233	3188	319	0	0	75.5	93.8
NH_3	0.6									
Na_2CO_3	20	8.5	1 day 20 min	931	398	1408	0	1128	5.2	37.7
NH_3	0.2									

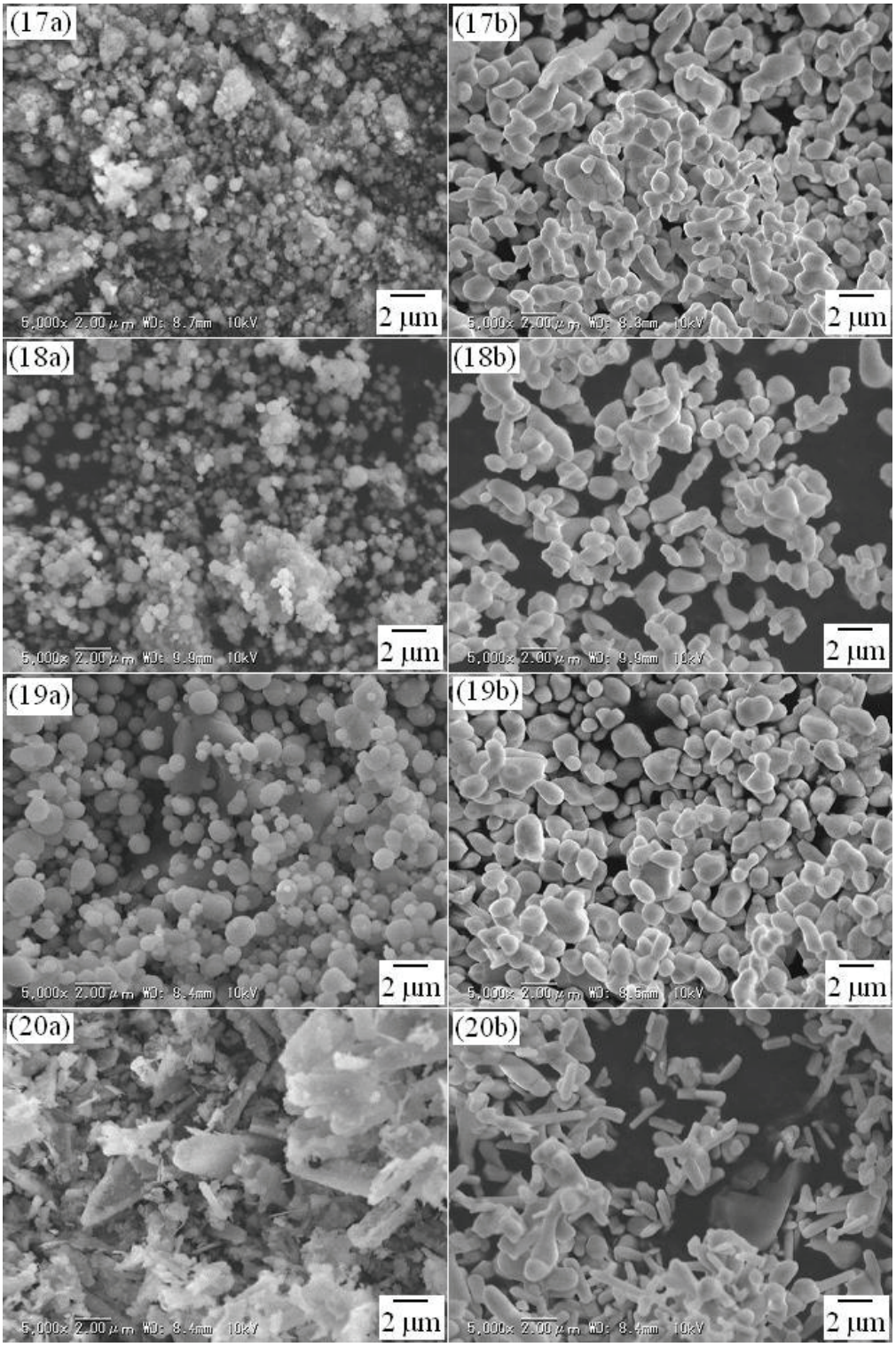

Figure 3.3.8 SEM images of crystals

Additive amount of Na_2CO_3 is (1) 5 mL, (2) 10 mL, (3) 15 mL, and (4) 20 mL.

(a) before firing (b) after firing

In the cases NH_3 was combined with Na_2CO_3 and stirred for 1 day, $YB(OH)_4CO_3$ crystal precursor was formed regardless of additive timing of NH_3. Uniform spherical microcrystals showing relatively high crystallinity were likely to form in the range of additive amount of Na_2CO_3 from 10 mL to 15 mL. On the other hand, in the cases 5 mL of Na_2CO_3 was added, non-uniform coarse crystals were incorporated and precursor showed lowest crystallinity among these cases. This is because fundamental lack of CO_3^{2-} prevents formation of $YB(OH)_4CO_3$ crystals. In the cases 20 mL of Na_2CO_3 was added, irregular-shaped crystals such as needle-like crystals or plate-like crystals were formed.

In almost all cases additive amount of Na_2CO_3 is less than 15 mL, crystallinity of $YB(OH)_4CO_3$ tended to be lower than that of the cases Na_2CO_3 only was used. The reasons of precursor crystallinity decrease are as follows. In the cases Na_2CO_3 and NH_3 are added simultaneously, rapid nucleation and rapid growth continuing from beginning of reaction will form precursor with relatively large size. However, at the same time, not also microparticles resulting from mass nucleation or secondary nucleation but also amorphous particles will incorporate due to excessively rapid reaction rate, which will decrease precursor crystallinity. On the other hand, in the cases NH_3 was added after Na_2CO_3, $YB(OH)_4CO_3$ crystals already formed before adding NH_3 must have uniform spherical shape and show high crystallinity like the cases Na_2CO_3 only is used and stirred for 1 day. However, already-formed $YB(OH)_4CO_3$ crystals will be destroyed by pH increase caused by NH_3 addition. Destroyed $YB(OH)_4CO_3$ crystals and unreacted raw materials will precipitate together as amorphous precursor due to high supersaturation produced by NH_3. Though spherical microcrystals remains because of short stirring time after adding NH_3, destruction of already-formed $YB(OH)_4CO_3$ crystals and incorporation of amorphous precursor will decrease precursor crystallinity.

When precursor crystallinity was compared by additive timing of NH_3, precursor formed in

the cases Na_2CO_3 and NH_3 were added simultaneously showed higher crystallinity in the range of additive amount of Na_2CO_3 was less than 10 mL. In contrast, precursors formed in the cases NH_3 was added after Na_2CO_3 tended to show higher crystallinity in the range of additive amount of Na_2CO_3 was more than 15 mL, and this crystallinity was also higher than that of the cases Na_2CO_3 only was used. The mechanisms providing these results are assumed to be as follows. Although NH_3 added after Na_2CO_3 promotes crystallization of unreacted H_3BO_3, whether precursor crystallinity will increase or decrease is decided by concentration of unreacted raw materials. For example, unreacted raw materials will precipitate rapidly and form amorphous precursor when concentrations of unreacted raw materials are high like the case 5 mL of Na_2CO_3 is used. On the other hand, unreacted raw materials will precipitate slowly and form $YB(OH)_4CO_3$ crystal precursor when concentrations of unreacted raw materials have been already decreased like the cases more than 15 mL of Na_2CO_3 is used. However, difference of precursor crystallinity caused by difference of additive timing of NH_3 was small when 5 mL of Na_2CO_3 was used because lack of CO_3^{2-} affected much greatly to decrease of precursor crystallinity. When Na_2CO_3 20 mL was used, crystallinity of $YB(OH)_4CO_3$ was increased by NH_3 addition regardless of additive timing because B atoms were unlikely to be taken into precursor prevented by high concentration of CO_3^{2-} and OH^- originating from Na_2CO_3.

These tendencies on precursor crystallinity in the cases NH_3 was combined with Na_2CO_3 and stirred for 1 day were different with the cases NH_3 was combined with Na_2CO_3 and stirred for 20 min. This is because $YB(OH)_4CO_3$ crystallization does not finish during stirring for 20 min. Precursor growth and crystallinity increase are inefficient in the cases Na_2CO_3 is only used and stirred for 20 min, and therefore they can be improved by combining NH_3 which promotes $YB(OH)_4CO_3$ crystallization. On the other hand, $YB(OH)_4CO_3$ crystallization by Na_2CO_3 usually finishes during stirring for 1 day, and therefore NH_3 addition negatively affects on crystallinity of

precursor by destroying already-formed $YB(OH)_4CO_3$ crystals while yield of $YB(OH)_4CO_3$ and YBO_3 after firing are improved. NH_3 combination also affects negatively on crystallinity of precursor in the cases Na_2CO_3 and NH_3 are adding simultaneously. This is mainly because amorphous incorporation due to excessively rapid growth of precursor by high pH from beginning of reaction.

YBO_3 was formed after firing, however, Y_3BO_6 was likely to incorporate like as Na_2CO_3 only was used. When 20 mL of Na_2CO_3 was used and NH_3 was added after Na_2CO_3, main product was Y_3BO_6 in contrast to the cases Na_2CO_3 was only used or Na_2CO_3 and NH_3 were simultaneously added, whose main product was Y_2O_3. Crystals angulated and partly aggregated after firing in all cases. When NH_3 was combined, crystal size also increased after firing. This result indicates NH_3 promotes particle adhesion during firing. Crystallinity after firing was higher in the cases NH_3 was added after Na_2CO_3 than the cases Na_2CO_3 only was used or Na_2CO_3 and NH_3 were added simultaneously. Moreover, amount of incorporated Y_3BO_6 was also decreased in the cases NH_3 was added after Na_2CO_3. This is assumed to be the result that $YB(OH)_4CO_3$ crystal precursor was partly dissolved or its crystal structure was changed when NH_3 was added after Na_2CO_3, and outer shell whose crystallinity was relatively low or containing amorphous precursor with excess B atom was formed.

In the cases NH_3 was combined with Na_2CO_3 and stirred for 1 day, luminance was improved in the cases NH_3 was added after Na_2CO_3 compared with the cases Na_2CO_3 only was used. This is assumed to be the result that outer shell with excess B atom formed after adding NH_3 improved YBO_3 crystallinity and luminance. On the other hand, luminance was not so improved or decreased in the cases Na_2CO_3 and NH_3 were added simultaneously. These results means NH_3 (or NH_4^+) has effects to prevent Y_3BO_6 incorporation and to improve YBO_3 crystallinity and luminance only in the case NH_3 is added after Na_2CO_3 and stirred for short time. Luminance was maximized when 10 mL

of Na_2CO_3 was used in both cases similarly to the cases Na_2CO_3 only was used.

Chromaticity was slightly decreased in the range additive amount of Na_2CO_3 was less than 10 mL regardless of addition timing of NH_3 compared with the cases Na_2CO_3 only was used. This is assumed to be the result that crystal size became larger by combining NH_3, and therefore chromaticity improvement by roughness of crystal surface did not work well. On the other hand, chromaticity was slightly increased when additive amount of Na_2CO_3 was 15 mL. This is assumed to be the result that Y_3BO_6 incorporation was prevented by combining NH_3, and as therefore chromaticity decrease by Y_3BO_6 was eliminated. Chromaticity was maximized when using 10 mL of Na_2CO_3, which was different result to the cases Na_2CO_3 only was used. Chromaticity was slightly improved in the cases NH_3 was added after Na_2CO_3 compared with the cases Na_2CO_3 and NH_3 were added simultaneously.

3.3.4 Conclusions

$YB(OH)_4CO_3$ spherical microcrystals before firing and YBO_3 microcrystals showing good chromaticity after firing are obtained by controlling additive amount of Na_2CO_3 as molar ratio of C atom to B atom (C/B) is less than 1.5 and stirring for sufficient time (about 1 day). Formation of mono-dispersed $YB(OH)_4CO_3$ spherical microcrystals before firing is the most important to form mono-dispersed YBO_3 microcrystals after firing because crystal size is maintained during firing in the conditions $YB(OH)_4CO_3$ spherical microcrystals are formed before firing. Na_2CO_3 pH adjuster enables to synthesize $YB(OH)_4CO_3$ spherical microcrystals easily and certainly, and moreover, combination of NH_3 enables to improve yield. However, PEI reaction field or PEI addition during firing is indicated to be essential to maintain crystal shape and to prevent aggregation.

3.4 Overall conclusions on $(Y,Gd)BO_3:Eu^{3+}$

Non-acidified PEI is the most suitable for reaction field to synthesize mono-dispersed YBO_3 microcrystals. In addition, appropriate concentration of non-acidified PEI exists. However, the most important requirement to form uniform YBO_3 microcrystals is to synthesize uniform $YB(OH)_4CO_3$ microcrystals before firing.

Chapter 4

The relationship between crystal habit and relative intensity of XRD peaks on $CaSO_4 \cdot 2H_2O$

Chapter 4

4.1 Introduction

Crystal morphology changes according to reaction conditions such as additives, pH, and reaction time. At the same time, intensity of each XRD peak also changes. This phenomenon is observed in various materials such as YBO_3, however, few studies correlate morphology with XRD peak, so the detail of the relationship between them remains unclear.

This study aims to clarify the detailed relationship between crystal morphology and XRD peak intensity. In this study, $CaSO_4 \cdot 2H_2O$ was selected as model substance because it shows crystal face and crystal shape clearly. $CaSO_4 \cdot 2H_2O$ crystals showing various morphologies were synthesized by reaction crystallization with various additives chosen randomly. Morphology (crystal shape, average longitude and aspect ratio), absolute intensity and relative intensity of major XRD peaks on synthesized $CaSO_4 \cdot 2H_2O$ were examined. Focused major five XRD peaks are (020), (021), (130), (041), and (-221) peaks. Positions (2θ) of them are 11.6°, 20.7°, 23.4°, 29.1°, and 31.1°, respectively. From these results, relationships between morphology and XRD peak intensities were clarified as well as the most suitable additive to control crystal nucleation and crystal growth to synthesize mono-dispersed $CaSO_4 \cdot 2H_2O$ microcrystals was determined. Moreover, crystal growth mechanism and crystal structure of $CaSO_4 \cdot 2H_2O$ were discussed by analyzing crystal size, XRD absolute intensity and XRD relative intensity.

4.2 Experimental procedure

In this research, $CaSO_4 \cdot 2H_2O$ crystals showing various morphologies were synthesized by reaction crystallization with various additives. Additives were chosen randomly among acids, bases, inorganic salts, organic compounds, and polyelectrolytes. $CaCl_2$ solution and Na_2SO_4 solution were used as raw materials. Concentration and volume of raw materials were basically standardized as 0.3 mol/L and 50 mL respectively. Exceptionally, concentrations of raw materials were increased to

0.6-1.5 mol/L when using additives which can increase solubility or can suppress nucleation of $CaSO_4 \cdot 2H_2O$. Applied materials and experimental conditions are shown in Table 4.1 and Table 4.2, respectively. Reaction crystallization was carried out at room temperature.

Table 4.1 Materials

Reagent	Grade	Purity [%]	Production company
$CaCl_2$	Special	95.0	Kanto Chemical Co. Inc
Na_2SO_4	Special	99.0	Kanto Chemical Co. Inc
HCl	Special	35.0-37.0	Wako Pure Chemical Industries, Ltd.
NaOH	Special	97.0	Wako Pure Chemical Industries, Ltd.
NaCl	Special	99.5	Wako Pure Chemical Industries, Ltd.
Citric acid	Special	98.0	Wako Pure Chemical Industries, Ltd.
Urea	Special	99.0	Wako Pure Chemical Industries, Ltd.
PEI70000	P-1000	29.0-31.0	Nippon Shokubai Co., Ltd.
PVP	K-30W	29.0-31.0	Nippon Shokubai Co., Ltd.
PAA250000	First	—	Wako Pure Chemical Industries, Ltd.
CMC-Na	Practical Grade	—	Wako Pure Chemical Industries, Ltd.
$Ca_2SO_4 \cdot 2H_2O$	First	—	Wako Pure Chemical Industries, Ltd.

Table 4.2 Experimental conditions

Series	Raw materials							
	$CaCl_2$		Na_2SO_4		Additives		Deionized water [mL]	Ripening time after nucleation
	Concentration [mol/L]	Volume [mL]	Concentration [mol/L]	Volume [mL]	Type	Amount		
$CaSO_4 \cdot 2H_2O$ reagent	—	—	—	—	—	—	—	—
Without additives	0.3	50	0.3	50	—	—	200	30 min
Without additives (ripened for 5 min)	0.3	50	0.3	50	—	—	200	5 min
HCl (Static)	0.9	50	0.9	50	35% HCl	10 mL	200	4 day
NaOH	0.3	50	0.3	50	1 mol/L NaOH	0.3 mL	200	30 min
NaCl (ripened for 1 day)	0.3	50	0.3	50	NaCl	2 g	200	1 day
Concentrated citric acid	0.9	50	0.9	50	Citric acid	100 g	200	30 min
Citric acid (Static)	0.3	50	0.3	50	Citric acid	2 g	200	25 day
Urea	0.3	50	0.3	50	Urea	2 g	200	30 min
PEI	0.3	50	0.3	50	15 g/L PEI70000	200 mL	—	30 min
Acidified PEI (concentrated raw materials)	1.5	50	1.5	50	10 g/L PEI70000 35% HCl	200 mL 10 mL	—	30 min
PVP	0.3	50	0.3	50	10 g/L PVP	200 mL	—	30 min
PAA250000	0.6	50	0.6	50	1 g/L PAA250000	200 mL	—	2 hour
CMC-Na	0.9	50	0.9	50	10 g/L CMC-Na	200 mL	—	25 min

200 mL of deionized water or additive solution was put into 300 mL beaker reactor and agitated by magnetic stirrer. 50 mL of $CaCl_2$ solution and 50 mL of Na_2SO_4 solution with predetermined concentrations were added in order. Through this operation $CaSO_4 \cdot 2H_2O$ was formed. Formed $CaSO_4 \cdot 2H_2O$ was ripened in agitating condition or static condition for predetermined time. $CaSO_4 \cdot 2H_2O$ crystals were separated from $CaSO_4 \cdot 2H_2O$ slurry by suction filtration, and dried in oven at 40℃ for more than 24 hours.

After drying, crystal morphology (crystal shape and crystal size) was observed by optical microscope (VH-Z450, KEYENCE) or SEM (VE-8800, KEYENCE). Average longitude (major axis), average latitude (minor axis), crystal size distribution, coefficient of variation (CV) and aspect ratio were calculated from micrographs. Crystallinity of each product was analyzed by XRD (Rint-UltimaⅢ, Rigaku). XRD absolute intensity (crystallinity) was determined from the strongest diffraction peak. XRD relative intensity was calculated by defining XRD intensity of (020) peak, ordinarily the strongest peak, as 100. Morphology, XRD absolute intensity and XRD relative intensity of synthesized $CaSO_4 \cdot 2H_2O$ were examined and the relationships between them were discussed.

4.3 Results and discussions

XRD relative intensities of major peaks on (020) peak were varied with additives. Especially, relative intensity of (021) peak on (020) peak was varied the most widely from under 10 to over 100. Therefore, the relationship between crystal morphology and XRD relative intensity on $CaSO_4 \cdot 2H_2O$ was examined by classifying results into four types according to XRD relative intensity of (021) peak: (a) 0-10, (b) 10-20, (c) 20-50, (d) 50-100 and more than 100. Experimental results organized from the view of XRD relative intensity of (021) peak are shown in Table 4.3 and Table 4.4. Examples of micrographs and XRD charts are shown in Fig. 4.1 - 4.4 and Fig. 4.5, respectively.

Table 4.3 Experimental results

(XRD absolute intensity and XRD relative intensity to (020) diffraction face)

XRD relative intensity of (021) face [%]	Series	XRD absolute intensity (020) [cps]	(021)	(130)	(041)	(-221)	XRD relative intensity to (020) face (020) [%]	(021)	(130)	(041)	(-221)
0-10	Acidified PEI (concentrated raw materials)	43575	2153	4826	3707	369	100	4.9	11.1	8.5	0.8
	Concentrated citric acid	16028	1528	2881	2753	431	100	9.5	18.0	17.2	2.7
	Citric acid (Static)	33059	2159	5606	2818	228	100	6.5	17.0	8.5	0.7
	HCl (Static)	65558	6533	15722	6714	97	100	10.0	24.0	10.2	0.1
	0-10 average	39555	3093	7259	3998	281	100	7.7	17.5	11.1	1.1
10-20	Without additives	27557	3213	3492	5046	569	100	11.7	12.7	18.3	2.1
	PEI	11883	2215	2623	2833	904	100	18.6	22.1	23.8	7.6
	PVP	17430	2926	2163	3959	513	100	16.8	12.4	22.7	2.9
	NaCl (ripened for 1 day)	32365	4044	5820	4104	272	100	12.5	18.0	12.7	0.8
	10-20 average	22309	3100	3525	3986	565	100	14.9	16.3	19.4	3.4
20-50	$CaSO_4 \cdot 2H_2O$ reagent	12598	2664	1830	2988	894	100	21.1	14.5	23.7	7.1
	Without additives (ripened for 5 min)	10470	2705	2201	3280	598	100	25.8	21.0	31.3	5.7
	NaOH	7928	2522	1370	3204	770	100	31.8	17.3	40.4	9.7
	Urea	12375	3363	2457	4320	793	100	27.2	19.9	34.9	6.4
	20-50 average	10843	2814	1965	3448	764	100	26.5	18.2	32.6	7.2
50-100	PAA250000	2693	2093	476	1352	1386	100	77.7	17.7	50.2	51.5
100-	CMC-Na	2142	2906	384	1984	1388	100	135.7	17.9	92.6	64.8

Table 4.4 Experimental results (Crystal shape, crystal size and aspect ratio)

XRD relative intensity of (021) face [%]	Series	Crystal shape	Longitude Average [μm]	CV [-]	Latitude Average [μm]	CV [-]	Aspect ratio Average [-]	CV [-]
0-10	Acidified PEI (concentrated raw materials)	needle, indefinite plate or granular	12.96	0.672	4.41	0.924	4.15	0.878
	Concentrated citric acid	indefinite plate or granular	11.06	0.698	5.56	0.892	2.46	0.527
	Citric acid (Static)	needle or indefinite plate	100.78	0.858	28.98	0.757	4.08	0.678
	HCl (Static)	needle or granular	40.24	1.797	8.52	0.682	5.51	1.649
	0-10 average	coarse needle or coarse plate	41.26	1.006	11.87	0.814	4.05	0.933
10-20	Without additives	needle or plate	17.27	0.447	3.52	0.808	7.29	0.741
	PEI	plate or granular	11.47	0.624	3.47	0.619	3.62	0.494
	PVP	needle, indefinite plate or granular	6.46	0.554	2.43	0.674	3.24	0.653
	NaCl (ripened for 1 day)	needle	18.45	0.871	3.12	0.710	7.74	1.069
	10-20 average	needle or plate	13.41	0.624	3.13	0.703	5.47	0.739
20-50	$CaSO_4 \cdot 2H_2O$ reagent	granular or indefinite plate	7.58	0.799	3.33	1.008	2.72	0.555
	Without additives (ripened for 5 min)	broken needle or broken plate	4.07	0.502	1.37	0.554	3.57	0.680
	NaOH	broken needle or granular	7.77	0.447	2.00	0.649	5.34	0.812
	Urea	needle, plate or granular	3.42	0.585	1.11	0.559	3.43	0.649
	20-50 average	needle, plate or granular	5.71	0.583	1.95	0.692	3.77	0.674
50-100	PAA250000	granular or aggregated	2.38	0.490	1.20	0.445	2.06	0.359
100-	CMC-Na	granular	2.21	0.520	1.17	0.475	1.99	0.426

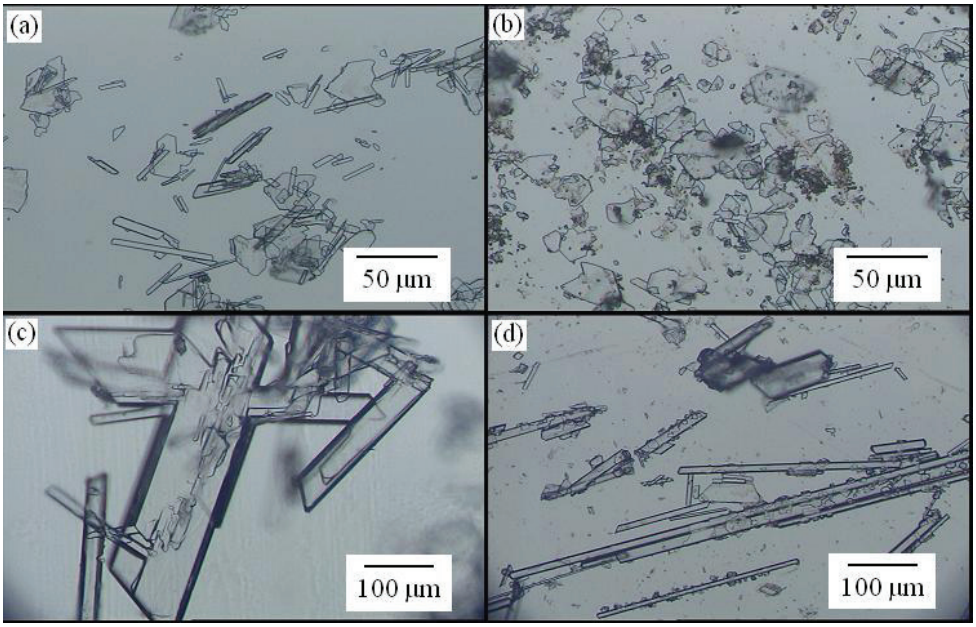

Figure 4.1 Micrographs of crystals whose XRD relative intensity of (021) peak is 0-10

(a) Acidified PEI (concentrated raw materials) (b) Concentrated citric acid

(c) Citric acid (static) (d) HCl (static)

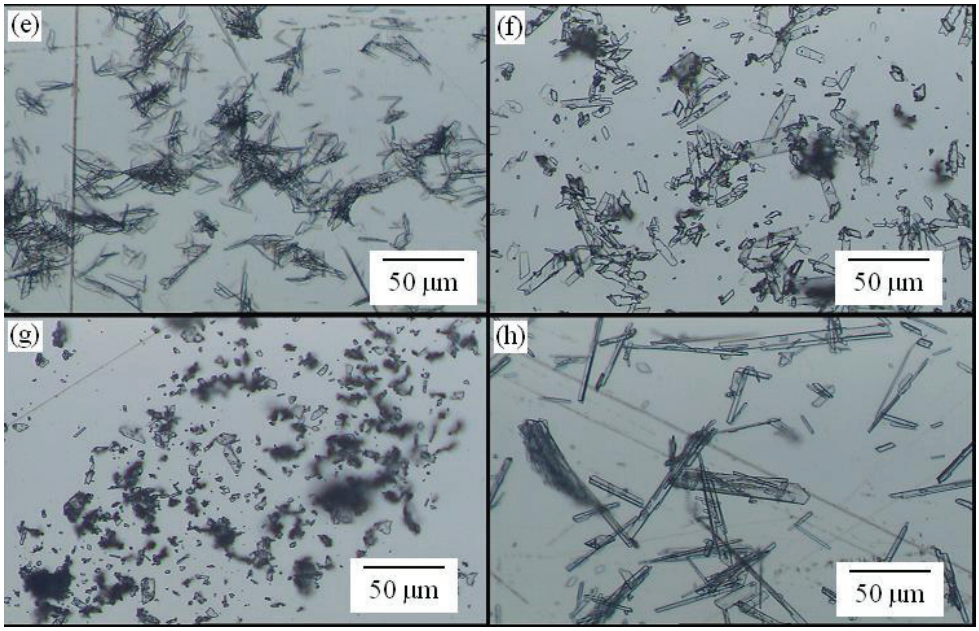

Figure 4.2 Micrographs of crystals whose XRD relative intensity of (021) peak is 10-20

(e) Without additives (f) PEI (g) PVP (h) NaCl (ripened for 1 day)

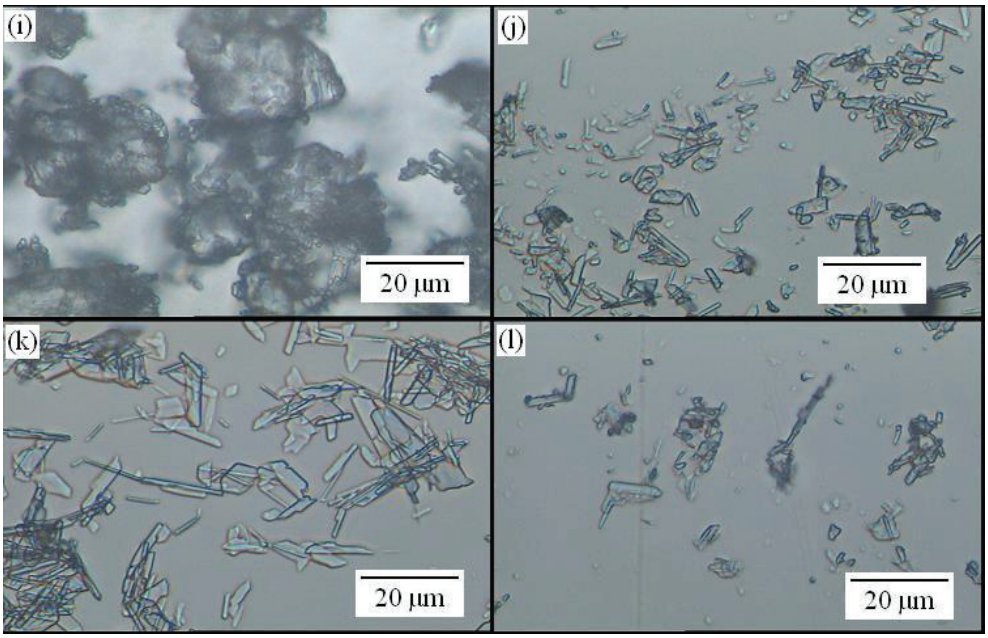

Figure 4.3 Micrographs of crystals whose XRD relative intensity of (021) peak is 20-50

(i) $CaSO_4 \cdot 2H_2O$ reagent (j) Without additives (ripened for 5 min) (k) NaOH (l) Urea

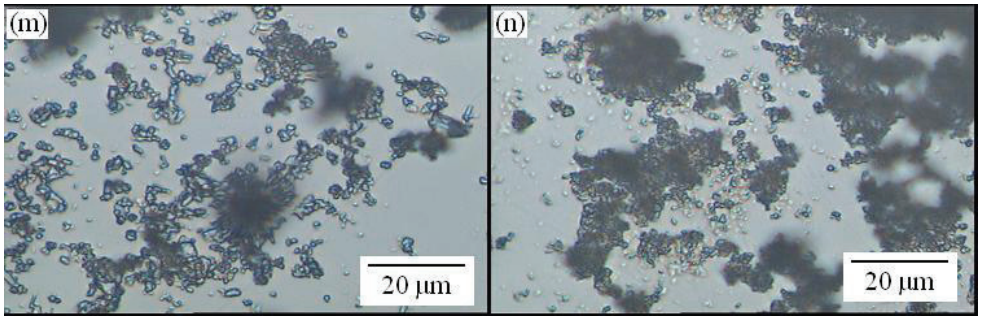

Figure 4.4 Micrographs of crystals

whose XRD relative intensity of (021) peak is 50-100 and more than 100

(m) PAA250000 (n) CMC-Na

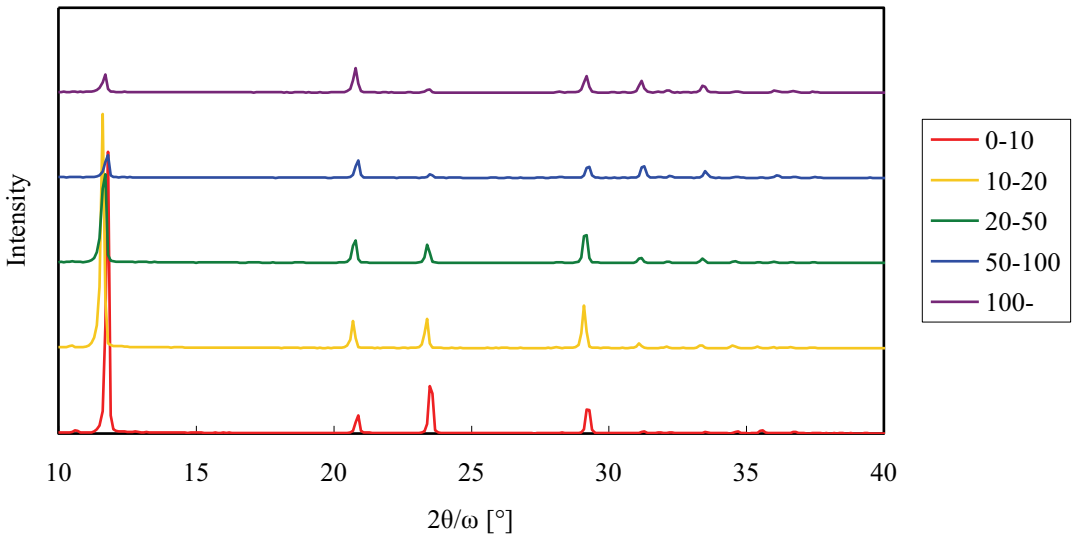

Figure 4.5 Examples of XRD charts whose XRD relative intensity of (021) peak is 0-10, 10-20, 20-50, 50-100, and more than 100

4.3.1 Crystal habits caused by additives

4.3.1.1 Detailed characteristics of crystals classified by XRD relative intensity of (021) peak

(a) The cases XRD relative intensity of (021) peak is 0-10

The cases XRD relative intensity of (021) peak is 0-10 occurred when adding concentrated citric acid, HCl or citric acid in static condition, or using concentrated raw materials' solutions with acidified PEI. In these cases, needle-like or plate-like large crystals with large aspect ratio were dominant. Especially in static conditions, coarse crystals whose longitude reached to hundreds of micrometer or mm order were formed. These results were assumed to be led by slow and precise growth resulting from solubility increase by acidic additives. In the case of using acidified PEI, large crystals were formed, which was opposite result to that observed in previous studies synthesizing mono-dispersed poorly-soluble sulfate microcrystals in acidified PEI reaction field. In reaction crystallization of $CaSO_4 \cdot 2H_2O$ from concentrated raw materials, $CaSO_4 \cdot 2H_2O$ crystals

were assumed to grow rapidly but stably in the presence of PEI behaving as stabilizer. In contrast, when using concentrated citric acid, irregular plate-like or wide plate-like crystals with relatively small aspect ratio were dominant though crystal size was still large. This result indicates high concentration of citric acid have an effect to change crystal habit by preventing crystal growth along longitude direction. Similarly-shaped microcrystals or granular microcrystals assumed to be broken crystals or secondary crystals were also observed in these cases. Coexistence of coarse crystals and microcrystals decreased CV especially in the case using HCl in static condition.

(b) The cases XRD relative intensity of (021) peak is 10-20

The cases XRD relative intensity of (021) peak is 10-20 occurred when adding PVP, PEI, NaCl, or using no additives. $CaSO_4 \cdot 2H_2O$ crystals synthesized from raw material solutions with appropriate concentrations without additives correspond to this case (Fig. 4.2 (e)), in other words, this case, XRD relative intensity of (021) peak is 10-20, is the most popular on reaction crystallization of $CaSO_4 \cdot 2H_2O$. In these cases, needle-like or plate-like large crystals with large aspect ratio and some microcrystals formed together similarly to the case XRD relative intensity of (021) peak is 0-10. Coarse crystals were formed only in the case using NaCl, however, this result is mainly ascribed to longer ripening time (1 day).

(c) The cases XRD relative intensity of (021) peak is 20-50

The cases XRD relative intensity of (021) peak is 20-50 occurred when adding NaOH or urea, or the case ripened 5 min without additives. In these cases, granular crystals as well as plate-like or needle-like crystals were formed. Both average longitude and aspect ratio of these crystals were smaller than the cases XRD relative intensity of (021) peak is 0-10 and 10-20. These results were assumed to be led by following mechanisms; slow growth resulting from solubility increase and

growth suppression by urea, mass nucleation and minimization of crystals resulting from solubility decrease by NaOH, or insufficient growth resulting from shorter ripening time. In these cases, broken crystals and chipped crystals were also included, which indicates durability of crystals decreased. Although secondary particles were certainly included, it was difficult to distinguish between them from originally-small crystals. $CaSO_4 \cdot 2H_2O$ reagent also corresponded to this case, however, it showed unique morphology: thick and coarse granular crystals.

(d) The cases XRD relative intensity of (021) peak is 50-100 and more than 100

The cases XRD relative intensity of (021) peak is 50-100 and more than 100 occurred when adding PAA250000 or CMC-Na, respectively. Both additives were polyelectrolytes having carboxyl groups. In these cases, morphology of synthesized $CaSO_4 \cdot 2H_2O$ dramatically changed from needle-like or plate-like large crystals to granular microcrystals, whose average size was about 2.3 μm. These results were assumed to be led by slow growth rate resulting from nucleation suppression and/or solubility increase by polyelectrolytes, growth suppression resulting from steric hindrance of polyelectrolytes, and prevention of aggregation resulting from electrostatic attractive force between Ca^{2+} and carboxyl groups in polyelectrolytes. This result indicates polyelectrolytes having carboxyl groups are the most suitable to synthesize mono-dispersed $CaSO_4 \cdot 2H_2O$ microcrystals. It was impossible to distinguish between primary crystals and secondary crystals, broken crystals and originally-small crystals. In addition, $CaSO_4 \cdot 0.5H_2O$ impurities were included in these cases.

4.3.1.2 Differences of effects of polyelectrolytes based on differences of interaction mechanisms

From above results, polyelectrolytes having carboxyl groups are considered to be the most appropriate reaction field to synthesize mono-dispersed $CaSO_4 \cdot 2H_2O$ microcrystals. On the other hand, acidified PEI, determined as the most effective reaction field to synthesize mono-dispersed

poorly-soluble sulfates microcrystals in previous studies, was ineffective to $CaSO_4 \cdot 2H_2O$, nor showed remarkable change on XRD charts. Therefore, mechanisms to control crystal nucleation and crystal growth, and to prevent crystal aggregation are assumed to vary with types of polyelectrolytes and target materials interacting with them.

Effectiveness of polyelectrolyte reaction field is assumed to be decided by interaction type and interaction strength between polyelectrolyte and target metals. Examples of interaction types are electrostatic attractive force in polyelectrolytes having carboxyl groups, PAA or CMC-Na, and formation of coordination bond in PEI. Examples of factors having possibility to affect interaction strength are atomic weight, ionic radius, and ion valence of target metals. In addition, difference of electronegativity between metal ions and particular atoms in functional groups in polyelectrolyte can affect interaction strength. Effectiveness of major three polyelectrolytes, non-acidified PEI, acidified PEI and PAA, are discussed as follows.

Interaction between PEI and metal ions are formation of coordination bond. Non-acidified PEI is effective for YBO_3 system though it has appropriate concentration range. However, non-acidified PEI is ineffective for $CaSO_4 \cdot 2H_2O$. Assumed reason is that attractive force between Ca^{2+} and unshared electron pairs on N atoms in PEI is too weak to form coordination bond due to lightness of Ca^{2+}. Non-acidified PEI is also inappropriate for poorly-soluble sulfates containing relatively heavy metal ions like Pb^{2+}, Ba^{2+}, and Sr^{2+} in previous studies. This is because direct reaction between these metal ions and non-acidified PEI immediately forms poorly-soluble hydroxide precipitation. Although target materials will form by continuous stirring, it will take a long time to exchange OH^- for target anion and formed crystals will be mixture of target compound and hydroxide with non-uniform shape and non-uniform size.

On the other hand, acidified PEI is effective for poorly-soluble sulfates in previous studies. Acidified PEI prevents direct reaction between metal ions and unshared electron pairs on N atoms

in PEI because unshared electron pairs on N atoms are masked by H^+. Moreover, H^+ bonded to PEI is gradually displaced by metal ions, which enables to form mono-dispersed microcrystals of poorly-soluble sulfates free from aggregation. However, acidified PEI is ineffective for YBO_3 and $CaSO_4 \cdot 2H_2O$. This is because relatively light metal ions such as RE^{3+} and Ca^{2+} cannot displace H^+ on N atom in acidified PEI because coordination bond formed between PEI and these metal ions is weaker than that formed between PEI and relatively heavy metal ions. In addition, high stability of metal ions resulting from high solubility of target materials in acidic conditions will prevent formation of coordination bond to PEI. Other factors may affect the effectiveness of acidified PEI in previous studies: less solubility of sulfates containing heavy metal ions and different pH adjuster like CH_3COOH having possibility to work as antisolvent.

Interaction between PAA and metal ions is electrostatic attractive force, which is stronger interaction than formation of coordination bond. PAA (and CMC-Na) is effective only for $CaSO_4 \cdot 2H_2O$. This is because electrostatic attractive force is adequately strong to adsorb relatively light metal ions like Ca^{2+}. PAA is ineffective for other systems because electrostatic attractive force is too strong to maintain poorly-soluble salts dissolved. PAA tends to gelate and precipitate in basic conditions, which restricts reaction conditions using PAA reaction field and decreases usefulness of PAA like YBO_3 systems.

4.3.1.3 Investigation of interaction mechanism between $CaSO_4 \cdot 2H_2O$ crystals and additives

In this research, aspect ratio of synthesized crystals dramatically decreased when using concentrated citric acid, PAA and CMC-Na; additives having carboxyl groups. This result indicates that crystal growth along longitude direction is suppressed by electrostatic attractive force between carboxyl groups of additives and crystal growth point on latitude of $CaSO_4 \cdot 2H_2O$ crystals. If such interactions exist, Ca atoms should locate on the side surface along latitude direction.

To examine this hypothesis, abundance ratio of S atom to Ca atom (S/Ca) on each crystal surface was analyzed by X-ray photoelectron spectroscopy (XPS) (PHI5000 Versa Probe WS, ULVAC-PHI) on $CaSO_4 \cdot 2H_2O$ crystals synthesized without additives. As a result, S/Ca on the side surface along latitude direction was about 0.9. In contrast, S/Ca on the largest surface and on the side surface along longitude direction were more than 1.0. S/Ca on the side surface along latitude direction and those of other crystal surfaces can be considered to differ significantly because abundance of S atom and that of Ca atom in $CaSO_4 \cdot 2H_2O$ crystal are basically equal. These results mean that Ca atoms are more likely to locate on the side surface along latitude direction of plate-like crystals or at the point of needle-like crystals than any other surface of $CaSO_4 \cdot 2H_2O$ crystals. This tendency will be the same in the presence of additives. Therefore, crystal growth along longitude direction will be suppressed when using additives having carboxyl groups by electrostatic attractive force between carboxyl groups of additives and Ca atoms at crystal growth point on the side surface along latitude direction. This interaction will change crystal shape by preserving growth-suppressed surfaces, and as a result, aspect ratio of these crystals will decrease. Moreover, when using polyelectrolytes having carboxyl groups, not only crystal shape change but also crystal size decrease will proceed simultaneously, which will change needle-like or plate-like large crystals into granular microcrystals. Concerning additives that will not interact electrostatically with $CaSO_4 \cdot 2H_2O$ crystals, they will adsorb equally to each surface of $CaSO_4 \cdot 2H_2O$ crystals and will not affect their crystal shapes.

4.3.2 Relationships among XRD absolute intensity, XRD relative intensity and crystal morphology

4.3.2.1 The relationship between XRD absolute or relative intensity and crystal size

The relationships between XRD absolute or relative intensity and longitude are shown in Fig. 4.6 and Fig. 4.7, respectively.

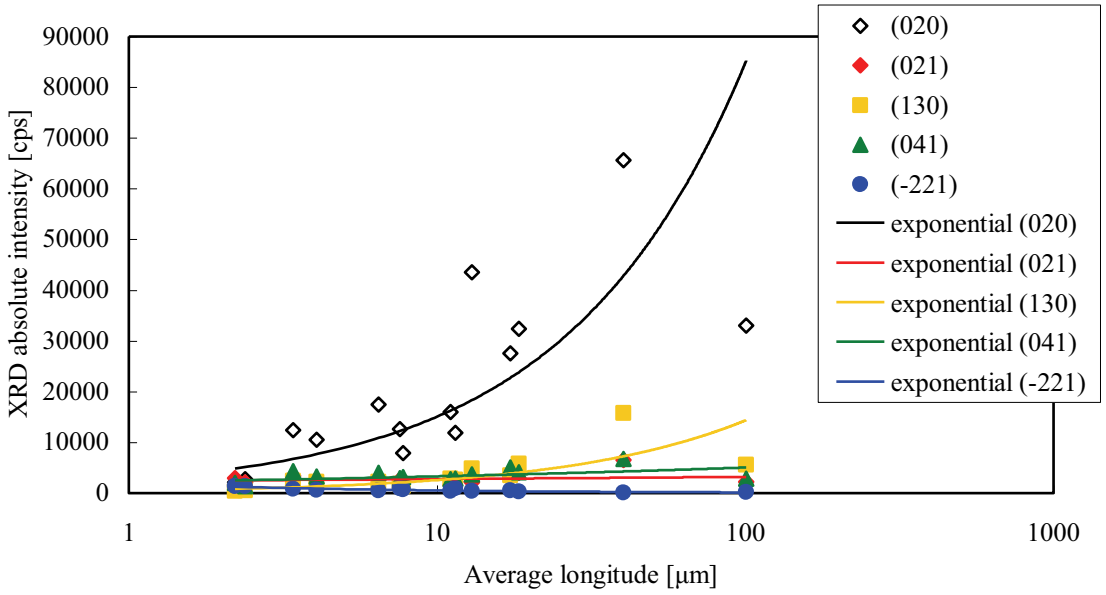

Figure 4.6 The relationship between average longitude and XRD absolute intensity

Exponential approximate equations of each diffraction face are as follows:

(020): $y = 2676.2x^{0.7504}$ $R^2 = 0.6703$ (021): $y = 2387.6x^{0.0632}$ $R^2 = 0.0375$

(130): $y = 457.61x^{0.7477}$ $R^2 = 0.6788$ (041): $y = 2158.4x^{0.1841}$ $R^2 = 0.2485$

(-221): $y = 1935.9x^{-0.5675}$ $R^2 = 0.6798$

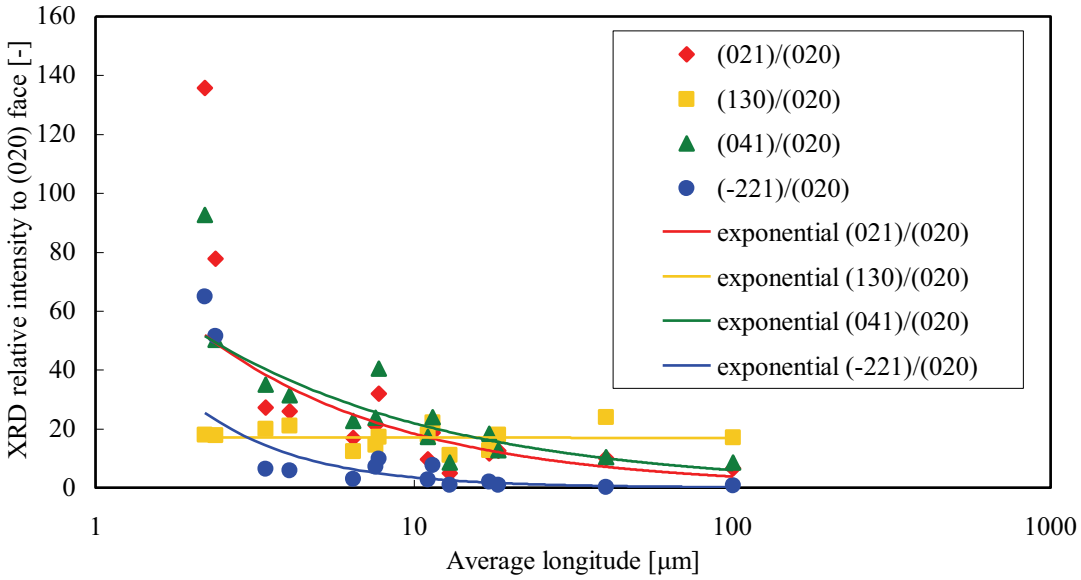

Figure 4.7 The relationship between average longitude and XRD relative intensity

Exponential approximate equations of each diffraction face are as follows:

(021) / (020): $y = 89.215x^{-0.6872}$ $R^2 = 0.6514$ (130) / (020): $y = 17.099x^{-0.0027}$ $R^2 = 0.0002$

(041) / (020): $y = 80.651x^{-0.5663}$ $R^2 = 0.7522$ (-221) / (020): $y = 72.338x^{-1.3179}$ $R^2 = 0.7163$

As longitude increased, XRD absolute intensity of (020) face and (130) face increased exponentially (Fig. 4.6). This result suggests (020) face and (130) face are parallel to longitude. In contrast, XRD absolute intensity of (-221) face decreased exponentially as longitude increased. This result suggests (-221) face grows rapidly and disappears as crystal grows along longitude direction. XRD absolute intensities of (021) face and (041) face were hardly affected by longitude increase, in other words, they were kept nearly constant regardless of longitude. This result suggests (021) face and (041) face are vertical to longitude. Because XRD absolute intensity of (021) face and (041) face are kept constant, these peaks outstands when granular microcrystals are dominant. However, XRD absolute intensity of (041) face can be considered to increase slightly as longitude increased. This result suggests (041) face slightly grows under the influence of crystal growth along longitude

direction though (041) face is not to be parallel to longitude. The relationship between XRD absolute intensity and latitude was less clear than longitude, however, (020) face, (130) face and (-221) face showed similar tendency to those of longitude. Concerning (021) face and (041) face, relationship to latitude was unclear.

Meanwhile, XRD relative intensity to (020) face decreased exponentially except for (130) face as longitude increased (Fig. 4.7). This result means the area of (021), (041) and (-221) faces relatively decrease as the area of (020) face increases by crystal growth along longitude direction. In other words, crystal shape changes from granular to needle or plate as the area of (020) face increases. In contrast, XRD relative intensity of (130) face was kept constant. This result ensures the theory that (130) face is parallel to longitude as well as (020) face and these faces grow together. On (-221) face, not only XRD absolute intensity but also XRD relative intensity was correlated with longitude. In fact, XRD relative intensity of (-221) face became larger as granular microcrystals became dominant. This result ensures the theory that (-221) face grows rapidly and disappears as crystal grows along longitude direction. The change of XRD relative intensity against latitude was similar to that against longitude.

Correlation coefficients on the relationships between XRD absolute or relative intensity and crystal size were 0.7 at the best. This is because XRD absolute intensity depends not on representative length but on the surface area of each diffraction face. For example, shape of grown crystal can be needle-like or plate-like though surface areas of them are equal. In addition, increase of crystal thickness will be error source.

4.3.2.2 Relationships between XRD relative intensity of (021) face and crystal morphology, XRD relative intensity of (021) face and that of other faces

The relationships between XRD relative intensity of (021) face and crystal morphology are

shown in Fig. 4.8. Decrease of average longitude and average latitude means that $CaSO_4 \cdot 2H_2O$ crystals become smaller by increase of XRD relative intensity of (021) face. However, because average longitude decreases more rapidly than average latitude, aspect ratio decreases as XRD relative intensity of (021) face increases. As a result, shape of synthesized $CaSO_4 \cdot 2H_2O$ changes from needle-like or plate-like to granular as XRD relative intensity of (021) face increases. Crystal shape changed the most dramatically when XRD relative intensity of (021) face was around 50.

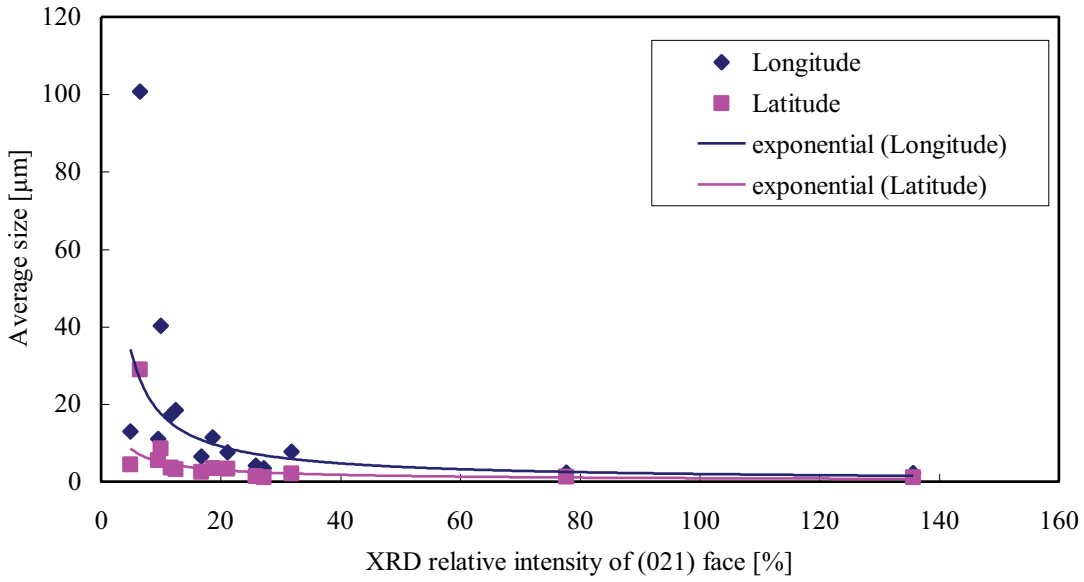

Figure 4.8 The relationship between XRD relative intensity of (021) face and average size

Exponential approximate equations of longitude and latitude are as follows:

Longitude: $y = 155.58x^{-0.948}$ $R^2 = 0.6514$ Latitude: $y = 28.696x^{-0.7571}$ $R^2 = 0.5888$

The relationships between XRD relative intensity of (021) face and XRD relative intensity of each diffraction face are shown in Fig. 4.9. As XRD relative intensity of (021) face increased, XRD relative intensities of (041) face and (-221) face also increased. On (-221) face, XRD absolute intensity increased as well as XRD relative intensity (Table 4.3). In contrast, XRD relative intensity

of (130) face kept constant. These changes of XRD relative intensities correspond to morphology changes, in other words, as relative area of (021) face increases, relative areas of (041) face and (-221) face also increase, as a result, synthesized $CaSO_4 \cdot 2H_2O$ changes from needle-like or plate-like large crystals to granular microcrystals.

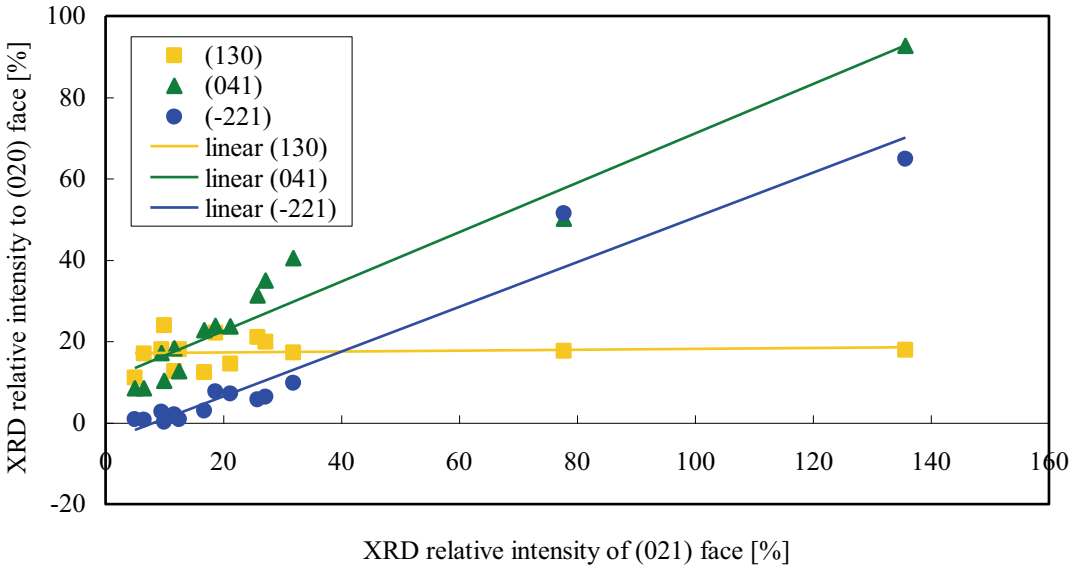

Figure 4.9 The relationship between XRD relative intensity of (021) face and those of other faces

Linear approximate equations of each diffraction face are as follows:

(130): $y = 0.0113x + 17.055$ $R^2 = 0.0117$ (041): $y = 0.6067x + 10.464$ $R^2 = 0.9387$

(-221): $y = 0.5495x - 4.4445$ $R^2 = 0.9487$

4.3.2.3 Estimation of crystal axis and crystal face of $CaSO_4 \cdot 2H_2O$

Analysis of intensity ratio of major XRD peaks enables us to trace the changing process of crystal habit of $CaSO_4 \cdot 2H_2O$. This knowledge also enables us to estimate crystal axis and crystal face of $CaSO_4 \cdot 2H_2O$. Crystal axes and approximate crystal structure of $CaSO_4 \cdot 2H_2O$ are estimated to be as Fig. 4.10. X-Y-Z coordinate system is defined not to be inconsistent with each crystal face.

(020) face is usually largest and the most outstanding face, therefore, longitude and latitude of crystals are usually decided from (020) face. (020) face is parallel to x axis and z axis, and vertical to y axis. (130) face is parallel to z axis similarly to (020) face. This face extends to depth direction, in other words, (130) face has the component of crystal thickness. (021) face and (041) face are vertical to z axis, in other words, these faces are vertical to (020) face and (130) face. However, inclination is different between (021) face and (041) face. (-221) face is assumed to be trace level in Fig. 4.10. This face is assumed to exist at the corner of crystal because this face is not parallel to any axes. This face outstands only at the beginning of crystal growth or in the case that granular microcrystals are dominant, and disappears rapidly as crystal grows along longitude direction. Other crystal faces showing lower XRD absolute intensity may appear at edge or corner of crystal, however, they will not affect approximate crystal structure of $CaSO_4 \cdot 2H_2O$.

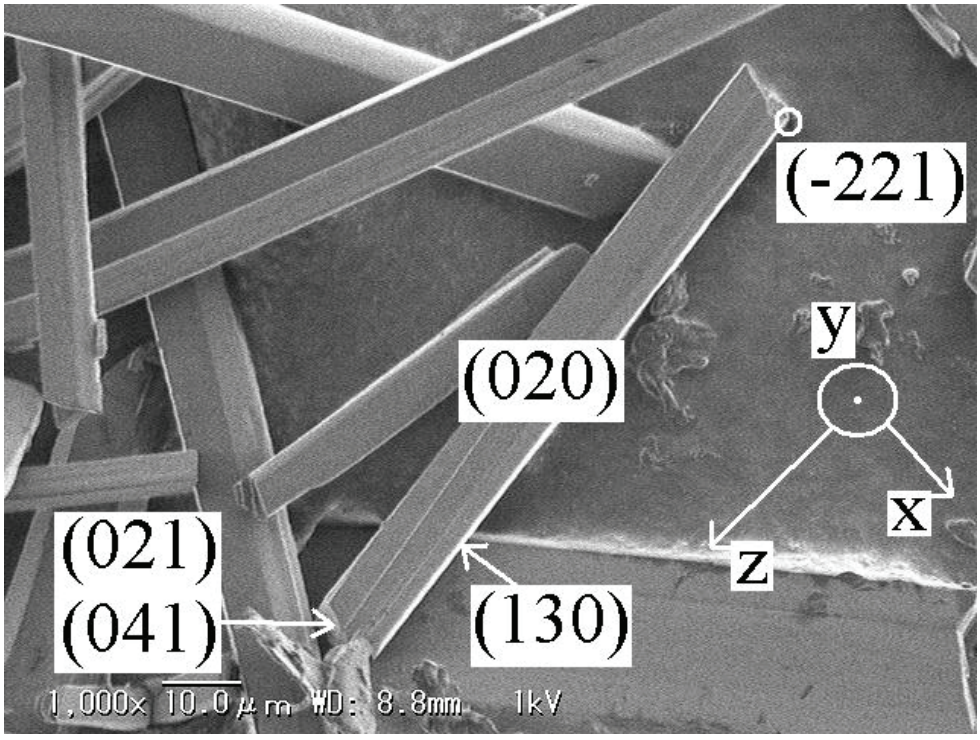

Figure 4.10 Assumed crystal axes and crystal faces of $CaSO_4 \cdot 2H_2O$

4.4 Critical problem for above research: preferred orientation

Preferred orientation of coarse crystals with large aspect ratio in powder X-ray diffraction can be fatal problem for the relationship between crystal habit and XRD absolute or relative intensity. In other words, observed relationship between them can only be the probability that particular face of crystals orients to the direction X-ray is irradiated. Preferred orientation of crystals will be eliminated as crystal size decreases, and finally XRD relative intensities will converge to the same values as JCPDS data regardless of crystal shape.

Certainly, XRD charts having particular peak much stronger than any other peak indicate the possibility of preferred orientation. However, synthesis method and/or synthesis condition of $CaSO_4 \cdot 2H_2O$ in this research is different from that of JCPDS. This means it is natural result that crystal habit and XRD relative intensities are different from those of JCPDS. In addition, although crystal size and crystal shape changed according to additives, the tendency that (020) peak is the strongest unchanged except for the case CMC-Na was added. Especially, $CaSO_4 \cdot 2H_2O$ reagent comprised of thick and coarse granular crystals showed similar XRD chart to other cases comprised of needle-like or plate-like crystals. These results mean the relationship between crystal habit and XRD absolute or relative intensity clearly exists though preferred orientation may affect to some extent.

Preferred orientation has to be prevented especially when precision measurement is carried out on large crystals with large aspect ratio. For example, preferred orientation can be almost solved by grinding crystals to less than 20 μm [25, 26]. However, preferred orientation may still remain on crystals with large aspect ratio because crystal shape is unchanged while crystal size is decreased by grinding. In addition, grinding cannot be applied in the cases grinding can cause change of crystal structure or chemical composition, crystal distortion and amorphous transition. These adverse impacts can occur on quite stable materials by heavy grinding and can change XRD chart. X-ray

photographic method or parallel beam method with capillary rotation stage is recommended for precision measurement of crystals likely to have preferred orientation.

4.5 Conclusions

Polyelectrolytes having carboxyl groups such as PAA or CMC-Na are the most suitable for synthesizing mono-dispersed $CaSO_4 \cdot 2H_2O$ microcrystals due to slow growth rate resulting from nucleation suppression and/or solubility increase by polyelectrolytes, growth suppression resulting from steric hindrance of polyelectrolytes, and prevention of aggregation resulting from electrostatic attractive force between Ca^{2+} and carboxyl groups in polyelectrolytes.

XRD relative intensity of each diffraction face on $CaSO_4 \cdot 2H_2O$ changes according to crystal morphology. As XRD relative intensity of (021) face increases, XRD relative intensities of (041) face and (-221) face also increase. At the same time, average longitude and aspect ratio decrease and needle-like or plate-like large crystals transform into granular microcrystals. In addition, XRD absolute intensity and XRD relative intensity on particular crystal faces are correlated with longitude. However, correlate coefficients are 0.7 at the best because XRD absolute intensity is depend not on representative length but on total area of each diffraction face.

Chapter 5

Overall conclusions and contribution of these researches

Type, concentration and pH of polyelectrolyte reaction field must be decided considering type and strength of interaction between polyelectrolyte and target materials to synthesize mono-dispersed microcrystals free from aggregation. For example, non-acidified PEI, whose interaction mechanism is formation of coordination bond between unshared electron pairs on N atoms in PEI and metal ions, is effective for synthesizing mono-dispersed YBO_3 microcrystals though appropriate concentration of PEI exists. However, PEI is ineffective for $CaSO_4 \cdot 2H_2O$ regardless of its pH due to weakness of coordination bond between PEI and Ca^{2+}. Considering other poorly-soluble sulfates containing relatively heavy metal ions such as Sr, Ba and Pb, only acidified PEI is effective by preventing direct reaction between unshared electron pairs on N atoms in PEI and metal ions, and by proceeding mild reaction through displacement reaction between H^+ and metal ions and following reaction crystallization on N atoms in PEI. On the other hand, electrostatic attractive force between carboxyl groups in PAA or CMC-Na and metal ions is adequately strong for compounds containing relatively light metal ions such as $CaSO_4 \cdot 2H_2O$ while it is too strong for YBO_3 or other poorly-soluble sulfates containing Sr, Ba and Pb. In addition, the tendency of polyelectrolytes having carboxyl groups to gelate and precipitate in basic conditions restricts reaction conditions. The above knowledge will be useful for similar compounds containing other anions, or compounds containing other cations with similar atomic weight, ionic radius, ion valence or electronegativity.

The most important requirement to form uniform YBO_3 microcrystals is to synthesize uniform $YB(OH)_4CO_3$ microcrystals before firing. In addition, PEI reaction field with appropriate concentration helps to maintain crystal shape and to prevent crystal aggregation not only during reaction crystallization but also during firing. Uniform YBO_3 microcrystals will shorten firing time, which will save the energy during firing. In addition, uniform YBO_3 microcrystals will allow making flat emission surface with less phosphor particles in high packing density, which will reduce market

price.

Morphology of $CaSO_4 \cdot 2H_2O$ changes from needle-like or plate-like large crystals into granular microcrystals synthesized in polyelectrolytes having carboxyl groups. From this aspect, polyelectrolytes having carboxyl groups such as PAA or CMC-Na are the most suitable for synthesizing mono-dispersed $CaSO_4 \cdot 2H_2O$ microcrystals. In addition, XRD relative intensity of each diffraction face correlates with crystal morphology. As XRD relative intensity of (021) face increases, average longitude and aspect ratio decrease and needle-like or plate-like large crystals transform into granular microcrystals. This knowledge enables us to trace changing process of crystal morphology from intensity ratio of major XRD peaks.

The above researches will contribute not only to control crystal characteristics, to improve production process of phosphors and to reduce production cost, but also to save resource and energy, and to develop crystallization itself.

Appendices

CMC-Na: sodium carboxymethylcellulose

CV: coefficient of variation

FT-IR: Fourier transform infrared spectroscopy

PAA: polyacrylic acid

PDP: plasma display panel

PEI: polyethyleneimine

PVP: polyvinylpyrrolidone

r_1[-]: a distance between the chromaticity coordinate of reference synthesized by solid-state reaction and chromaticity coordinate of ideal red

r_2[-]: a distance between chromaticity coordinate of sample synthesized by reaction crystallization and chromaticity coordinate of ideal red

RE: rare earth

SEM: scanning electron microscope

VUV: vacuum ultraviolet

XPS: X-ray photoelectron spectroscopy

XRD: X-ray diffraction

References

[1] A. Katayama et. al., *J. Cryst. Growth*, **2004**, *260*, 500-506

[2] T. Mikami et. al., *Chem. Eng. Res. Des.*, **2010**, *88*, 1200-1205

[3] T. Mikami et. al., *J. Chem. Eng .Jpn.*, **2010**, *43*, 698-703

[4] C. H. Kim et. al., *J. Alloys. Compd.*, **2000**, *311*, 33-39

[5] H. C. Lu et. al., *J. Electron. Spectrosc. Relat. Phenom.*, **2005**, *144-147*, 983-985

[6] Jisedai PDP kaihatsu center, "Tokoton Yasashii Plasma Display no Hon", p.88, 120 (2006)

[7] M. Kawamura, "Yokuwakaru Purazuma Terebi", p.128 (2005)

[8] T. Uchida, "Zukai Denshi Display no Subete", p.186-187 (2006)

[9] Y. Wang et. al., *J. Solid State Chem.*, **2004**, *177*, 2242-2248

[10] C. Xiangzhong et. al., *J. Rare Earths*, **2006**, *24*, 149-152

[11] Z. Wei et. al., *J. Appl. Phys.*, **2003**, *93 (12)*, 9783-9788

[12] G. Lee, S. Kang, *J. Electrochem. Soc.*, **2006**, *153 (5)*, H105-H109

[13] X. Jiang et. al., *J. Solid State Chem.*, **2003**, *175*, 245-251

[14] K. Kim et. al., *J. Mater. Res.*, **2002**, *17 (4)*, 907-910

[15] Y. Zhijian et.al., *J. Rare Earths*, **2004**, *22 (6)*, 829-832

[16] N. Joffin et. al., *Opt. Mater.*, **2006**, *28*, 597-601

[17] Ernest M. Levin et. al., *Am. Mineral.*, **1961**, *46*, 1030-1055

[18] J. A. Zaykoski et.al., *J.Am. Ceram. Soc.*, **2011**, *1 (7)*, 1-7

[19] Y. Wang, L. Wang, *Mater. Lett.*, **2006**, *60*, 2645-2649

[20] M. Ooki et.al., "Kagaku Daijiten", p.2492 (1989)

[21] B. Simon and M. Bienfait, *Acta Cryst*., **1965**, *19*, 750

[22] W. M. M. Heijnen and P. Hartman, *J.Crystal Growth*, **1991**, *108*, 290

[23] Elly van der Voort and P. Hartman, *J.Crystal Growth*, **1991**, *112*, 445-450

[24] K. Sohn et. al., *J. Mater. Res.*, **2002**, *17 (12)*, 3201-3205

[25] M. Kato, “Ceramics Kiso Koza 3 X Sen Kaisetsu Bunseki”, p.21,158-167,201 (1990)

[26] Rigaku, “X Sen Kaisetsu Handbook”, p.41,42,57,58 (1998)

Acknowledgements

This research was supported by Global Center of Excellence (GCOE) Practical Chemical Wisdom, Konica Minolta, Nippon Shokubai, Professor Hirasawa, Professor Noda, Assistant Professor Kohori, researchers in laboratory, and my parents.

早稲田大学大学院 先進理工学研究科

博 士 論 文 概 要

論 文 題 目

Reaction Crystallization Field to Control Crystal Characteristics

結晶特性を制御するための反応晶析場

申 請 者

Mikiyasu	INOUE
井上	幹康

応用化学専攻 化学工学研究

2013 年 12 月

反応晶析は液相法の一種であり、液体原料を混合、反応させて結晶製品を得る方法である。反応晶析は、反応により生じる過飽和により結晶化が急速に進むという長所がある一方、核化・成長の制御が困難であり、粒子が凝集しやすいという問題点を抱えている。

本研究では、核発生と結晶成長の制御、凝集抑制を目的として、高分子電解質を反応場として用いる反応晶析を利用した。この方法により$(Y,Gd)BO_3:Eu^{3+}$を合成し、最適な高分子電解質反応場および反応条件を決定した。さらに、高分子電解質使用時に見られたYBO_3の晶癖変化とX線回折ピーク強度変化の関係について、結晶面、結晶形状がより明瞭な$CaSO_4 \cdot 2H_2O$をモデル物質として研究を進め、同時に$CaSO_4 \cdot 2H_2O$についても結晶特性制御に有用な反応晶析場を探索した。以上の結果を統合し、反応晶析場による結晶特性の制御の概念を提出した。

本論文は全五章から構成される。各章の概要について以下に述べる。

第一章　反応晶析の特徴および高分子電解質反応場の作用

反応晶析は液相法の一種であり、液体原料を混合して結晶製品を得る方法である。反応晶析の最大の長所は、反応により生じる過飽和により結晶化が急速に進む点である。加えて、常温・常圧で反応が進むため、エネルギーの節約も可能である。一方で、反応晶析は核化・成長制御が困難であり、粒子が凝集しやすいという問題点を抱えている。

凝集を防ぐための合成法の一つとして、高分子電解質を反応場として用いる反応晶析がある。この方法を用いることで、高分子電解質と溶質分子および結晶核との静電的相互作用、高分子鎖の立体障害により核化段階と成長段階が分離でき、単分散微粒子の合成が可能になると示唆されている。実際に、難溶性硫酸塩の単分散微粒子合成の既往研究においては、ポリエチレンイミン(PEI)酸性条件が特に有効であるという結果が得られている。

第二章　対象物質$(Y,Gd)BO_3:Eu^{3+}$および$CaSO_4 \cdot 2H_2O$の結晶特性

$(Y,Gd)BO_3:Eu^{3+}$は真空紫外(VUV)蛍光体の一種であり、プラズマディスプレイパネル(PDP)用赤色蛍光体として広く利用されるほか、水銀フリー蛍光灯への応用も検討されている。商業用$(Y,Gd)BO_3:Eu^{3+}$は固相法で合成され、大粒径で形状が不均一であるが、反応晶析を利用すれば改善が可能である。ただし、反応晶析では非晶質前駆体が生成するため、焼成操作によりYBO_3に変換する必要がある。

$CaSO_4 \cdot 2H_2O$はアルカリ土類金属硫酸塩の中では最も式量が小さく、最も水に溶けやすいが、物質全体では難溶性塩に分類される。この点から、$CaSO_4 \cdot 2H_2O$は、反応晶析で合成する際に核化・成長制御、凝集抑制が難しい物質の一つであり、既往研究における難溶性硫酸塩と同様に単分散微粒子合成法を探索する価値

のある物質であるといえる。常温・常圧下では通常 2 水和物が析出するが、0.5 水和物をはじめとして異なる水和数のものが生成する場合もある。

第三章　高分子電解質反応場を用いた反応晶析による$(Y,Gd)BO_3:Eu^{3+}$単分散微粒子の合成

1 g/L または 10 g/L の PEI およびポリアクリル酸(PAA)を高分子電解質の候補とし、YBO_3単分散微粒子の合成に最適な高分子電解質反応場および操作条件を探索した。その結果、1 g/L PEI を反応場として用い、塩基性側から操作した場合に、3 つの興味深い現象が見られた。まず、CO_3^{2-}源を添加していないにもかかわらず、通常の非晶質前駆体ではなく $YB(OH)_4CO_3$ 結晶質前駆体が生成した。次に、生成した前駆体は粒径・形状ともに均一な球状微粒子であった。さらに、焼成後もこの粒径と形状は維持された。これに対して、PEI 酸性条件は 1 g/L、10 g/L とも非晶質前駆体が生成し焼成後も凝集しているという点で、10 g/L PEI 塩基性条件は粒径・形状が不均一かつ焼成後に不純物が混入するという点で不適であった。PAA は、YBO_3 前駆体が生成する塩基性領域ではゲル状となり分離するという点で明らかに不適であった。以上より、高分子電解質反応場としては 1 g/L PEI 塩基性条件が最適であると結論づけられた。

一連の研究として、$YB(OH)_4CO_3$ 結晶質前駆体の生成条件の解明、Na_2CO_3 を pH 調整剤として用いた $YB(OH)_4CO_3$ 結晶質前駆体の合成の検討も行った。その結果、$YB(OH)_4CO_3$ 結晶質前駆体を得るには、希薄条件、最終 pH 弱酸性、1 日程度の撹拌という 3 つの条件が必要であることを見出した。また、Na_2CO_3 使用時には、前駆体中の B 原子と C 原子のモル比(C/B)を 1.5 以下に抑え、1 日撹拌した場合に均一な $YB(OH)_4CO_3$ 球状微粒子が生成した。さらに、$YB(OH)_4CO_3$ 球状微粒子が生成すれば焼成後にも粒径が維持されることから、YBO_3 単分散微粒子の合成には、焼成前の均一な $YB(OH)_4CO_3$ 球状微粒子の生成が最も重要であることを見出した。Na_2CO_3 により $YB(OH)_4CO_3$ 球状微粒子が確実かつ簡便に合成でき、NH_3 を併用すれば収率の向上も可能である。ただし、焼成中の形状維持、凝集抑制には課題が残り、焼成中の PEI の必要性が示唆された。

第四章　$CaSO_4・2H_2O$ の晶癖と XRD ピーク強度の関係

結晶形状（晶癖）は反応条件により変化し、同時に X 線回折ピーク強度も変化する。これらの変化は YBO_3 を含めさまざまな物質で観察されるが、晶癖と XRD ピーク強度の関係は明らかにされていない。本研究では、モデル物質 $CaSO_4・2H_2O$ を各種添加物存在下で合成し、核化・成長制御に有用な反応晶析場を探索するとともに、添加物による晶癖変化、晶癖と XRD ピーク強度の関係を調査した。

その結果、PAA（平均分子量 25 万）、カルボキシメチルセルロースナトリウム(CMC-Na)など、カルボキシル基をもつ高分子電解質を用いると、$CaSO_4・2H_2O$ の

形状および X 線回折図形が大きく変化した。通常の $CaSO_4・2H_2O$ 結晶は針状・板状粗大晶だが、PAA25 万、CMC-Na を反応晶析場として用いると粒状微結晶が生成した。しかし、他の難溶性硫酸塩の単分散微粒子合成に有効であった PEI 反応場は $CaSO_4・2H_2O$ には効果がなく、X 線回折図形にも目立った変化はなかった。また、酸・塩基、無機塩、低分子有機化合物などの各種低分子添加物についても、カルボキシル基をもつ高分子電解質に匹敵する微小化・単分散化効果を示すものはなかった。一方で、粗大粒子のまま短径方向の成長を促進させる低分子添加物が存在し、静置条件では mm オーダーの粗大晶が生成するなど、微小化とは対極にある現象も観察された。以上のことから、$CaSO_4・2H_2O$ 単分散微粒子の合成には、カルボキシル基をもつ高分子電解質が最も有力な反応晶析場であることが見出された。X 線回折図形に関しては、カルボキシル基をもつ高分子電解質使用時、通常最強ピークとなる(020)面のピーク強度が大きく低下した一方、(021)面のピーク強度が増大し、最強ピークになることもあった。また、(041)面、(-221)面など、通常の $CaSO_4・2H_2O$ 回折図形ではあまり目立たないピークの強度も増大した。

(020)面に対する各回折ピークの相対強度を算出し、最も変化の大きい(021)面の相対強度に関して結果を分類すると、特定の XRD 相対強度間、あるいは XRD 相対強度と平均粒径、アスペクト比の間に相関関係があることが確認された。さらに、各回折ピーク強度の変化を解析することで、$CaSO_4・2H_2O$ の晶癖変化の過程を追跡できることを見出した。

第五章　結果の総括と今後の展開および本研究の貢献可能性

$(Y,Gd)BO_3:Eu^{3+}$反応晶析における高分子電解質反応場としては 1 g/L PEI 塩基性条件が最適である。そして、YBO_3 単分散微粒子の合成には、焼成前に均一な $YB(OH)_4CO_3$ 球状微粒子を生成させることが最も重要である。均一な YBO_3 微粒子の合成が可能になると、焼成時間の短縮により省エネルギー化が達成される。また、均一な微粒子はより少量で高充填密度の発光面が作製可能であり、商品価格も低減されると期待される。

$CaSO_4・2H_2O$ は、カルボキシル基をもつ高分子電解質中で合成すると粒状微結晶となる。また、XRD 相対強度と晶癖の間には相関関係があり、(021)面の XRD 相対強度が増大するにつれて平均長径、アスペクト比は減少し、$CaSO_4・2H_2O$ 結晶は針状・板状粗大晶から粒状微結晶に変化する。この知見は主要な XRD ピーク強度比からの晶癖の推定を可能にし、凝集が激しく個々の結晶形状が不明瞭な場合、結晶の向きが不明な場合などに特に有用である。

以上のように、本論文の成果は、単分散微粒子合成をはじめとする結晶特性制御、蛍光体生産プロセス改良・製造コスト削減のみならず、省資源・省エネルギー、さらには学問としての晶析工学の発展に寄与するものである。

早稲田大学　博士（工学）　学位申請　研究業績書

氏 名　井上　幹康　　印

（2013　年　11　月　現在）

種 類 別	題名、　発表・発行掲載誌名、　発表・発行年月、　連名者（申請者含む）
1. 論文	○Mikiyasu Inoue and Izumi Hirasawa, “The relationship between crystal morphology and XRD peak intensity on $CaSO_4$・$2H_2O$”, Journal of Crystal Growth, **380** (2013) pp.169-175 ○Mikiyasu Inoue and Izumi Hirasawa, “Synthesis of (Y,Gd)BO_3:Eu^{3+} by reaction crystallization using polyelectrolyte reaction field”, Chemical Engineering & Technology (in press) Akio Tanahashi, T.Ikehara, M.Inoue, R.Shinozuka and Izumi Hirasawa, “Effect of excess boric acid on (Y,Gd)BO_3:Eu red phosphor for plasma display panel through reaction crystallization”, BIWIC2008, pp.303-309 (2008)
2. 講演	井上幹康，平沢泉，“Synthesis of (Y,Gd)BO_3:Eu^{3+} by Reaction Crystallization using PEI Reaction Field”，第 6 回 G-COE 国際シンポジウム，P20，要旨集 p.70，東京（2011 年 12 月） 井上幹康，平沢泉，“Effects of Polyelectrolyte on Reaction Crystallization of (Y,Gd)BO_3:Eu^{3+}”，第 3 回 NIMS (MANA) - Waseda 国際シンポジウム，PS37，要旨集 p.47，東京（2011 年 11 月） 井上幹康，平沢泉，“The Relationship between Morphology and Relative Intensity of XRD Peaks on $CaSO_4$･$2H_2O$”，第 5 回 G-COE 国際シンポジウム，P16，要旨集 p.34，東京（2011 年 1 月） 井上幹康，平沢泉，“Effects of Polyelectrolyte on Reaction Crystallization on $CaSO_4$･$2H_2O$”，第 2 回 NIMS(MANA)-Waseda 国際シンポジウム，PS16，要旨集 p.24，茨城（2010 年 12 月） 井上幹康，篠塚力樹，斎藤祐亮，平沢泉，“The Synthesis of (Y,Gd)BO_3:Eu^{3+} by Coprecipitation Method Using Buffer Solution”，第 4 回 G-COE 国際シンポジウム，P39，要旨集 p.43，東京（2010 年 1 月） 井上幹康，棚橋昭夫，池原与人，平沢泉，“沈殿法による PDP 用(Y,Gd)BO_3:Eu^{3+}の合成における操作条件の最適化“，分離技術会 2007，SFa-P2，要旨集 p.121，愛知（2007 年 6 月）